UNIVERSITY OF CALIFORNIA,
IRVINE

Cosmological Implications of Quantum Gravity

DISSERTATION

submitted in partial satisfaction of the requirements
for the degree of

DOCTOR OF PHILOSOPHY

in Physics

by

Lu Heng Sunny Yu

Dissertation Committee:
Professor Herbert W. Hamber, Chair
Professor Jonathan L. Feng
Professor Mu-Chun Chen

2021

DEDICATION

To my parents,
my advisor Prof. Herbert W. Hamber,
and the continued exploration of the Universe.

TABLE OF CONTENTS

LIST OF FIGURES

LIST OF TABLES

ACKNOWLEDGMENTS

Firstly and most importantly, I would like to thank my advisor Herbert Hamber for his guidance and kindness, his deep insights, wit, and passion to physics, and above all, his unwavering support throughout my academic career. Every meeting I had with you brightened my day and gained deeper perspectives in physics.

Special thanks to Professor Stan Brodsky, who had provided many enlightening discussions during my visit at SLAC (Stanford Linear Accelerator Center) National Accelerator Laboratory, Stanford University.

To all the people at University of California, Irvine (UCI) who generously provided me with valuable sources of knowledge, discussions, and support, including professors and colleagues in Particle Theory group: Mu-Chun Chen, Tim Tait, Jonathan Feng, Michael Ratz, Arvind Rajaraman, Yuri Shirman. My gratitude also goes to Laura Tucker, for many support and discussions on physics education.

I'd also like to especially thank all my friends and collaborators: Hasitha E. Pituwala Kankanamge, Milad Pourrahmani, Ron Shaeffer and Brian Casas. Thank you for all the companionship and the many many riveting mathematics, philosophy, and physics discussions. My life has become better and more inspiring because of your being part of it. Your friendships are truly invaluable and always be remembered. For making the graduate office fun as well as a decent working and learning environment, I want to thank Ben Lillard, Jordan Smolinsky, Arianna Braconi, Michael Waterbury, Frieda Rivera, Alexis Romero, Yvonne Wong, Alex Armstrong.

Also thanks to all the professors whom I had the privilege to work as a teaching assistant for – for providing the opportunity for me to refine my teaching skills, while sharing my love for physics. I'd also like to give special thanks to teachers including Rick Twyman, Yush Yuen, James Briggs, that were my early inspirations to the wonderful world of mathematics and physics.

Most important of all, this journey cannot be possible without the indispensable support of my parents, who always provided a strong fabric of love, values and affirmation. Especially, to my mother Paulina Leung for the uncountable times you have supported me when things are tough. And to my father Yuen T. Yu, who has been my primary inspiration for falling in love with the fascinating world of mathematics, physics, and all the wonders of the universe in the first place. I will be forever grateful for all the late nights you have both dedicated to me personally and academically in my whole life. I cannot be here without you. And I can only make the differences that I have made because of you.

Last but not least, thank you to My Banh and the administrative team at the UCI Physics department, for the numerous times I and other graduate students needed help. You have always been there for us. Finally, thank you to everyone at UCI and SLAC that I have had the pleasure to work with, who contributed to making this work possible.

CURRICULUM VITAE

Lu Heng Sunny Yu

EDUCATION

Doctor of Philosophy in Physics **2020**
University of California, Irvine *Irvine, California, USA, USA*

Master of Advanced Studies in Mathematics **2014**
University of Cambridge *Cambridge, UK*

Bachelor of Science in Mathematics and Physics **2013**
University College London (UCL) *London, UK*

RESEARCH EXPERIENCE

Graduate Research Assistant **2015–2020**
University of California, Irvine *Irvine, California, USA*

Visiting Research Scholar **2019**
SLAC National Accelerator Laboratory, Stanford University *Menlo Park, CA, USA*

TEACHING EXPERIENCE

Lecturer **2017, 2020**
University of California, Irvine *Irvine, California, USA*

Teaching Assistant **2015–2020**
University of California, Irvine *Irvine, California, USA*

WORK EXPERIENCE

Business Analyst **2014–2015**
Fidelity National Information Services, Inc. *London, UK*

REFEREED JOURNAL PUBLICATIONS

Dyson's Equations for Quantum Gravity in the Hartree-Fock Approximation 2021
with Herbert W. Hamber. *Symmetry* 2021, 13, 120

Gravitational Fluctuations as an Alternative to Inflation III: Numerical Results 2020
with Herbert W. Hamber, Hasitha E. P. Kankanamge. *Universe* 2020, 6, 92

Gravitational Fluctuations as an Alternative to Inflation II: Angular CMB Spectrum 2019
with Herbert W. Hamber. *Universe* 2019, 5, 216

Gravitational Fluctuations as an Alternative to Inflation 2018
with Herbert W. Hamber. *Universe* 2019, 5, 31 (Cover Article)

RESEARCH PRESENTATIONS AND CONFERENCES

Quantum Gravity as an Alternative to Inflation 2019
- Quantum and Gravity in Okinawa Workshop, Okinawa Institute of Science and Technology Graduate University (OIST), Japan
- SLAC (Stanford Linear Accelerator Center) National Accelerator Laboratory, Stanford University, USA
- The University of Melbourne, Australia
- The University of New South Wales, Australia

Cosmic Matter Power Spectrum from Quantum Gravity 2019
- SoCal Beyond Standard Model (BSM) Workshop, University of California, Los Angeles, USA

Explaining the Power Spectrum with Non-perturbative Quantum Gravity 2017
- W.E. Heraeus Summer School on "Foundations and New Methods in Theoretical Physics", Germany

ABSTRACT OF THE DISSERTATION

Cosmological Implications of Quantum Gravity

By

Lu Heng Sunny Yu

Doctor of Philosophy in Physics

University of California, Irvine, 2021

Professor Herbert W. Hamber, Chair

Quantum gravity – as defined in the Feynman path integral approach by a gravitational action and a functional measure over metrics – is in principle a unique theory. While additional higher derivative terms that are consistent with general covariance are in principle allowed in the action, they affect only the physics at very short distances. As shown by Feynman, the Einstein-Hilbert action plus a cosmological constant term represents the unique covariantly-quantized theory for a massless spin-two particle at large distances – much like the Yang-Mills theory and QED are for massless spin-one particles. While the theory is still infamously perturbatively nonrenormalizable, a wide range of modern analytical and numerical methods have been developed in the past decades to study precisely such theories. From the nonlinear Heisenberg magnet in three dimensions to QCD in four dimensions (in the nonperturbative limit), these methods have produced many useful predictions with remarkable accuracies. Furthermore, important new physics have been revealed with these nonperturbative methods – such as the existence of quantum condensates, anomalous dimensions in critical scaling exponents, and nontrivial phase transitions – that would otherwise be invisible with perturbation theory to any order.

In this dissertation, we explore the consequences of these techniques applied to gravity. Using a range of analytical to numerical methods, we derive a number of physical predictions to

the gravitational effects on cosmology. In particular, we explore the unique alternative explanation for the various cosmological power spectra (including the galaxy- and CMB-spectra) that is based on gravitational fluctuations, as derived using various nonperturbative quantum field-theoretical methods. This is contrasted with the currently popular inflationary models, which are based on fluctuations of scalar fields. Next, we also outline a number of testable predictions in this picture that deviate from the conventional picture of inflation. The key ingredients in this new picture are the appearance of a nontrivial gravitational vacuum condensate (directly related to the observed cosmological constant), and a calculable renormalization group running of Newton's G on cosmological scales. Finally, we compare these results to latest available cosmological observational data, and we find that the results fit very well with the majority of the data. However, the limited precision of the observational data on largest angular scales, which is where the deviations are most significant, does not yet allow us to clearly prove or disprove either set of ideas. Nevertheless, it is expected that with an influx of increasingly accurate observational data in the near future, the new quantum gravitational picture we presented here can be subjected to further stringent observational tests, thus helping us gain a deeper understanding of roles that quantum field theory and gravity play in our Universe.

Chapter 1

Introduction

1.1 The Mystery

In cosmology, we know that the Universe is not perfectly homogeneous and isotropic, but is rather comprised of inhomogeneous fluctuations in both matter and energy densities. Furthermore, these fluctuations are far from random, but are instead congregated and correlated in rather specific manners. Detailed measurements made from large scale galaxy and cosmic microwave background (CMB) surveys have revealed that the fluctuations of various sizes follow a well-defined pattern that scales with their distance apart. In cosmology, these correlations are quantified by what are known as correlation functions and power spectra [1–4]. The questions of why these density fluctuations are distributed and correlated the way they are, or why these correlation functions and power spectra scale the way they do, are thus important ones in cosmology.

The conventional explanation for the shapes of these power spectra are provided by inflation models. While there are variations in detail among different inflation models, they are all based on the hypothesis of at least one or more additional primordial scalar fields called

inflatons [5–7]. Inflation explains that the matter fluctuations are originated from quantum fluctuations of this scalar field, and is able to reproduce the observed power spectrum of matter and other fluctuations from those of the inflaton field fluctuations. This is known as one of the earliest quantitative "verification" of inflation, and the agreement of these predictions with observations to high accuracy has thus been widely regarded as a great triumph and confirmation for inflation [8].

However, this picture is not without controversy [9–12], including criticisms on the naturalness and uniqueness of the theory. The detailed model of inflation is still largely unknown, and many models suffer from fine-tuning problems. As a result, the goal of our work is to propose an explanation for the shapes of the various cosmological power spectra based on gravitational fluctuations alone, independent of inflation. This approach is not only highly unique by nature (in the sense of having very limited adjustable parameters), arguably more natural (in the sense of having essentially no extra ingredients, and only using well-established cosmology and quantum field theory), but also, to our knowledge, the first of its kind that addresses the power spectra without any additional scalar fields.

In the next section, we will first briefly outline the premise of this new picture, before we present and explore the detailed theoretical derivations and subsequent data analyses in the remaining of the dissertation.

1.2 A Unique Solution – Cosmological Fluctuations from Quantum Gravity

General relativity provides an unambiguous relation between curvature and matter distributions through the Einstein field equations

$$R_{\mu\nu} - \tfrac{1}{2}\, g_{\mu\nu} R = 8\pi\, G\, T_{\mu\nu} \ . \tag{1.1}$$

It is therefore natural that any fluctuations in matter are directly related to fluctuations in curvature. Now, in any quantum theory, quantities fluctuate. As a result, a quantum theory of gravity produces metric and curvature fluctuations for which their correlation functions are in principle calculable from first principles. It is then possible to relate unambiguously these correlation functions to those of matter fluctuations, via the Einstein field equations.

While the theory of quantum gravity remains speculative in the extreme short-distance, a.k.a. ultraviolet (UV), regime—due to both an infinite number of allowed higher-order operators consistent with general covariance together with a lack of experimental results in this regime, the long-distance or infrared (IR) limit of the theory is however in principle well-defined and unique, governed primarily by the concept of universality. Nevertheless, this long-distance quantum theory of gravity still suffers from being perturbatively nonrenormalizable, rendering perturbation theory useless for calculating any quantum corrections in gravity. However, in the past decades, well known field theory techniques have been extensively developed, applied and even tested to high accuracy in various disciplines of physics where perturbation theory fails (e.g., nonlinear sigma model, Heisenberg magnets). It is thus highly conceivable that these nonperturbative methods may find use in deriving physical consequences for another perturbatively nonrenormalizable theory such as gravity.

From previous works [13, 14], it was shown that quantum effects of gravity may manifest

themselves not only on the extreme small (UV) scales, but also on the extreme large (IR), cosmological scales. In particular, our works [15, 16] have shown that, utilizing nonperturbative field theory methods, much of the cosmological matter power spectrum can be derived and reproduced purely from Einstein gravity and standard ΛCDM cosmology alone, without the need of any additional scalar fields as advocated by inflation. We have shown that not only the predictions agree quite well with recent data by the Planck Collaboration [17], but also that additional quantum effects predict subtle deviations from the classical picture, which allows this approach to be testable in the near future with increasingly powerful cosmological experiments.

It should be pointed out that this approach only uses fundamental principles from quantum field theory and general covariance, well-established methods in nonperturbative physics and cosmological dynamics, and no further assumptions or extra ingredients such as any scalar fields. The highly constrained setup from first principles also as a result dictates a very limited number of adjustable parameters, making the theory, like QED and QCD, essentially unique. As a result, it can be argued that this provides a more natural and unique solution to the question of matter and energy correlations in cosmology.

In this dissertation, we will summarize the essential background of quantum gravitation and nonperturbative dynamics, explain in detail how they provide a natural explanation to the power spectra mystery, present quantitative analysis of the supporting observational data, discuss constraints on the (limited) parameters in this theory from the observational data, comparisons with the inflation-motivated picture, prospective developments that can distinguish the two pictures in the future, and potential future works related to this subject.

More specifically, the dissertation is organized as follows. In Section 2, we provide the key background concepts relevant to this dissertation, including the definitions of correlation functions and power spectra in cosmology, and the essential concepts and key results from a nonperturbative study of quantum gravity. In Section 3, we will derive the galaxy power

spectrum and the cosmological matter power spectrum from the results of quantum gravity, and then compare them to the latest cosmological observational data. We also derive the additional quantum effects that takes place in the largest scales that potentially deviates from the classical results (including the renormalization group running of Newton's G and the effects of IR regulations due to the existence of a quantum condensate). We contrast this picture and its results with the conventional inflation perspective, and point out areas where these pictures can be tested with upcoming observational experiments. We also study the (very few) adjustable parameters in this picture, and the constraints that current observational data set on them. In Section 4, we extend the predictions to the angular CMB temperature spectrum, the spectrum most studied by cosmologists, in an analytical way. And in Section 5, we further the analysis by re-deriving the spectrum, but this time using some of the most popular numerical programs in cosmology. With the help of these state-of-the-art cosmological programs, we also derive a number of related cosmological spectra (including ones with E- and B-mode CMB photon polarizations, and the lensing potential ϕ), and comment on the potential usefulness of these in future observational tests. Finally, Section 6 summarizes our study, and provide an account of possible future directions that can be further explored, based on our studies in this dissertation.

Chapter 2

Background

In this chapter, we will recount some essential background necessary for the scope of this dissertation. More detailed background for each of the respective topics below can be found in the references therein as well as the standard literature. Section 2.1 reviews the standard ways matter and energy fluctuations are quantified in cosmology (and measured in observations). Section 2.2 gives a brief outline of the nonperturbative approach of quantum gravity, as well as key results that are important to the derivations in subsequent chapters of this dissertation.

2.1 Power Spectra in Cosmology

In this section, as a background, we briefly summarize the two main quantities that are used in cosmology to parameterize matter fluctuations: (i) correlation functions in both real and momentum space, and (ii) their corresponding powers, or spectral indices. To begin, it is customary to describe the matter density fluctuations in terms of the matter density contrast $\delta(\mathbf{x}, t)$ [1, 18], which measures the fractional over-density of matter relative to the

background mean density $\bar{\rho}(t)$,

$$\delta(\mathbf{x},t) \equiv \frac{\rho(\mathbf{x},t) - \bar{\rho}(t)}{\bar{\rho}(t)} = \frac{\delta\rho(\mathbf{x},t)}{\bar{\rho}(t)}, \tag{2.1}$$

where $\bar{\rho}(t)$ evolves only with time, in a way that is governed by the background Friedmann-Robertson-Walker (FRW) metric.

From its definition, it is clear that the expectation value, or the "one-point function", for the density contrast averages to zero, i.e., $\langle\, \delta(\mathbf{x},t)\,\rangle = 0$. The first non-trivial and more interesting quantity is the "two-point function", also known as the real space correlation function[1] G_ρ, which measures the average correlation between the density contrast fluctuations at two spacetime points by averaging over all space. Explicitly,

$$G_\rho(\mathbf{x},t;\mathbf{x}',t') \equiv \langle\, \delta(\mathbf{x},t)\; \delta(\mathbf{x}',t')\,\rangle = \frac{1}{V}\int_V d^3\mathbf{y}\; \delta(\mathbf{x}+\mathbf{y},t)\; \delta(\mathbf{x}'+\mathbf{y},t') \tag{2.2}$$

or even more commonly, with its momentum space conjugate, known as the matter power spectrum

$$P(k) = (2\pi)^3 \langle\, |\delta(k,t_0)|^2\,\rangle = (2\pi)^3\, F(t_0)^2\, \langle\, |\Delta(k)|^2\,\rangle \quad . \tag{2.3}$$

In the second step of Equation (2.3), the time dependence [2] is factored out as $\delta(k,t) \equiv \Delta(k)F(t)$, so that the power spectrum explicitly compares fluctuations as they are measured today, at time $t = t_0$. The factor $F(t)$ then simply follows the standard GR evolution formulas as governed by the Friedmann–Robertson–Walker (FRW) metric. Furthermore, both the real and momentum space correlation functions represent statistical averages, which satisfy homogeneity and isotropy, and hence are expected to only depend on the magnitudes

[1] The matter density correlation function for galaxies in real space is usually denoted as ξ_M, or simply ξ, in the cosmology literature. But in this paper it will be desirable to call it G_ρ, to avoid confusion with the quantum gravitational correlation length ξ that will be introduced later.

[2] $F(t)$ simply evolves according to the FRW background; its explicit evolution can be found in [18].

$r \equiv |\mathbf{x} - \mathbf{y}|$ and k.

Note that the power spectrum is directly related to the real space correlation function via a Fourier transform

$$\begin{aligned} G_\rho(r;t,t') &= \int \frac{d^3k}{(2\pi)^3}\, G_\rho(k;t,t')\, e^{-i\mathbf{k}\cdot(\mathbf{x}-\mathbf{y})} \\ &= \frac{1}{2\pi^2}\frac{F(t)F(t')}{F(t_0)^2} \int_0^\infty dk\; k^2\; P_m(k)\; \frac{\sin(kr)}{kr} \quad . \end{aligned} \tag{2.4}$$

In particular, most galactic observations are taken at relatively low redshifts, where $t \approx t' \approx t_0$, in which case the pre-factor ratio of $F(t)$'s reduces to unity. Furthermore, in the absence of expecting any extra critical scales in the physics, one often starts with *scale-invariant models* in cosmology, which assume the power spectrum follows a simple power law, characterized by a scaling index and an amplitude. For example, the real-space correlation function is usually parameterized by the index γ and amplitude r_0 [1],

$$G_\rho(r) = \left(\frac{r_0}{r}\right)^\gamma \quad , \tag{2.5}$$

and its momentum space version by the index s and a_0,

$$P(k) = \frac{a_0}{k^s} \quad . \tag{2.6}$$

While the amplitudes r_0, a_0 may be somewhat sensitive to normalization and regularization procedures, these so-called *spectral indices* γ, s are often methodology- or *scheme*-independent, often referred to as "universal" quantities, and thus play a critical role in capturing physics of the two-point correlations of their corresponding fluctuations.

It should also be noted that, with this parametrization, the Fourier transform (2.4) can be

evaluated formally and exactly in d dimensions

$$\int d^d x \; e^{-ik\cdot x} \frac{1}{x^{2n}} = \frac{\pi^{d/2} 2^{d-2n} \Gamma(\frac{d-2n}{2})}{\Gamma(n)} \frac{1}{k^{d-2n}} \quad , \tag{2.7}$$

which relates the spectral indices with

$$s \;=\; (d-1) - \gamma \;=\; 3 - \gamma \quad , \tag{2.8}$$

where the last equality is evaluated for $d = 4$.

Over the past few decades, these scale-invariant models have been compared against increasingly accurate astrophysical data measurements. Early data [1] supported this model with approximate values $\gamma = 1.77 \pm 0.04$ and $r_0 = 5.4 \pm 1 \; h^{-1}$Mpc for distances in the range $0.01 \; h^{-1}\text{Mpc} \lesssim r \lesssim 10 \; h^{-1}\text{Mpc}$, which then gives for the exponent $s \simeq 1.23$. More recent data [2, 19] again supports this model, with approximate values $\gamma = 1.8 \pm 0.3$ for distances in the range $0.1 h^{-1}\text{Mpc} \lesssim r \lesssim 50 \; h^{-1}\text{Mpc}$, which leads to $s \simeq 1.2$. Another set of recent estimates gives $\gamma = (1.79, 1.84)$ for distances up to 100Mpc, see for example [3, 4, 20–24] and references therein. Here we will focus on the most recent high statistics data from the Sloan Digital Sky Survey (SDSS) collaboration [25], which supports the above model with approximate values $s = 1.089$ (and thus $\gamma \simeq 1.91$) for distances in the range $0.01 \; h \; \text{Mpc}^{-1} \lesssim k \lesssim 0.3 \; h \; \text{Mpc}^{-1}$. This latest SDSS data is shown on Figure 3.2 in the next chapter.[3]

As a result, an important challenge in cosmology is to provide a theoretical explanation for these particular values of s and γ. At this point, it should be reminded that matter fields can be related to gravitational fields unambiguously via the Einstein field equations, and so can their respective correlation functions. In particular, as we will recount in the next

[3]For a comprehensive list of commonly accepted cosmological parameters and their uncertainties, we refer the reader to the recent authoritative reference [26].

section, the correlation functions for gravitational curvature fluctuations can also in principle be calculable from a quantum field theoretical treatment of gravity. Hence, while there are many technical subtleties in the calculation – which we will address in the following sections, in principle and conceptually, quantum gravity provides a natural framework for calculating and explaining these observed values for γ and s. This is the general picture we will discuss in detail in the following section and the remainder of this dissertation.

2.2 Nonperturbative Approach to Quantum Gravity

Many more details on the nonperturbative approach to Quantum Gravity used in this paper can be found in a number of earlier works [13,14], and many references therein. The current section will therefore only serve to summarize the key points and main results which will become relevant for the subsequent discussion.

Quantum gravity, in essence the covariantly quantized theory of a massless spin-two particles, is in principle a unique theory, as shown by Feynman some time ago [27,28], much like Yang-Mills theory and QED are for massless spin-one particles. In the covariant Feynman path integral approach, only two key ingredients are needed to formulate the quantum theory - the gravitational action $S[g_{\mu\nu}]$ and the functional measure over metrics $d[g_{\mu\nu}]$, leading to the generating function

$$Z = \int d[g_{\mu\nu}]\, e^{\frac{i}{\hbar}S[g_{\mu\nu}]} \quad , \tag{2.9}$$

where all physical observables could in principle be derived from. For gravity the action is given by the Einstein-Hilbert term augmented by a cosmological constant

$$S[g_{\mu\nu}] = \frac{1}{16\pi G}\int d^4x\sqrt{g}\,(R - 2\lambda) \quad , \tag{2.10}$$

where R is the Ricci scalar, g being the determinant of the metric $g_{\mu\nu}(x)$, G the Newton's constant, and λ the scaled cosmological constant (where a lower case is used here, as opposed to the more popular upper case in cosmology, so as not to confuse it with the ultraviolet-cutoff in quantum field theories that is commonly associated with Λ). The other key ingredient is the functional measure for the metric field, which in the case of gravity describes an integration over all four metrics, with weighting determined by the celebrated DeWitt form [29].

There are two important subtleties worth noting here. Firstly, in principle, additional higher derivative terms that are consistent with general covariance could be allowed in the action, but nevertheless will only affect the physics at very short distances and will not be necessary here for studying large-distance cosmological effects. Secondly, as in most cases that the Feynman path integral can be written down, from non-relativistic quantum mechanics to field theories, the formal definition of integrals requires the introduction of a lattice, in order to properly account for the known fact that quantum paths are nowhere differentiable. It is therefore a remarkable aspect that, at least in principle, the theory (in a nonperturbative context) does not seem to require any additional extraneous ingredients to properly define a quantum theory of gravity besides the standard ones mentioned above.

At the same time, gravity does present some rather difficult and fundamentally inherent challenges, including: the well-known fact that the theory is perturbatively nonrenormalizable (due to a badly divergent series in Newton's constant G), the intensive computational power needed in order for any concrete results to be numerically calculated (due to it being a highly nonlinear theory), the conformal instability which makes the Euclidean path integral potentially divergent, and further genuinely gravitational-specific technical complications (such as the fact that physical distances between spacetime points – which depend on the metric, which is a quantum entity – fluctuate).

Although these hurdles will ultimately need to be addressed in a complete and satisfactory

way, a comprehensive account is of course far beyond the scope of this dissertation. However, regarding the perturbatively nonrenormalizable nature, some of the most interesting phenomena in physics often stem from non-analytic behavior in the coupling constant and the existence of nontrivial quantum condensates, which are hidden from and impossible to probe within perturbation theory alone. It is therefore possible that certain challenges encountered in the case of gravity are likely the result of inadequate perturbative treatments, and not necessarily a reflection of some fundamentally insurmountable problem with the theory itself. Here, we shall take this as a motivation to utilize the plethora of well-established nonperturbative methods to deal with other quantum field theories where perturbation theory fails, and attempt to derive sensible physical predictions that can hopefully be tested against observations. More detailed accounts on the other various issues associated with the theory of quantum gravity can be found, for example, in [13, 14] and references therein.

So, to derive physical consequences from a perturbative nonrenormalizable and highly nonlinear theory, we can draw inspiration with methods used for theories of similar nature. As in the case of nonlinear theories such as QCD, Yang-Mills theories, and the $O(N)$ nonlinear sigma model, one can nevertheless extract universal quantities, such as critical exponents (such as the exponents ν, γ, δ, etc., in the nonlinear sigma model), and genuinely nonperturbative characteristic scales (such as correlation lengths or $\Lambda_{\overline{MS}}$ for QCD). Such predictions, despite obtained from a nonpertubative treatment, are today amongst some of the best tested results of quantum field theory. These results includes the measurement of the critical exponents for the nonlinear sigma model being the second-most accurate prediction in physics, after the prediction of the famous $g-2$ anomalous magnetic moment in QED [30,31]. Analogously, utilizing a number of nonperturbative approaches (such as $2+\epsilon$ expansion and numerical evaluations of the path integral) for gravity, one can extract universal scaling dimensions such as the exponent ν and the nonperturbative, renormalization group invariant, correlation length scale ξ. The latter is in turn related to the vacuum expectation value of curvature, which is measured via a large-scale cosmological constant λ_{obs}. Both the exponent

ν and the scale ξ have significant effects on correlation functions, which deviate from any semi-classical or free field (Gaussian) predictions. More importantly, these are potentially verifiable via observations, as we will show below.

For our present discussion, we will mention several main results and ingredients from this perspective. The nonperturbative treatments of quantum gravity via both Wilson's $2+\epsilon$ double expansion (both in G and the spacetime dimension) and the Regge–Wheeler lattice path integral formulation [32] reveal the existence of a new quantum phase, involving a nontrivial gravitational vacuum condensate [13]. Along with this comes a nonperturbative characteristic correlation length scale, ξ, and a new set of nontrivial scaling exponents ν, as is common for well-studied perturbatively nonrenormalizable theories [33–38]. Together, these two parameters characterize the quantum corrections to physical observables such as the long-distance behavior of invariant correlation functions, as well as the renormalization group (RG) running of Newton's constant G, which in coordinate space leads to a covariant $G(\Box)$ with $\Box = g^{\mu\nu}\nabla_\mu\nabla_\nu$ [14]. In particular, it can be shown [13, 39] that for $r < \xi$, the connected correlation function of the scalar curvature over large geodesic separation $r \equiv |x-y|$ scales as

$$G_R(r) = \langle\, \sqrt{g}R(x)\sqrt{g}R(y)\; \delta(|x-y|-r)\,\rangle_c \;\underset{r\ll\xi}{\sim}\; \left(\frac{1}{r}\right)^{2n}\,, \tag{2.11}$$

with the power $2n = 2(d-\frac{1}{\nu})$, and d is the dimension of spacetime. The subscript c stands for connected correlation functions. Furthermore, the RG running of Newton's constant can be expressed as

$$G(k) \;=\; G_0\left[1 + 2\,c_0\left(\frac{m^2}{k^2}\right)^{\frac{1}{2\nu}} + \mathcal{O}\left(\left(\frac{m^2}{k^2}\right)^{\frac{1}{\nu}}\right)\right], \tag{2.12}$$

where $m \equiv 1/\xi$ is a characteristic nonperturbative mass scale, and $2\,c_0 \approx 16.04$ a nonperturbative amplitude, which (unlike the universal exponent ν) cannot be obtained in perturbation

theory, and thus requires a genuinely nonperturbative approach, such as the Regge–Wheeler lattice formulation of gravity [40–47].

Here we note the important roles played by the quantum parameters ν and ξ. The appearance of a gravitational condensate is viewed as analogous to the (equally nonperturbative) gluon and chiral condensates known to describe the physical vacuum of QCD, so that the genuinely nonperturbative scale ξ (or equivalently $m = 1/\xi$) is in many ways analogous to the scaling violation parameter $\Lambda_{\bar{M}S}$ of QCD. (Note that gravitons nevertheless stay massless in the same way as gluons do in QCD, and there is no explicit violation of gauge or coordinate invariance.) Similarly, the overall magnitude of such a scale cannot be established from first principles, but should instead be linked with other length scales in the theory, such as the observed cosmological constant scale $\sqrt{1/\lambda}$, or equivalently the (scalar) curvature vacuum expectation value

$$\frac{\langle \int d^4x \sqrt{g}\, R \,\rangle}{\langle \int d^4x \sqrt{g} \,\rangle} \equiv \langle\, R \rangle. \tag{2.13}$$

The latter is related to the observed cosmological constant via the Einstein field equations

$$\langle\, R \rangle \,=\, 4\lambda \,. \tag{2.14}$$

It follows that the observed cosmological constant λ can be used to infer the magnitude of the gravitational vacuum condensate scale ξ. More specifically, the combination most natural to be identified with ξ is

$$\frac{\lambda}{3} = \frac{1}{\xi^2} \,, \tag{2.15}$$

such that $\xi \sim \sqrt{3/\lambda} \simeq 5300\,\text{Mpc}$ for the observed value of λ [13, 48, 49]. On the other hand, the other key quantity—the universal scaling dimension ν, can be extracted via a number of methods, many of which are summarized in [45–47, 50–70]. Multiple avenues (including a

simple geometric argument that suggests $\nu = 1/(d-1)$ for spacetime dimension of $d \geq 4$ [14]) point to a value of $\nu^{-1} \simeq 3.0$, which will serve as a sufficiently good working value for this parameter in the following.

It should be noted that the nonperturbative scale ξ should also act as an infrared (IR) regulator, such that, like in other quantum field theories, expressions in the "infrared" (i.e., as $r \to \infty$, or equivalently $k \to 0$) should be augmented by

$$\frac{1}{k^2} \to \frac{1}{k^2 + m^2} \tag{2.16}$$

where the quantity $m = 1/\xi \simeq 2.8 \times 10^{-4}\, h\,\mathrm{Mpc}^{-1}$, expressed in the dimensionless Hubble constant $h \simeq 0.67$ for later convenience. Consequently, the augmented expression for the running of Newton's constant G becomes

$$G(k) = G_0 \left[1 + 2\, c_0 \left(\frac{m^2}{k^2 + m^2} \right)^{\frac{1}{2\nu}} + \mathcal{O}\left(\left(\frac{m^2}{k^2 + m^2} \right)^{\frac{1}{\nu}} \right) \right] \quad . \tag{2.17}$$

The aim here is therefore to explore areas where these predictions can be put to a test. The cosmological power spectra, which are closely related to the correlation functions discussed, thus take effects over large distances, provide a great testing ground for these quantum gravity effects.

Chapter 3

The Matter Power Spectrum $P(k)$

In this chapter, we will show how the matter power spectrum $P(k)$ can be fully derived and constrained from gravitational fluctuations, without the need of inflation and scalar fields.

In Section 3.1, we first focus on the galaxy regime ($k > 0.15$), and show how the spectral indices s and γ from Eqs. (2.2) and (2.3) can be derived from gravitational fluctuations. Then, in Section 3.2 and 3.3, we will extrapolate the prediction to early times ($k < 0.15$), and show how the prediction compares favorably with the observational data, as well as compare this picture with that of inflation. In Section 3.4, we include additional, genuinely quantum, gravitational effects which are present at the extreme small k domain, and compare those with data. In Section 3.5 and 3.6, we discuss how the only two parameters in the theory can be constrained using current observed cosmological data. Finally, in Section 3.7, we summarize the analysis on $P(k)$, discuss how this gravitationally-motivated picture differs from that of inflation, and how it can be tested.

3.1 Matter Power Spectrum in the Galactic Regime

We begin by first deriving the matter power spectrum $P(k)$ in the galaxy domain.

Recall in Section 2.2, we showed that over large distances, the invariant scalar curvature correlation fluctuation at fixed geodesic distance behaves in accordance to Eq. (2.11), reproduced here for convenience,

$$G_R(r) = \langle\, \sqrt{g}R(x)\sqrt{g}R(y)\, \delta(|x-y|-r)\, \rangle_c \underset{r \ll \xi}{\sim} \left(\frac{1}{r}\right)^{2n} , \tag{3.1}$$

with the power $2n = 2(d - 1/\nu)$, and d is the dimension of spacetime. This shows that, for distances smaller than the aforementioned characteristic length scale ξ, this two-point correlation function follows a simple scaling law that is purely dependent on the universal exponent ν. The value for the critical exponent ν has been calculated and estimated through various means, including $2+\epsilon$ expansion [50–57], large d expansion [58,59], numerical lattice calculations [45], exact results in 2+1 dimensions [60, 61] and truncated continuum renormalization group methods [62, 64, 65, 67–76]. Many of these results have been summarized recently, for example, in [13], where it is argued that current evidence points to $\nu \simeq 1/3$ in $d = 4$ (see Figure 3.1). In particular, in the large-d limit, one finds $\nu = 1/(d-1)$ [58,59,64,65] in addition to the usual scaling results for the relation for the power in Eq. (3.1), namely $2n = 2(d - 1/\nu)$. This in turn implies for the power $2n = 2$ for $d = 4$ and above. In the following we will proceed on the assumption (supported by extensive numerical calculations on the lattice [45]) that $\nu = 1/3$ exactly in $d = 4$, and that consequently the power in Eq. (3.1) is exactly equal, or at least very close to, two. Another key quantity here is the renormalization group invariant scale ξ appearing for example in Eq. (3.1), and related to the quantum gravitational vacuum condensate. It was argued in [13, 14, 43, 44] that the renormalization group invariant ξ is most naturally identified with the scaled cosmological constant via $\xi \simeq \sqrt{3/\lambda}$. Modern observational values of $\lambda_{\rm obs}$ yield an estimate of $\xi \sim 5300$

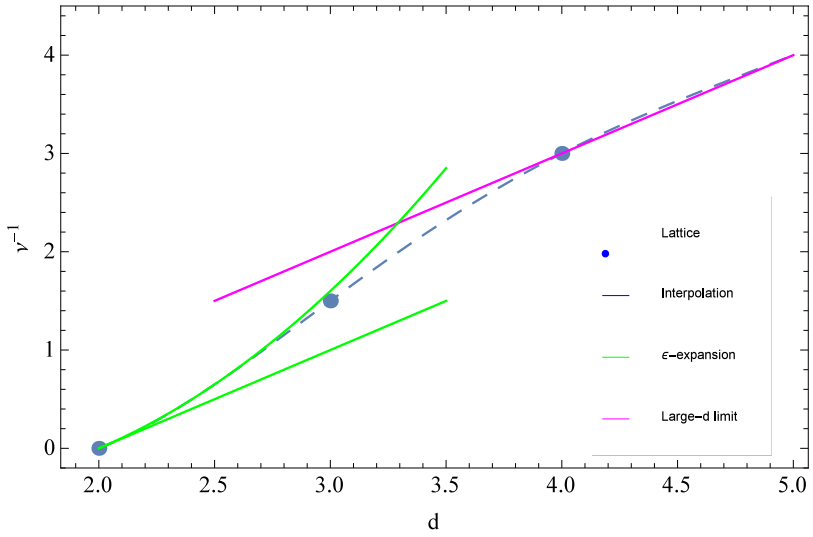

Figure 3.1: Universal scaling exponent ν as a function of spacetime dimension d. Shown are the $2+\epsilon$ expansion result to one and two loops, the value in $2+1$ dimensions obtained from the exact solution of the Wheeler-DeWitt equation, the numerical result in four spacetime dimensions, and the large d result $\nu^{-1} \simeq d-1$.

Mpc. Since galaxies and galaxy clusters involve distance scales of around $r = 1-10$ Mpc $\ll \xi$, the scaling relation in Eq. (3.1) should then be applicable for such matter. Using these values, one finds in Eq. (3.1) $2n = 2(4-3) = 2$, and therefore one expects the gravitational curvature fluctuations to scale as

$$G_R(r) = \langle\, \delta R(0)\, \delta R(r)\, \rangle \sim \frac{1}{r^2} \ , \tag{3.2}$$

where δR denotes the curvature fluctuation above the background (i.e., the connected part of the correlation function).

Next we proceed to relate the curvature fluctuations $G_R(r)$ to the matter fluctuations $G_\rho(r)$ defined in Section 2.1. As alluded in the introduction, this procedure is unambiguous through the Einstein field equations

$$R_{\mu\nu} \ - \ \tfrac{1}{2}\, g_{\mu\nu} R + \lambda g_{\mu\nu} \ = \ 8\pi G\, T_{\mu\nu} \ . \tag{3.3}$$

To a first approximation, by assuming galaxies follow a perfect non-relativistic (pressureless) fluid[1], the trace equation reads

$$R - 4\lambda = -8\pi G\, T \ . \tag{3.4}$$

(For a perfect fluid the trace gives $T = 3p - \rho$, and thus $T \simeq -\rho$ for a non-relativistic fluid.) Since λ is a constant, the variations, and hence correlations, are directly related as in

$$\langle\, \delta R\, \delta R\, \rangle \ = \ (8\pi G)^2\, \langle\, \delta\rho\, \delta\rho\, \rangle \ . \tag{3.5}$$

As described in Section 2.2 previously, quantum gravity predicts that the scalar curvature fluctuations G_R over large distances scale as

$$G_R(r) \equiv \langle\, \delta R(\mathbf{x})\, \delta R(\mathbf{y})\, \rangle \ \sim \ \frac{1}{r^2} \ . \tag{3.6}$$

Using the relation in Eq. (3.5), the galaxy density fluctuations G_ρ then follow a similar scaling relation

$$G_\rho = \Big(\frac{r_0}{r}\Big)^2 \tag{3.7}$$

as $r \to \infty$, or equivalently, for the galaxy power spectrum $P(k)$,

$$P(k) = \frac{a_0}{k} \tag{3.8}$$

as $k \to 0$, using the fact $s = 3 - \gamma$ from Eq. (2.8). Hence, we see that quantum gravity predicts for the critical scaling exponent $\gamma = 2$, or equivalently, $s = 1$.

It should be emphasized here that the scaling relation of Eq. (3.1) with $2(d - 1/\nu) = 2$, and

[1]This is justified since the clumping of matter, and hence galaxy formation, happens in a matter-dominated era of cosmology, where the perfect fluid and negligible pressure limit is applicable.

as a result $\gamma = 2$ or $s = 1$, does *not* follow from simple dimensional arguments, (indeed the relevant correlation function is dimensionless), and is instead a non-trivial result based on anomalous scaling dimensions associated with quantum gravity in four dimensions. Indeed, as discussed for example in [13], in the weak field expansion the scaling result of Eq. (3.1) would be rather different. In fact, the approximate value of $\gamma = 2$ for galaxy matter density correlations has been a long standing puzzle in observational cosmology, see for example the cosmology monograph [1].

Note that the prediction of $\gamma = 2$ or $s = 1$ is expected to be valid in the limit of the so-called "linear scaling regime" – i.e., in scales where galaxies can be treated essentially as pressureless point-particles, and that the long-range gravitational correlations are expected to be the dominant influence. More quantitatively, one observes that typical galaxy clusters have sizes around $3 - 10$ Mpc, and voids (the pockets of empty space between clusters) have typical diameters around 25 Mpc. As a result, one would expect the effects of scaling to be most explicit for separation scales larger than around $r > 50 - 100$ Mpc (or $k < 0.2 - 0.1\, h\text{Mpc}^{-1}$). These are the ranges where any effects of such nonlinear dynamics should become unimportant and, instead, long-range gravitational correlations are expected to dominate. It is over these separation scales that one expects the gravitationally-controlled scaling law to take place. In other words, Eq. (3.8) implies that in the limit of small k's (large scales) beyond $k < 0.2 - 0.1\, h\text{Mpc}^{-1}$, the power spectrum should approach a horizontal constant asymptotically on a $k \cdot P(k)$ vs. k plot, with the constant representing the amplitude a_0. And this is exactly what we see from the observational side, as we will show shortly below in Figure 3.2.

On the other hand, below these separations scales, nonlinear dynamics are expected to take over. Nonlinear effects can modify the scaling in two ways. Firstly, including the effect of pressure to the Freidman equations will induce fluctuations around the general scaling trend, known as baryonic acoustic oscillations (BAOs). Secondly, for separations scales below or

around the size of galaxy clusters, nonlinear multi-body dynamics become important. As a result, the spectrum is expected to diverge from the $s = 1$ scaling law at small distances (large k). This is again seen in Figure 3.2.

Nevertheless, despite the computational complexity, such nonlinear dynamics basically follow Newtonian dynamics and are thus well-understood and well-studied in standard literatures such as [1, 18, 77, 78]. At these scales, neither quantum nor general-relativistic effects are expected to play a huge role. Although it presents more technical complexity to include, no new physics is in play. Thus, we will focus mostly on the limit of large distances (small k).

Figure 3.2 shows the most recent observational results of the galaxy matter power spectrum from the 14th data release (DR14) of the Sloan Digital Sky Survey (SDSS), a galaxy survey which charted over 1.5 million galaxies, covering over one-third of the celestial sphere [25], for separations roughly from $r \simeq 500\,\mathrm{Mpc}$ ($k \simeq 0.02\,h\,\mathrm{Mpc}^{-1}$) to $r \simeq 30\,\mathrm{Mpc}$ ($k \simeq 0.30\,h\,\mathrm{Mpc}^{-1}$). Notice that as k decreases (r increases), the data indeed approach a constant on the $k \times P(k)$ vs. k plot. This agrees with the $s = 1$ scaling law, which claims

$$k \times P(k) = a_0 \ . \tag{3.9}$$

Via a one-parameter fit, one obtains a value of $a_0 \approx 686 \pm 87\,(\mathrm{Mpc/h})^2$ for the amplitude of the galaxy power spectrum. In particular, notice that in the linear scaling regime $k \lesssim 0.15\,h\,\mathrm{Mpc}^{-1}$ ($r \gtrsim 50\mathrm{Mpc}$), all of the 13–15 data points lie within a 3σ ($\sim 15\%$) variance of a_0. On the other hand, as expected, for separation scales smaller than $50\,\mathrm{Mpc}$ ($k \gtrsim 0.17\,h\,\mathrm{Mpc}^{-1}$), the spectrum deviates from the $s = 1$ scaling law, giving rise to a transient behavior into the nonlinear regime. In addition, subtle oscillations from BAOs can also be roughly observed about the average value given by a_0 and throughout the trend.

One can further extend the phenomenological analysis over the linear regime by performing a two-parameter fit, a_0 and s, using again the scale-invariant ansatz $P(k) = a_0/k^s$. This fit

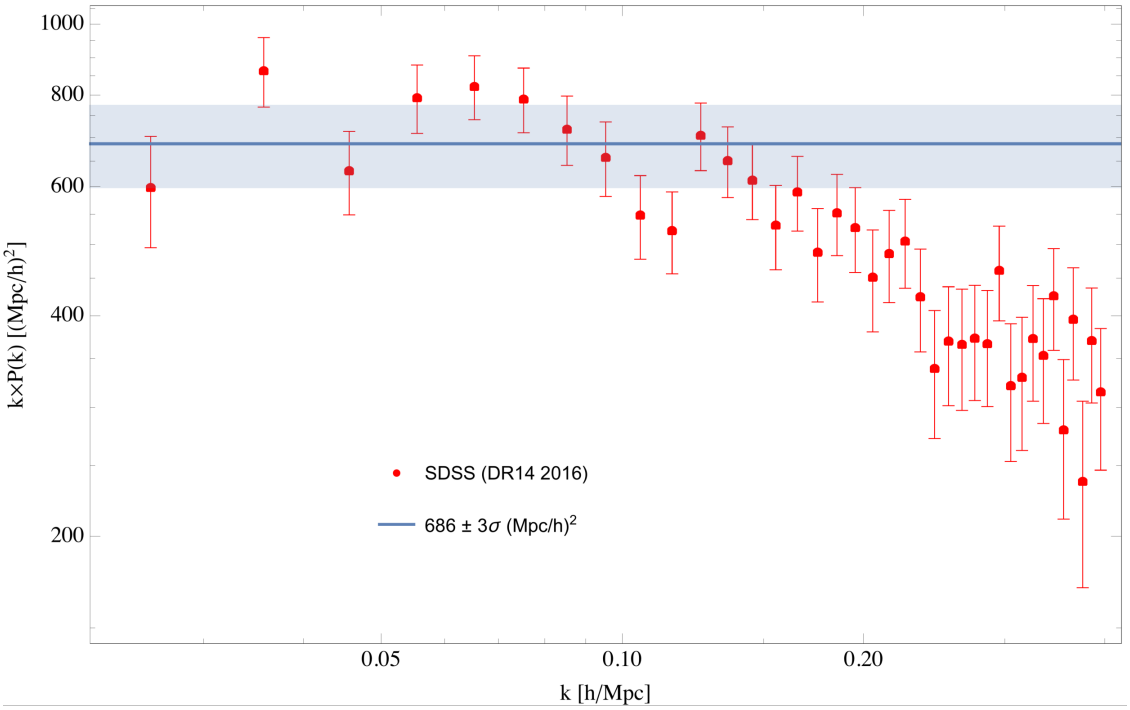

Figure 3.2: The observed galaxy power spectrum in $k \times P(k)$ versus wavenumber k. The data points are taken from the Sloan Digital Sky Survey (SDSS) collaboration's 14th Data Release (DR14) . Quantum gravity predicts that in the linear regime ($k \lesssim 0.15\,h\,\mathrm{Mpc}^{-1}$), as $r \to \infty$ (or $k \to 0$), $P(k)$ should approach a scale-invariant spectrum with $\nu = 1/3$ (i.e., $s = 1$), as in Eq. (3.8). In other words, $k \times P(k)$ should approach a constant. The solid line represents the asymptotic value of the $s = 1$ spectrum, with a one-parameter fit for the amplitude in Eq. (3.8) giving $a_0 \simeq 686\,(\mathrm{Mpc/h})^2$. The gray bands represent a 3σ ($\sim \pm 15$ %) variance to the fit. It can be seen that, below $k < 0.15\,h\,Mpc^{-1}$, the data generally approach a constant of approximately $a_0 \sim 686\ (\mathrm{Mpc/h})^2$, but beyond $k > 0.15\,h\,\mathrm{Mpc}^{-1}$ the data shows a transient region where the points deviate from the linear scaling, due to the relevant correlation function probing distances smaller than the linear scaling regime.

gives $s \simeq 1.09 \pm 0.08$ – i.e., about $9.0(\pm 8.0)\%$ around the predicted value of $s = 1$ and $a_0 = 540 \pm 115\,(\mathrm{Mpc/h})^2$. This is a decent expectation given a first order prediction, neglecting BAOs and other dynamical effects superimposed on the linear scaling. Further analysis by applying the fit over the full range of observational data ($k = (0.02, 0.30)\,h\,\mathrm{Mpc}^{-1}$) gives $s \simeq 1.31 \pm 0.04$, i.e., about 30% of the predicted $s = 1$ value, and an amplitude of $a_0 = 280 \pm 24\,(\mathrm{Mpc/h})^2$. The larger discrepancy in s is also expected, given that the nonlinear regime is now included in the fit. Nevertheless, it is still overall consistent with an $s \sim 1$ trend, satisfying the general trend created and set by the gravitational correlations. To even more accurately extrapolate the results to the nonlinear regime ($k > 0.15\,h\,\mathrm{Mpc}^{-1}$), the full nonlinear dynamics has to be addressed and solved. In fact, we will see that the nonlinear solutions can be extrapolated to even larger scales ($k < 0.02\,h\,\mathrm{Mpc}^{-1}$) into a radiation dominated era of the Universe. This will be the topic of the next section.

It should be noted here that the amplitude a_0, just like the scaling dimension ν or s, is in principle calculable from the lattice treatment of quantum gravity, as discussed for example in [13] and references therein. Nevertheless, unlike the universal, scheme-independent, scaling dimension s, a_0 represents a non-universal quantity, and will therefore depend to some extent on the specific way the ultraviolet cutoff is implemented in the quantum theory. This fact is already well known from other lattice gauge theories such as lattice QCD. Therefore it seems more appropriate here to take this non-universal amplitude a_0 as an adjustable parameter, to be fitted and constrained by astrophysical observational data. Nevertheless, quantum gravity provides a direct prediction for the general $s = 1$ scaling of galaxy correlations.

Notice that since galaxy scales from the SDSS survey are of the order $50 - 500\,\mathrm{Mpc}$, which is at least one to two orders of magnitude below $\xi \simeq 5300\,\mathrm{Mpc}$, the RG running of Newton's G as governed by Eq. (2.12) is highly suppressed, and Newton's constant can be treated as a constant. Later on we will explore these additional effects as we turn to fluctuations on even larger scales in the next section.

3.2 Matter Power Spectrum Beyond Galactic Regime

So far, our analysis asserted that the scaling of galaxy distributions, which is governed by that of matter fluctuation correlations $G_\rho(r)$, is directly calculable from curvature fluctuation correlation functions $G_R(r)$ in the quantum theory of gravity. In particular, the matter and curvature fluctuations are unambiguously connected via the Einstein field equations. Usually there is an implicit assumption that the $T_{\mu\nu}$ on the right hand side takes the perfect fluid form, which involve an equation of state of pressure-less matter. The latter assumption is certainly valid for the matter-dominated universe[2], an era in which we expect galaxy-formations to take place. As can be seen in Figure 3.2, the observational data is in rather good agreement with the $s = 1$ prediction of quantum gravity for the scale of galaxy clusters (i.e., $k \lesssim 0.15$ hMpc^{-1}).

In principle, quantum gravity with its long-range correlations and n-point functions should also govern and make predictions beyond galactic observation scales. Below galactic scales (large k), complex and nonlinear interactions between matter arises, and gravitational correlations are expected to become subdominant effects and not easily discernible. On the other hand, beyond the scale associated with galaxy clusters and superclusters (small k), gravity is again undoubtedly the dominant long-range force. There we expect fluctuations in curvature to again play a dominant role in governing long-range correlations. However, observationally, larger spatial scale corresponds to looking at increasingly earlier epochs of the universe, perhaps even before galaxies are formed. Therefore data from galaxy surveys cannot serve as a test to the predictions in these regimes. Fortunately, modern astronomy has provided very detailed measurements of the cosmic microwave background (CMB), which encodes fluctuations over a wide range of cosmological scales. This can then be used as an additional test for the quantum gravity predictions.

[2]see comment of footnote 1 from Section 3

In this section, we will discuss how we can utilize the so-called transfer function to extrapolate the quantum gravity prediction to increasingly small k far beyond galaxy scales, and compare to how it fits observed CMB data. It should be noted that in the current CMB literature one often refers to the angular power spectrum C_l as the primary quantities obtained. Nevertheless, $P(k)$ is directly related to C_l, as described in many standard literature works on the subject [1, 8, 18, 77]. However here instead we focus on $P(k)$, since, as mentioned above, it is this quantity whose scaling is most directly related to that of curvature fluctuations, the quantity that is predicted from quantum gravity. According to the Friedman equations, wavelengths that enter the horizon before matter-radiation equality evolve differently than those that enter after. As a result, as we look at even larger scales (smaller k's), the $s = 1$ slope discussed previously is expected to change. Nevertheless, we can use a well-known function in cosmology, the so-called transfer function $\mathcal{T}(\kappa)$, to relate small wavelength behaviors to large wavelength behaviors. Details of the transfer function can be found in standard texts such as [18]; for explicit numerical results see also [79]. Here we outline below how the transfer function can be applied to our predictions.

We recall the definition of the spectral function

$$P(k) = (2\pi)^3 F(t_0)^2 \langle\, |\Delta(k)|^2 \,\rangle \ . \tag{3.10}$$

Here $F(t)$ can be calculated from the Friedmann equations, giving

$$F(t) = \frac{3}{5}\left[\frac{a(t)}{a_L}\right] C(x) \ , \tag{3.11}$$

where $x = x(t) = (\Omega_\Lambda/\Omega_M)\, a(t)^3$, and the correction factor $C(x)$ is given by

$$C(x) \equiv \frac{5}{6}\, x(t)^{-\frac{5}{6}} \sqrt{1+x(t)} \int_0^{x(t)} du\, \frac{1}{u^{\frac{1}{6}}(1+u)^{\frac{3}{2}}} \ . \tag{3.12}$$

Detailed steps in the above derivations can be found in [18]. As for the function $\Delta(k)$ in

Eq. (3.10), it can be calculated from the Boltzmann transport equations, again presented in detail in [18] and references therein, giving

$$\Delta(q) \approx \delta(q, t_L) - t_L\, \psi(q, t_L) = \frac{2}{3} \cdot \frac{q^2\, \mathcal{R}_q^0\, \mathcal{T}(\kappa)}{H_L^2 a_L^2} \quad , \tag{3.13}$$

where the comoving wavenumber q is often used in place of the physical wavenumber k, the two being related by $k \equiv q/a(t)$. Here $\delta(q,t)$ is the matter density contrast defined in Eq. (2.1) in momentum space, $\psi(q,t)$ is the gravitational perturbation in Newtonian gauge, t_L is the time of decoupling of radiation from matter, associated with the recombination of hydrogen, and H_L and a_L are the Hubble rate and scale factor correspondingly evaluated at t_L. The last equality is obtained by conveniently parameterizing the combination of δ and ψ with $\mathcal{R}_q$ and $\mathcal{T}(\kappa)$, known as the comoving curvature perturbation and transfer function, respectively [18]. The transfer function $\mathcal{T}(k)$ is usually expressed with an argument $\kappa \equiv \sqrt{2}\,(k/k_{EQ})$, where k_{EQ} is the scale at matter-radiation equality. Inserting these results into the definition for $P(k)$ in Eq. (3.10) then gives

$$P(k) = \frac{4(2\pi)^2 a_0^3\, C^2(\frac{\Omega_\Lambda}{\Omega_M})}{25\, \Omega_M^2 H_0^4}\, \mathcal{R}_q^{0^2} k^4 \, \left[\mathcal{T}\left(\sqrt{2}\frac{k}{k_{EQ}}\right)\right]^2 \quad . \tag{3.14}$$

Again, following common convention [18], the function $\mathcal{R}_q$ is often parametrized as a simple power of q

$$\mathcal{R}_q \simeq N q^{-3/2} \left(\frac{q}{q_*}\right)^{(n_s-1)/2} , \tag{3.15}$$

where q_* is some arbitrarily chosen reference scale, and n_s is referred to as the spectral index. Then $P(k)$ can be conveniently factorized into

$$P(k) = C_0\, A\, k^{n_s} \left[\mathcal{T}(\kappa)\right]^2 , \tag{3.16}$$

with

$$A \equiv \frac{N^2}{k_*^{n_s-1}} \text{ , and } C_0 \equiv \frac{4\,(2\pi)^2 \left[C\left(\frac{\Omega_\Lambda}{\Omega_M}\right)\right]^2}{25\,\Omega_M^2 H_0^4} \ , \tag{3.17}$$

so that C_0 is a prefactor that encodes exclusively cosmological model parameters. It was Harrison and Zel'dovich who originally suggested in the seventies that n_s should be close to one [80–82].

It is known that the transfer function $\mathcal{T}(\kappa)$ is entirely determined from classical cosmological evolution and by the solutions of the associated coupled Boltzmann transport equations for matter and radiation. It will turn out to be useful here that the function in question can be accurately described by the semi-analytical formula given explicitly by D. Dicas as quoted in [18, 79],

$$\mathcal{T}(\kappa) \simeq \frac{\ln[1+(0.124\kappa)^2]}{(0.124\kappa)^2} \left[\frac{1+(1.257\kappa)^2+(0.4452\kappa)^4+(0.2197\kappa)^6}{1+(1.606\kappa)^2+(0.8568\kappa)^4+(0.3927\kappa)^6}\right]^{1/2} \ , \tag{3.18}$$

which will be used here in the following discussion. For later reference, the shape of the function $\kappa|\mathcal{T}(\kappa)|^2$ is shown below in Figure 3.3; particularly noteworthy here is the inverted-v shape reflecting the cosmological evolution transition from a radiation dominated to a matter dominated universe, again as discussed in great detail in [18].

Now, both C_0 and $\mathcal{T}(\kappa)$ are fully determined, the former by cosmological measured parameters from, for example, the latest Plank satellite data [83, 84], and the latter theoretically from the Boltzmann transport equations, numerically evaluated in [18, 79] and further references cited therein. Therefore the end result is that $P(k)$ is essentially parameterized by two quantities, an overall amplitude A and the spectral index n_s. The next step is to use quantum gravity to theoretically constrain the value of n_s, and analyze how well a power spectrum with the predicted value of n_s fits the current observational data. As discussed previously in Section 3.1, quantum gravity predicts $P(k) \sim a_0/k^s$ with an exponent $s = 1$

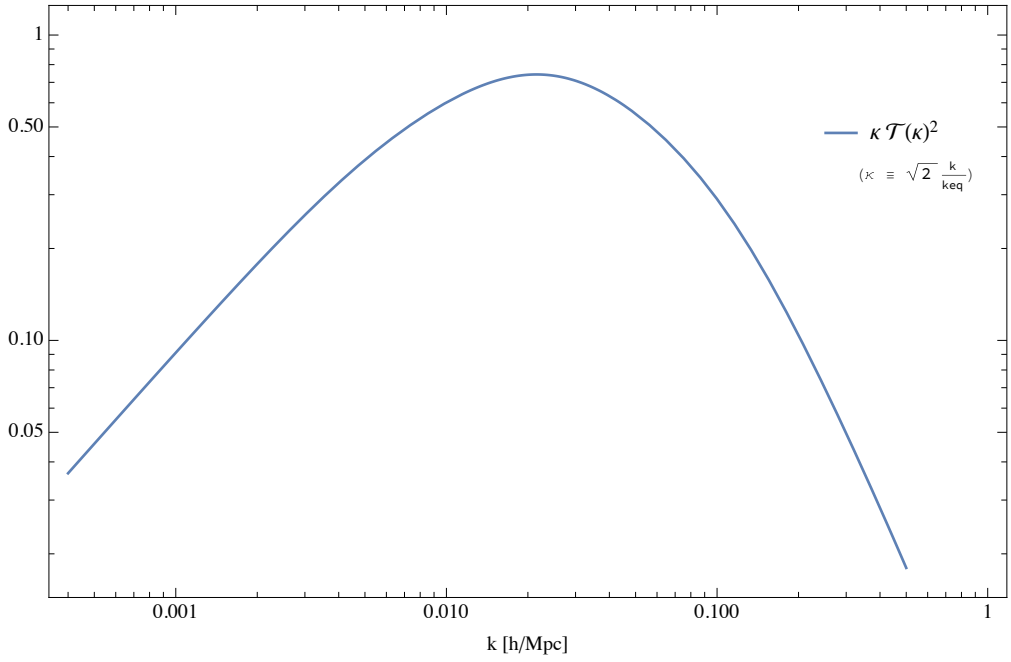

Figure 3.3: Shape of the transfer function $\kappa\,|\mathcal{T}(\kappa)|^2$ using the interpolating formula of Eq. (3.18). What is of interest here is the significant turnover happening at wavenumbers $k \sim 0.02$ which is known to correspond to a cosmological time scale associated with matter-radiation equilibrium. This marked turnover here is the primary reason for the peculiar inverted-v shape of the power spectrum in the following plots.

in the galaxy regime (i.e., $k \sim 0.01$ to $0.3\ h\mathrm{Mpc}^{-1}$). We also noted that although a_0 is in principle calculable, additional subtleties arise. Hence, for the current purpose, we simply use the value that fits best the galaxy data at the largest scales, namely $a_0 \simeq 689$. As a result, within the galaxy regime, we should have a matching

$$P(k) \equiv C_0\ A\ k^{n_s}\ \mathcal{T}(\kappa)\ \approx \frac{689}{k} \quad (\text{ for } k \sim 0.01 \text{ to } 0.3\ h\mathrm{Mpc}^{-1})\ . \tag{3.19}$$

As mentioned earlier under Eq. (3.18), both C_0 and $\mathcal{T}(\kappa)$ are fully determined from the classical cosmological FRW evolution equations, leaving this essentially an equality with two unknowns, namely A and n_s, that holds in the galaxy regime. Therefore, by appropriately selecting two points from the quantum gravity prediction within this regime, we can derive the values for A and n_s. Since the left hand side is supposedly valid for all scales, with the two values A and n_s determined, these will then give us a power spectrum that allows us to extrapolate the quantum gravity prediction within the galaxy regime to much larger scales.

Within the galaxy regime, there is a certain flexibility in which two points one may choose. For the purpose of a first estimate, we select two points relatively apart, but not too close to the margins of the available galaxy data. Although the data set ranges from $0.025 \lesssim k \lesssim 0.3\ h\ \mathrm{Mpc}^{-1}$, the linear scaling regime is only valid up to around $k \lesssim 0.15\ h\ \mathrm{Mpc}^{-1}$, as discussed in Section 1.2. On the other hand, extreme small k's (large distances) are expected to be less representative, as they suffer from limited statistical samples within the ensemble. Thus, an appropriate preliminary choice, for first-estimation purpose, would be:

$$\begin{aligned} k_1 &= 0.035\ h\ \mathrm{Mpc}^{-1} \\ k_2 &= 0.10\ h\ \mathrm{Mpc}^{-1}\ . \end{aligned} \tag{3.20}$$

These correspond to real space scales of

$$\begin{aligned} &\lambda_1 \sim 250 \text{ Mpc} \\ &\lambda_2 \sim 90 \text{ Mpc} \ . \end{aligned} \tag{3.21}$$

Using these test points in Eq. (3.19) gives

$$n_s = 1.108 \ , \ \ A = 5.97 \times 10^{11} \ . \tag{3.22}$$

The best fit from the Plank 2015 data gives a fit of $n_s = 0.9667 \pm 0.0040$ [83, 84]. This suggests our preliminary analysis, using the two above selected points, yields a value of n_s that is around $\sim 15\%$ of the best fit value of the data.

There are two flexible aspects in this analysis. Firstly, there is a flexibility in choosing k_1 and k_2, and secondly there are intrinsic statistical errors in the observational data. As an example, by purely adjusting the former, it is possible to get a value of $n_s \approx 0.9827$ if we use $k_1 \sim 0.040 \ h \text{ Mpc}^{-1}$ and $k_2 \sim 0.065 \ h \text{ Mpc}^{-1}$, which correspond to $\lambda_1 \sim 230$ Mpc and $\lambda_2 \sim 140$ Mpc, respectively. Though this normalization choice seems to yield a value for n_s closer to that of Plank, the two points do not seem sufficiently apart to normalize the spectrum properly in our quantum gravity picture. Nevertheless, this methodology also provides a rough estimate for the overall uncertainty in n_s.

3.3 Comparison with Inflationary Models

A popular attempt to explain the matter power spectrum is through inflation models, which proposes that the structures visible in the Universe today are formed through fluctuations in a hypothetical primordial scalar inflaton field. Although the precise behavior and dynamics

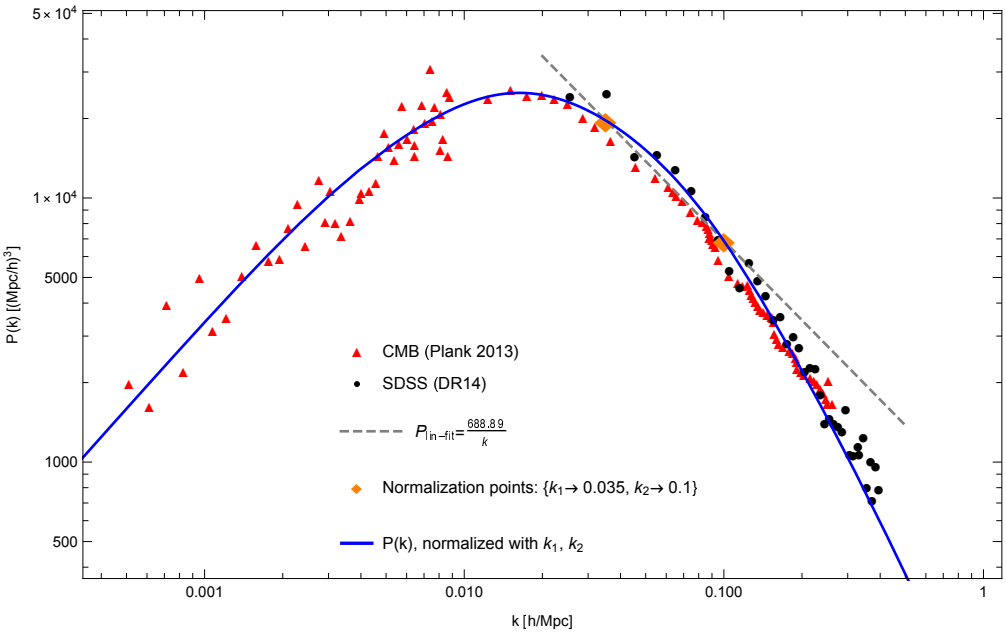

Figure 3.4: Full Power Spectral Function $P(k)$ (blue solid) normalized by $P_{lin} = a_0/k^s$ with $s = 1$, $a_0 = 688.89$ (gray dashed), and two reasonable normalization points (orange). This choice of normalization yields a value of $n_s = 1.10777$ and $A = 5.97 \times 10^{11}$, which fits well with both CMB and SDSS data.

of the inflaton field are still largely controversial [9–12,85,86], there are some general features common among these models that allow one to derive predictions about the shape of the power spectrum. Here we very briefly outline the inflation perspective, and how it radically differs from the quantum gravity perspective we have presented here. For more details and reviews on the inflation mechanism, we refer to recent literatures such as the books [8,18,77].

Cosmic inflation was first advocated in [5–7] as a possible solution to the horizon and flatness problem in standard big bang cosmology, by proposing a period of exponential expansion in the early phases of the universe. This exponential expansion is expected to be driven by a hypothetical"inflaton field", usually scalar in nature, which dominates the energy density in the early universe, causing a de Sitter type accelerated expansion. In these models, the gravitational perturbations that ultimately cause gravitational collapse and structure formations are also due to fluctuations in this inflaton field. Scalar field fluctuations are assumed to be Gaussian for large enough distances (small k), which then naturally results

in a value for the spectral index $n_s = 1$. More realistic models with non-zero tensor to scalar ratio predicts n_s between 0.92 and 0.98 [10,78,87,88], without assuming excessive fine-tuning of parameters [10][3]. The above value of $n_s = 1$ is then used in Eqs. (3.16) and (3.18), leaving only one free parameter, the amplitude A in Eq. (3.16), which can then be determined by normalizing to the CMB data at very large scales (i.e., small k).

Notice that the gravitational perspective we pose in this thesis differs fundamentally from that of inflation, both in procedure and, most importantly, in origin. Firstly, inflation models suggest that gravitational perturbations are due to fluctuations in an inflaton field, whereas here perturbations are intrinsically gravitational and quantum mechanical in origin. Secondly, inflation models use the corresponding inflaton correlation function, $G_\phi(r)$, or power spectrum, $P_\phi(k)$, which are mostly scalar/Gaussian in nature, to derive those of matter $G_\rho(r), P(k)$. Such a perspective is distinctly different from ours. In our gravitational picture, the correlation function that constrains $G_\rho(r)$ and $P(k)$ is the curvature $G_R(r)$, which is highly non-Gaussian. Finally, while both perspectives provide a prediction for n_s which governs the shape of $P(k)$, both leave the overall normalization A in Eq. (3.16) uncertain.

Modern renormalization group theory would imply that the critical exponent ν, and the scaling dimensions n that follow from it [see Eq. (3.1)], are expected to be *universal*, and as such only dependent on the spacetime dimension, the overall symmetry group, and the spin of the particle. The same cannot be said of the critical amplitudes, such as the amplitude associated with the curvature two-point function of Eq. (3.1). In principle it is possible to estimate from first principles the amplitude A and thus the normalization constant N is Eq. (3.15), since these can be regarded as wave function normalization constants in the underlying lattice theory. A rough estimate was given in [13]; nevertheless a number of reasonable assumptions had to be made there in order to relate correlations of small gravitational Wilson loops to

[3]The measured value of n_s is often used to back infer the inflation tensor to scalar ratio, r, which gives around $r \lesssim 0.11$ for $n_s = 0.968 \pm 0.006$ [83, 84].

very large (macroscopic) ones. As a result, the estimate for the amplitude quoted there is still two orders of magnitude smaller than the observed one. Nevertheless it is understood that amplitudes are expected to be regularization and scheme dependent, and will differ by some amount depending on the specific form of the ultraviolet cutoff scheme chosen, whether it is a lattice one, or a continuum inspired momentum cutoff, or dimensional regularization. This phenomenon is well known in scalar field theory as well as lattice gauge theories, and allows the relative correction factors to be computed to leading order in perturbation theory [89], thus reducing the regularization scheme dependent uncertainties. In the following we choose to leave, for now, the overall amplitude in Eqs. (3.7) or (3.8) as a free parameter, and constrain it instead directly by the use of observational data.

Inflation models on the other hand often normalize the curve at large scales with CMB data or at the turnover point $P_{\max}$ [18], but our picture normalizes it with the slope within the galaxy domain, where we argue that the curvature-matter relation is most direct, as discussed in Section 1.2.

We contend that there are a number of reasons that the gravitation-induced picture is more natural for matter distributions than the inflaton-induced one. Firstly, the gravitational field is a well-established interaction and is supposed to have long-range influences with cosmological consequences, whereas the scalar inflaton field remains an observationally unconfirmed quantum field whose precise properties, such as its potential and interaction with standard model fields, remain unknown. Secondly, the Feynman path integral treatment is an unambiguous procedure to quantize a theory covariantly, producing in principle a unique theory with essentially no free parameters (as in the case of QED and QCD).

On the other hand, there is little consensus on the precise dynamics of the inflation field, the number of competing models is far from unique, and almost all suffer from fine-tuning problems, leading to ad-hoc potentials. Many physicists also question the falsifiability of such theories. Well-known cosmologists, including some of the creators of the theory, have

expressed various issues with this paradigm [9]. Therefore, whether or not inflation theories are a satisfactory solution to the cosmological problems are still unsettled.

At this stage, despite the differences in perspective, there is yet no clear-cut preference over each other except for the naturalness arguments given above. However, a number of second order effects due to quantum gravitational fluctuations could yield diverging and distinct predictions, including the IR regulation from ξ, the RG running of G, and n-point functions, which should be testable in the near future with increasingly accurate measurements. So in contrast, the predictions from quantum gravitation are (i) unique and (ii) falsifiable. Therefore, we believe this provides a compelling alternative to inflation. We will now discuss these new effects in the next section.

3.4 Matter Power Spectrum in Extreme Small-k Regime

So far we have introduced the alternative picture that matter perturbations are directly resulted from, and hence governed by, underlying quantum fluctuations from gravity, instead of the inflaton. However, when it gets to large separation scales $k \sim m$, additional genuinely quantum effects will become important. In this section we discuss the two additional quantum-mechanical effects as a result of gravitational condensates, which would be explicitly distinct from any scalar field inflationary models, and potentially provide a window to test between these pictures. These effects are (i) the presence of an infrared (IR) regulator, and (ii) the renormalization group (RG) running of Newton's constant G.

In a quantum field treatment of gravity, like most nonlinear quantum field theories such as QCD and the nonlinear sigma model, a nonperturbative "condensate" scale ξ is dynamically generated which regulates the otherwise serious infrared divergences associated with a zero-mass graviton. In addition, Newton's constant G is seen to "run" with scale as a result of

quantum corrections, precisely in analogy to what happens in QED and QCD. In momentum space, the formula for the running of G is found by [13, 40] to be

$$G(k) \;=\; G_0 \left[1 \,+\, 2c_0 \left(\frac{m^2}{k^2} \right)^{3/2} \,+\, \mathcal{O}\left(\frac{m^2}{k^2} \right)^3 \right] \;. \tag{3.23}$$

Here G_0 is the classical (i.e., $k \gg m$) "laboratory" value of the Newton's constant, or simply G henceforth in the paper, m is the renormalization scale in momentum space related to ξ by $m = 1/\xi$, and c_0 the coefficient for the overall amplitude of the quantum correction, which is generally expected to be of order one. As for the nonperturbative scale ξ, it is most naturally related to the cosmological constant λ_0 [14, 43, 44] by

$$m^2 \equiv \frac{1}{\xi^2} \simeq \frac{\lambda_{\rm obs}}{3} \;\; . \tag{3.24}$$

It should be emphasized again that these two quantum effects are not unique to gravity, but common in quantum field theories. The latter is most representative in the well-studied theories of QED and QCD, where quantum corrections result in the running of coupling constants e and α_s, respectively. It is well known that a dynamically generated infrared cutoff arises in other nonperturbative theories such as the nonlinear sigma model, QCD and generally non-Abelian gauge theories. The scale ξ therefore plays a role analogous to the scaling violation parameter $\Lambda_{\overline{MS}}$ in QCD. ξ also serves directly as a characteristic scale in the theory that, much like the $\Lambda_{\overline{MS}}$ scale in QCD, distinguishes the small distance from the large distance domain. Both effects are discussed in detail in [13, 14].

The formal implementation of the dynamically generated scale ξ is to be inserted as a lower infrared cutoff in any momentum integrals. This would mean amending

$$\int_{-\infty} dk \;\; \rightarrow \;\; \int_{m} dk \;\; . \tag{3.25}$$

However, a more straightforward implementation is to simply make replacements $k^2 \to k^2 + m^2$ with $m = 1/\xi$, which phenomenologically works well in other nonperturbative theories (such as QCD) and partially includes the effects of infrared renormalons [90]. As a result, for the power spectrum given in Eq. (3.16) one obtains

$$\begin{aligned} P(k) &= C_0 \cdot A \cdot k^{n_s} \left[\mathcal{T}(\sqrt{2}\,\frac{k}{k_{EQ}})\right]^2 \\ \to \quad P(k)_{\rm reg} &= C_0\; A \cdot (k^2+m^2)^{\frac{n_s}{2}} \;\; \left[\mathcal{T}\left(\sqrt{2}\,\frac{(k^2+m^2)^{1/2}}{k_{EQ}}\right)\right]^2 \quad . \end{aligned} \tag{3.26}$$

The effect of this modification can be seen as the orange curve in Figure 3.5 below. It is most visible in the extreme long distance (small k) domain where $k \sim 1/\xi$.

Secondly, the other important expected quantum effect is the renormalization group running of Newton's G. To implement this, it can be done either through a scale dependence in momentum space $G(k)$ or by the use of a set of covariant nonlocal effective field equations containing a $G(\Box)$, where $\Box \equiv g^{\mu\nu}\nabla_\mu\nabla_\nu$ is the covariant d'Alembertian acting on n-th rank tensors. More subtleties can be found in works from [14, 40, 43, 44]. Here, to implement the running of Newton's G, the crucial step is to identify where the Newton's G would appear in the power spectrum. Recall the matter correlations are related to curvature correlations via the Einstein field equations by

$$G_\rho(x) = \frac{1}{(8\pi G)^2}\,(\bar{\rho})^{-2}\,G_R(x)\;, \tag{3.27}$$

or in momentum space, via a Fourier transform

$$P(k) = \frac{1}{(8\pi G)^2}\,(\bar{\rho})^{-2}\,P_R(k)\;, \tag{3.28}$$

where, as usual, $P(k)$ is the spectrum for matter fluctuations, and $P_R(k) \equiv < |\delta R(k)|^2 > \sim 1/k^s$ with index $s = 1$ is the spectrum for curvature fluctuations. Observing that $P(k) \propto$

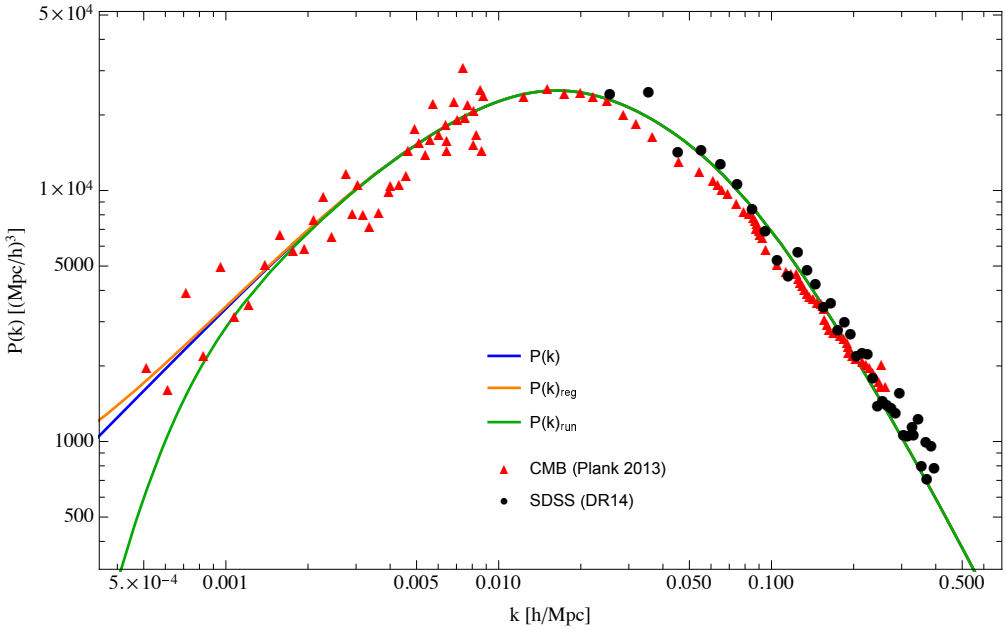

Figure 3.5: Effects of the IR regulator and RG running of G. The red triangles here show the 2015 Planck CMB data . The blue curve represents the full power spectral function $P(k)$ as derived and shown previously in Figure 3.4. The orange curve $P(k)_{\rm reg}$ includes the effect of an IR regulator. The green curve $P(k)_{\rm run}$ includes the effect of an IR regulator together with the RG running of Newton's G.

$1/G^2$ dimensionally, promoting $G \to G(k)$ can be achieved by the replacement

$$P(k) \to \quad P(k)_{\rm run} = \left[\frac{G}{G(k)}\right]^2 P(k) \tag{3.29}$$

with $G(k)$ given in Eq. (3.23). In addition, since the running of G is again an effect that is most significant on small k's, the strong infrared divergence near $k \simeq 0$ should similarly be regulated as discussed above correspondingly by the replacement $k^2 \to k^2 + m^2$ in $G(k)$. As a consequence, the fully IR regulated expression with the running factor is

$$P(k)_{\rm run} = \left[1 + c_0 \left(\frac{m^2}{k^2+m^2}\right)^{\frac{3}{2}}\right]^{-2} \cdot C_0\, A \left(k^2+m^2\right)^{\frac{n_s}{2}} \cdot \left[\mathcal{T}\left(\sqrt{2}\,\frac{(k^2+m^2)^{1/2}}{k_{EQ}}\right)\right]^2 \tag{3.30}$$

This expression is plotted as the green curve in Figure 3.5 and 3.6 against two sets of observational data by the SDSS collaboration.

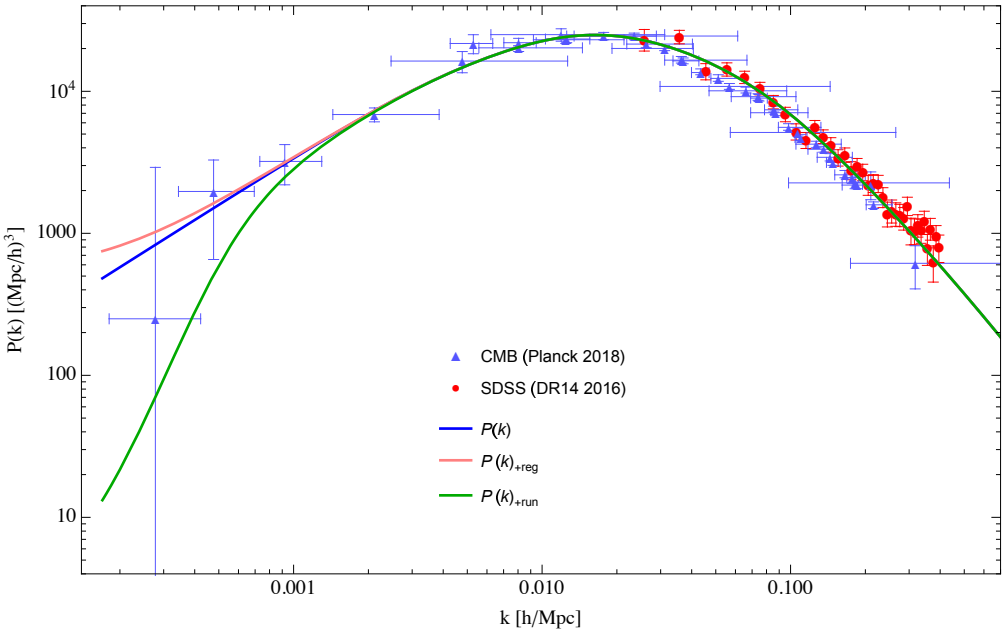

Figure 3.6: Same plot as in Figure 3.5, but now using the latest July 2018 Planck data release (blue triangles), showing again the effect of the IR regulator and of the RG running of G. As before, the blue curve represents the full power spectral function $P(k)$ as derived and shown previously in Figure 3.4, the orange curve $P(k)_{\rm reg}$ includes the effect of an IR regulator, and the green curve $P(k)_{\rm run}$ includes the effect of an IR regulator together with the RG running of Newton's G. Notice that this new observational data set consists of additional low-k data, which seems to support (within large errors) the lowest $P(k)$ (green) curve which is here implemented with the IR regulator and the running of G.

From Figures 3.5 and 3.6, one can see that the effects of the IR regulator alone serves to level off the curve at a low $k \sim m = 1/\xi$ (orange curve), whereas the full modification including both the IR regulator and the RG running of G (green curve) bends the curve downwards below the original classical curve (blue).

Figure 3.6 represents the newest observational data set at the time of writing – which was actually published shortly after our first analysis was done (see version 1 of the preprint [15]). It is interesting here to study the consistency and improvements, if any, of the data. In fact, as one compares the first plot (Figure 3.5) with this new release, we find that the refined observational data not only remain consistent with our original theoretical prediction, but also an additional data point at an even lower value of $k \approx 2.9 \times 10^{-4}\, h\mathrm{Mpc}^{-1}$ was found – which seems to actually suggest a downwards dip in the spectrum at low-k regime, as a running Newton's constant due to quantum gravity would suggest. It is clear that the error bars on the points are too large to make any conclusive statements. However, it is still interesting that it expresses such a downwards bend. Therefore this should remain an interesting development to study, and one is hopeful that as the observational resolution continues to improve, error bars for the data in the low-k regime will continue to narrow down, to eventually confirm or falsify this important prediction.

3.5 Constraints on the Scaling Dimension ν from Cosmology

It is also possible to utilize these latest cosmological observations to constrain the theoretical values of the microscopic parameters, and thus further shed insight into the underlying theory. A handful of parameters in the theory are investigated, including the universal critical scaling exponent ν, the coefficient for the amplitude of quantum effects c_0, and the characteristic nonperturbative correlation length scale ξ. Our analyses show that while the latter (c_0 and ξ) may only be constrained up to an order of magnitude, the data actually puts rather stringent constraints on the universal scaling exponent ν.

It should by now be apparent that the universal scaling index ν plays an important role in the theory of quantum gravity. Sections 2.2 and 3.1 summarized various methods, both analytical and numerical, to determine this value. Furthermore, Section 3.1 shows that the numerically derived value is in generally good agreement with recent observational data. It is therefore of academic interest to see if the logic can be reversed – by taking advantage of the variance in the data, to provide a constraint on this important theoretical parameter ν.

Figure 3.7 shows the same plot as in Figure 3.6 but with a 1% and 2% variance added to the value $\nu = 1/3$ (and ignoring the effect of IR regulation and RG running of Newton's constant G that is only important in the last three data points). It can be seen that, should one want to stay within most of the error bars on the left, only a maximum of 1% variance in ν is allowed. A 2% variance would already significantly protrude away from the rather stringent vertical error bars in the 4^{th} point from the left. One can therefore conclude that current cosmological data provides a very stringent constraint on the theoretical value of the scaling exponent ν - supporting the value of $\nu \simeq 1/3$, with a maximum allowed deviation of $1 - 2\%$. This observational constraint for ν, which should be emphasized that is the first of

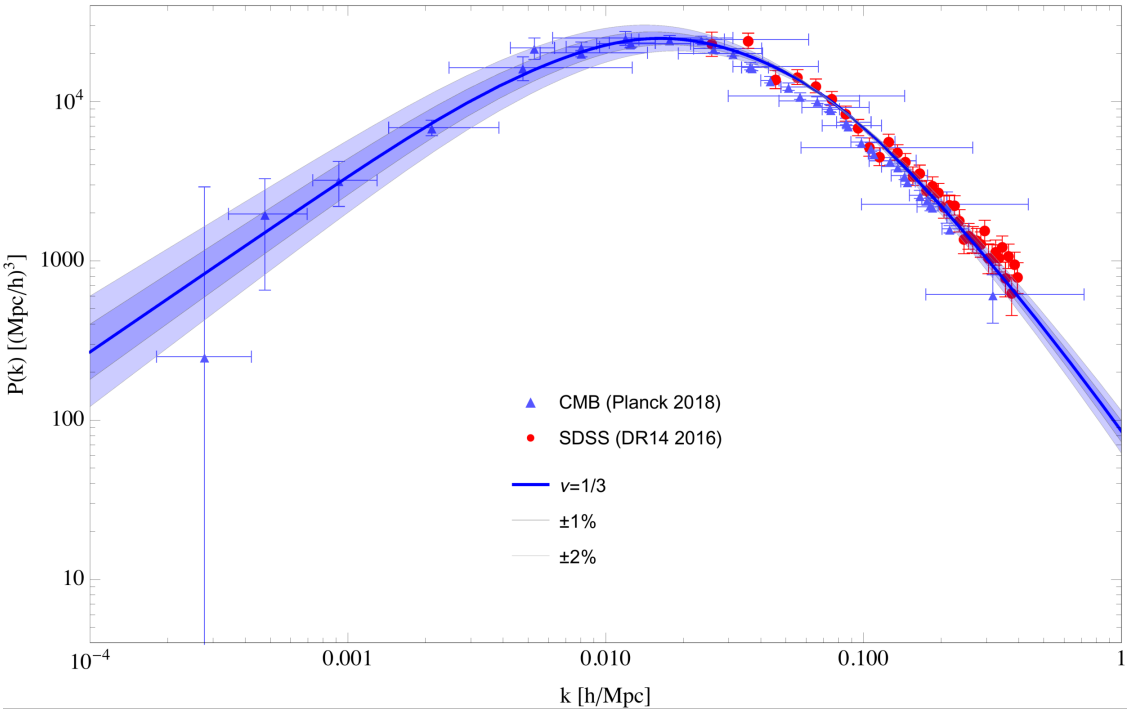

Figure 3.7: Matter power spectrum $P(k)$ with various choices for the scaling exponent ν. The middle (blue) curve shows the matter power spectrum as predicted by quantum gravity with a value of $\nu = 1/3$ as before, with two bands showing variance of $1 - 2\%$ in the value of ν. Notice that in order to obtain general consistency with current CMB data, ν cannot deviate by more than $\sim 2\%$ from the theoretically predicted value of $1/3$. This can be viewed as a rather stringent constraint on the value of the exponent ν arising from cosmology.

its kind, is extremely consistent with the various other numerical methods, and analytical- and semi-analytical approximations mentioned in Sections 2.2 and 3.1 for this value.

3.6 Constraints on the Running of G from Cosmology

A similar study can be performed for the magnitude of the RG running of Newton's constant G, and specifically the key quantum amplitude c_0. Recall that the running of Newton's G is given by

$$G(k) = G_0 \left[1 + 2c_0 \left(\frac{m^2}{k^2 + m^2} \right)^{3/2} + \mathcal{O}\left(\left(\frac{m^2}{k^2 + m^2} \right)^3 \right) \right] \ , \tag{3.31}$$

where G_0 is the currently established laboratory value for Newton's constant, the quantum amplitude is $2\,c_0 \approx 16.04$, and the nonperturbative gravitational condensate scale is estimated at $\xi \equiv m^{-1} \sim \sqrt{3/\lambda} \simeq 5300$ Mpc. The value of $2\,c_0 \approx 16.04$ is computed from the Regge-Wheeler lattice formulation of Quantum Gravity [45]. This is largely in exact analogy, both in concept and in practice (via the lattice), to the evaluation of the $\beta(g)$ function in QCD. The latter represents a quantity that has been extensively tested in collider experiments, and is by now in extremely good agreement with accelerator experiments. At this stage, unlike $\beta(g)$ from QCD, the same level of precision has not yet been achieved for c_0, and it seems possible at this stage, given various numerical uncertainties inherent in the calculation of c_0, to have deviations that could modify it by up to an order of magnitude.

As a result, one can parallel the previous study of ν, and utilize cosmological data to provide a best-fit value, and thus a constraint, on the quantum amplitude c_0. Also, the same type investigation for the variance in ξ will be done at the end of this section. Figure 3.8 shows the best fit to c_0, which corresponds to roughly 1/7-th, or 15%, of the original value for c_0, i.e., $2\,c_0 = 16.04/7 \simeq 2.29$ (in solid purple). The bands above and below the solid purple

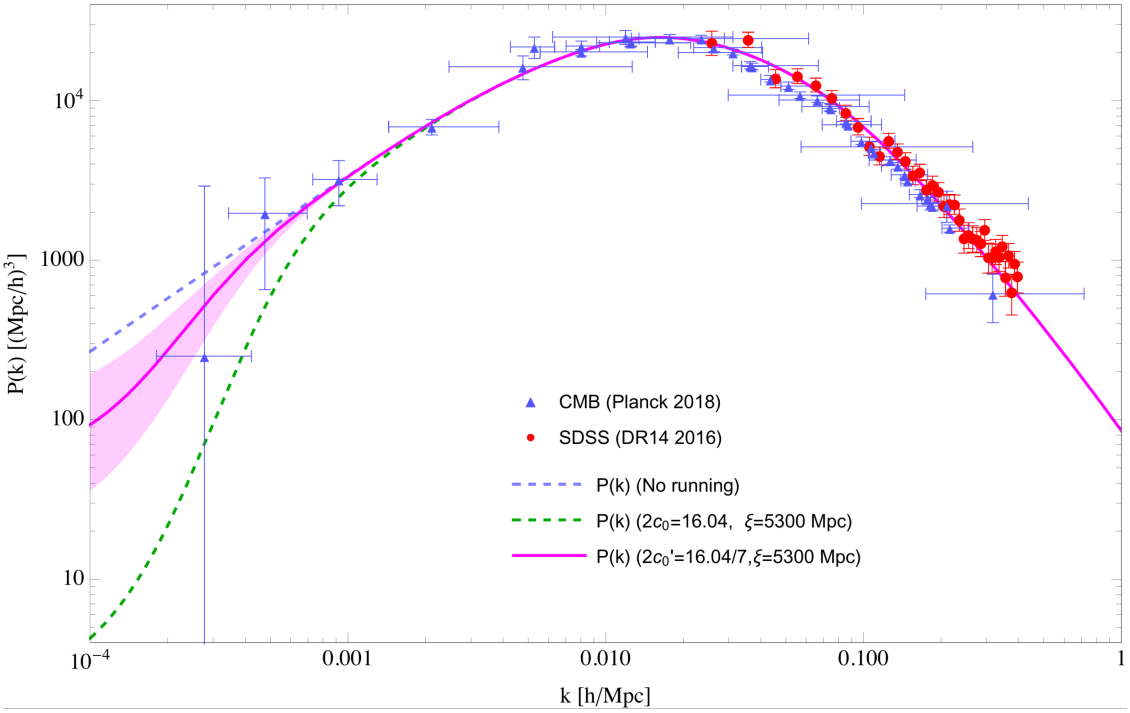

Figure 3.8: Matter power spectrum $P(k)$ shown for various choices of the quantum amplitude c_0. The middle (purple) solid curve shows a best fit through the last few low-k data points via an RG running of Newton's constant G, with an amplitude of running $2\,c_0 \approx 16.04/7 \approx 2.29$, i.e., around 15% of the preliminary value of 16.04 from the lattice. The shaded (purple) band represents a variance in $2\,c_0 \approx 2.29$ by a factor of 2 and 1/2. The original spectrum with no running (top, blue, dashed) and the spectrum with running of Newton's constant G, with the original coefficient of $2\,c_0 \approx 16.04$, (bottom, green, dashed) are also shown for reference. Note that the middle (purple) curve with $2\,c_0$ modified to 16.04/7 can also be mimicked by instead tuning the nonperturbative scale ξ to $\sim 2.5 \times 5300\,\text{Mpc}$ ($\approx 13,000\,\text{Mpc}$) and keeping the quantum amplitude $2\,c_0 = 16.04$.

curve represent a further factor of 1/2 and 2 respectively. Note that the middle solid (purple) curve with $2\,c_0$ modified to 16.04/7 can also be mimicked by instead tuning ξ to $\sim 2.5 \times 5300$ Mpc ($\approx 13,000$ Mpc) and keeping the lattice value for the amplitude at $2\,c_0 = 16.04$. The initial association of $\xi \sim \sqrt{3/\lambda} \approx 5300$ Mpc is theoretically motivated by connecting the curvature vacuum condensate scale in the theory, $\sqrt{3/\lambda}$, to the nonperturbative correlation length ξ [48, 49], and again in close analogy to what happens in QCD (the factor of 1/3 is often accompanied with λ in the equations of motions, such as the classical Friedmann equations). It is thus conceivable that the order of estimate ξ can be varied by a factor up

to an order of magnitude. The above analysis shows that, if the lattice value of $2\,c_0 = 16.04$ is to be taken rigorously, then an increase of ~ 2.5 on the vacuum scale ξ would best fit the data. In essence, the RG running of Newton's constant G requires two parameters, the quantum amplitude c_0 and the correlation length ξ, to fully determine its form. The former is in principle calculable from the lattice, while the latter is best associated with the scale $\sqrt{3/\lambda}$ provided by the theory, which determines the long-distance decay of Euclidean curvature correlation functions at a fixed geodesic distance. Nevertheless, the error bars in the last data point in Figure 3.8 are too wide to provide any definite conclusions at this stage. It is conceivable that further satellite experiments might put further constrains on the errors in these points, and thus provide more insight on these fundamental microscopic parameters.

Here we note that it is of some interest to explore analytical (as opposed to numerical) methods related to the running of Newton's constant G. One possibility briefly mentioned earlier is the $2+\epsilon$ expansion [50–57], which provides an estimate for the scaling exponent ν^{-1} to be between 2 and 4.4, through a one- and two- loop double expansion (in G and the dimension) respectively, giving additional confidence in the numerically computed value $\nu^{-1} \simeq 3$. Similar estimates for the exponent ν are found within a set of truncated RG equations, directly in four dimensions [62, 70].

Another recently explored idea is a nonperturbative approach via a mean field approximation, which in this context is essentially the Hartree-Fock (HF) self-consistent method applied to quantum gravity [91], used here for the running of Newton's constant G. One finds the following expression for the running of G,

$$G \;\to\; G_{\rm HF}(k) = G_0 \left[1 - \frac{3m^2}{2k^2} \log\left(\frac{3m^2}{2k^2}\right)\right] \tag{3.32}$$

The result of this exercise is shown in Figure 3.9. The middle solid orange curve shows the

Hartree-Fock expression for the running of Newton's constant G, while the bottom dashed green curve and the top blue dotted curve show the original lattice running of Newton's constant G (with original lattice coefficient $2\,c_0 = 16.04$), as well as no running respectively for reference. It seems that the Hartree-Fock running of G is in good consistency with the lattice expression, except for the eventual unwieldly upturn beyond $k < 2 \times 10^{-4}$. However, this upturn is most likely an artifact from the Hartree-Fock expression being just a first-order analytical approximation after all (it is well known that the Hartree-Fock approximation can be extended to higher order, by including increasingly complex higher loop diagrams, with dressed propagators and vertices still determined self-consistently by a truncated version of the Schwinger-Dyson equations). Nevertheless, the Hartree-Fock approximation shows good consistency with both the latest available observational data sets, as well as with the lattice results. The fact that it exhibits a gentler dip at small k perhaps also provides support for the reduced lattice running coefficient of $2\,c_0 = 16.04/7 \approx 2.29$ from Figure 3.8.

3.7 Comparison with Inflationary Models 2

It should be emphasized again that the two quantum gravity predictions of an emerging IR dynamical regulator and an RG the running of Newton's G – of which the combined effects on the large cosmological scales are shown by the green curves in the various $P(k)$ plots in this paper – are *independent* on whether the origin of matter fluctuations is inflation-driven or gravity-governed. Thus, conceptually, even if one insists that the power spectrum to be inflation-driven, or some sort of combined effect between inflation and gravitation, the effects of IR regulation and RG running of Newton's G should be taken into account, due to the non-trivial condensate effects from gravity by applying standard nonperturbative methods of quantum field theory. And, as we have shown, the data seem to reflect and support this. Or, at the very least, the inclusion of these nonperturbative quantum gravitational effects

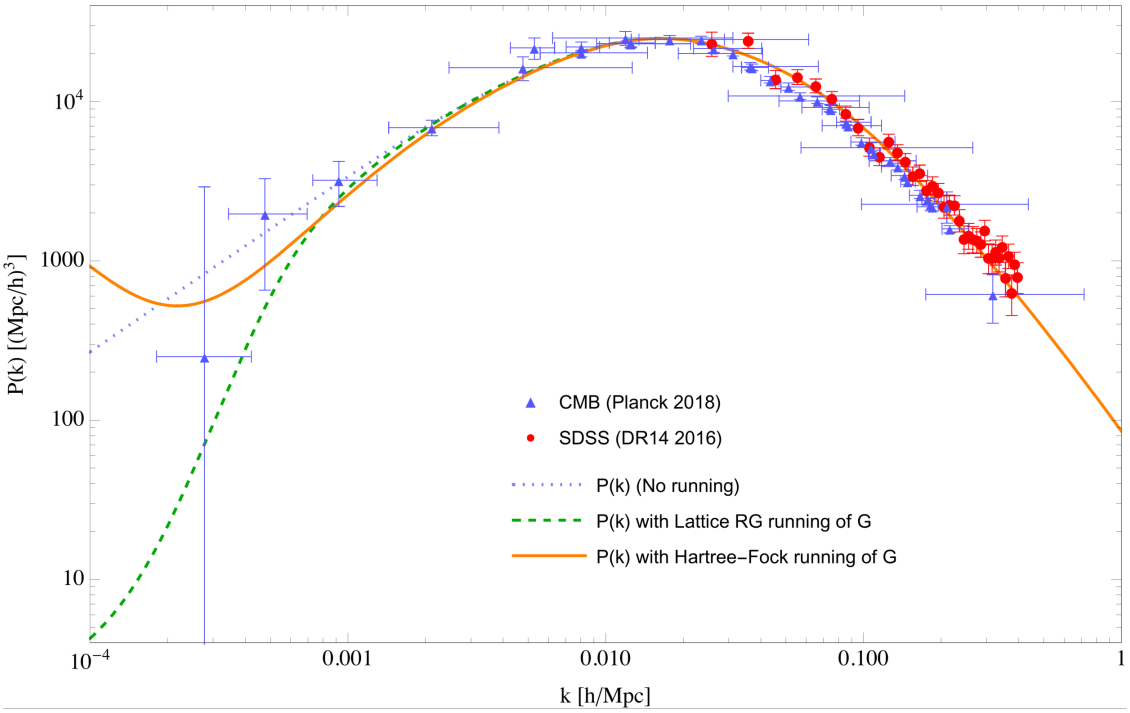

Figure 3.9: Lattice versus Hartree-Fock running of Newton's constant G. The middle solid (orange) curve shows $P(k)$ implemented with the Hartree-Fock running of Newton's constant G factor. The lower dashed (green) curve shows the original lattice RG running of Newton's constant G (with the original lattice coefficient $2\,c_0 = 16.04$) for comparison. The original spectrum with no running is also displayed by the top dotted (blue) curve for reference.

form a rather compelling explanation for the observed dip in the low-k limits of $P(k)$.

Once again, it should be stressed that these two additional, genuinely-quantum, effects are fairly concrete predictions associated with standard quantum modifications to classical gravity, and are quite distinct from any effects from inflationary models – both in procedure and in origin. With the advance of increasingly accurate astrophysical and cosmological satellite observations, it is hoped that these new predictions could be verified, or falsified, in the near future.

Chapter 4

Angular CMB Power Spectrum C_l

Cosmological power spectra always play an important role as the testing ground for the theories of inflation. In particular, the ability to reproduce the CMB temperature angular power spectrum C_l – in additional to the galaxy matter power spectrum $P(k)$ – to high accuracy is often considered a triumph of inflation. In the previous chapter, we presented an alternative explanation for the matter power spectrum based on nonperturbative quantum field-theoretical methods applied to Einstein's gravity, instead of inflation models based on scalar fields. In this chapter, we extend our predictions to the angular CMB temperature spectrum coefficients C_l. Then we investigate further the potential freedoms and uncertainties associated with the fundamental parameters that are part of this picture, and show how recent cosmological data provides significant constraints on these quantities. Overall, we have found good general consistency between theory and data, will summarize our results by outlining how this picture may be tested in the near future with increasingly accurate astrophysical measurements.

4.1 Introduction

In the previous chapter, we offered an alternative explanation based on gravitational fluctuations alone without inflation [15], which to our knowledge is the first-of-its-kind. While the short-distance theory of quantum gravity may still be highly uncertain due to both the flexibility of higher-order operators consistent with general covariance and the lack of experimental results, the long-distance or infrared limit of the theory is however in principle well-defined and unique, governed largely by the concept of universality. Although this long-distance quantum theory of gravity still suffers from being perturbatively nonrenormalizable, well known field theory techniques have been extensively developed, applied and tested in many other fields of physics where perturbation theory fails, usually due to a non-trivial vacuum structure. As a result, it is thus conceivable that these nonperturbative methods may find use in deriving physical consequences of perturbatively nonrenormalizable theories such as gravity. Previous efforts [13, 14] have shown that many such effects may manifest themselves and become important on very large cosmological scales. In particular, we found that much of the matter power spectrum can be derived and reproduced from Einstein gravity and standard ΛCDM cosmology alone, utilizing nonperturbative quantum field methods, without the need of additional scalar fields as advocated by inflation. We have shown that not only the predictions agree quite well with recent data, but also that additional quantum effects predict subtle deviations from the classical picture, which may become testable in the near future.

In this chapter, we further investigate consequences from the above picture. Most importantly, we translate our quantum gravity prediction of the matter wavenumber power spectrum $P(k)$ to a prediction for the angular temperature power spectrum coefficients C_l's. The angular temperature power spectrum, which expresses the power as coefficients of spherical harmonics (instead of plane waves, like the matter power spectrum) serves as a more di-

rect comparison with observation, since after all the CMB measurements are performed over the sky. Unsurprisingly, we again find a general agreement between the observations and the gravitationally motivated prediction. Furthermore, additional quantum gravitational effects are expected to affect the low-l regime of the C_l spectrum. As discussed in [15], new quantum effects become significant when the separation-distances r become comparable to a characteristic vacuum condensate scale of gravity ξ, which is expected to be extremely large ($\sim 5300\,\mathrm{Mpc}$), affecting very small l's in angular harmonic space. The additional quantum effects include the infrared (IR) regulator effects from the gravitational vacuum condensate and the renormalization group (RG) running of Newton's constant G. Such modifications are usually implemented via sophisticated numerical programs (such as CMBFAST and CAMB) in cosmology. While that would produce the most sophisticated predictions, the procedure and details become rather obscured and nontransparent. So, here we first attempt to derive these effects in a mostly analytical manner, apart from a few standard approximations and the help of Mathematica to perform a few final numerical integrals, instead of relying on a "black-box" program from the start. From this derivation, we find a small dip in power in the low-l regime. It is possible that this, the quantum effects of gravitation, may be the cause for the well-known $l = 2$ anomaly in the C_l spectrum. Although it is impossible to make conclusive statements so far due to the large cosmic variance in that region, one might hope that there may be incremental improvements in systematic and experimental uncertainties in the near future, or that certain statistical likelihood-arguments for this effect can be made. After this, in the next chapter, we proceed to employ more state-of-the-art programs in cosmology to revisit this (and other) calculations, compare against them in detail.

This chapter is organized as follows. Section 4.2 serves to outline the key theory of angular temperature spectrum C_l, and how it relates to the matter power spectrum $P(k)$. Section 4.3 relates the quantum gravity predictions on the matter power spectrum $P(k)$, as discussed in the last chapter, to the angular temperature spectrum C_l's, as well as the quantum effects of an IR regulator and the RG running of Newton's constant G on the C_l's. Section 4.4

discusses, summarizes and contrasts the current quantum gravity motivated picture with that of inflation, in view of explaining the measured power spectra. The section concludes by outlining a number of future issues of interest to this study.

4.2 Angular CMB Temperature Power Spectrum

The most accurate recent measurements of the CMB are actually represented by the angular temperature power spectrum, represented by a set of angular Fourier coefficients denoted by C_l. It is therefore useful to translate the quantum gravity prediction to the angular temperature spectrum represented by the C_l's. The angular temperature spectrum C_l coefficients relate to a two-point correlation function of the temperature, when expanded in terms of spherical harmonics labelled by l and m. The C_l coefficients themselves are defined as

$$C_l \equiv \frac{1}{4\pi} \int d^2\hat{n} \int d^2\hat{n}' \; L_l(\hat{n} \cdot \hat{n}') \, \langle \, \Delta T(\hat{n}) \, \Delta T(\hat{n}') \, \rangle \quad , \tag{4.1}$$

where $\hat{n}, \hat{n}'$ are two different directions in the sky, and $L_l(\theta)$ the Legendre polynomials. Here we avoid the usual common notation, "$P_l(\theta)$", for the Legendre polynomials, in order to avoid unnecessary confusion with the various power spectra. Following [18], fluctuations in the CMB temperature ΔT can be expanded in plane waves,

$$\left(\frac{\Delta T(\hat{n})}{T_0} \right) = \int d^3q \; e^{i\mathbf{q}\cdot\hat{n}\, r(t_L)} \, (\, F_1(q) + i\hat{q} \cdot \hat{n} \; F_2(q) \,) \quad , \tag{4.2}$$

where $T_0 = 2.725$ K (the average CMB temperature measured today), t_L the time of recombination, and $F_{1,2}(q)$ form factors given by

$$F_1(q) = -\frac{1}{2} a^2(t_L) \ddot{B}_q(t_L) - \frac{1}{2} a(t_L) \dot{a}(t_L) \dot{B}_q(t_L) + \frac{1}{2} E_q(t_L) + \frac{\delta T_q(t_L)}{\bar{T}(t_L)} \quad , \tag{4.3}$$

$$F_2(q) = -q\left(\frac{1}{2}a(t_L)\dot{B}_q(t_L) + \frac{\delta u_{\gamma q}(t_L)}{a(t_L)}\right) \quad , \tag{4.4}$$

The B and E functions describe suitable decompositions of the metric perturbations, and δu_γ is the velocity potential for the CMB photons. These form factors simplify for certain gauge choices. In the synchronous gauge, $E = 0$, whereas in the Newtonian gauge $B = 0$ and $E = 2\Phi$, which then gives

$$F_1(q) = \Phi_q(t_L) + \frac{\delta T_q(t_L)}{\bar{T}(t_L)} \quad , \tag{4.5}$$

$$F_2(q) = -\frac{\delta u_{\gamma q}(t_L)}{a(t_L)} \quad . \tag{4.6}$$

The functions Φ and δu_γ, as well as the scale factor $a(t)$ and $T(t)$, can all be obtained as solutions of the classical Friedmann equations combined with the Boltzmann transport equations, as is done in standard cosmology, which will then in principle lead to unambiguous predictions for the C_l's. Note that $F_1(q)$ and $F_2(q)$ are referred to as "$F(q)$" and "$G(q)$" respectively in [18]. Here we will use the former in order to avoid confusion with the expression for the running of Newton's constant $G(k)$, as it will be implemented below. We also make the usual approximation of a sharp transition at t_L during recombination, which is quite acceptable since we are primarily interested in the general trend, and not exceedingly precise features, of the spectrum at this stage.

Perturbations in the above form factors are fully governed by the classical Friedmann and Boltzmann transport equations. These lead to standard solutions in terms of transfer func-

tions $\mathcal{T}(\kappa)$, $\mathcal{S}(\kappa)$ and $\Delta(\kappa)$, given by

$$F_1(q) = \frac{\mathcal{R}_q^0}{5}\left[3\,\mathcal{T}\left(\frac{q\,d_T}{a_L}\right)R_L \;-\; (1+R_L)^{-\frac{1}{4}}\;e^{-\left(\frac{q\,d_D}{a_L}\right)^2}\mathcal{S}\left(\frac{q\,d_T}{a_L}\right)\;\cos\left[\frac{q\,d_H}{a_L}+\Delta\left(\frac{q\,d_T}{a_L}\right)\right]\right]\quad, \tag{4.7}$$

$$F_2(q) = \sqrt{2}\,\frac{\mathcal{R}_q^0}{5}\,(1+R_L)^{-\frac{3}{4}}\;e^{-\left(\frac{q\,d_D}{a_L}\right)^2}\mathcal{S}\left(\frac{q\,d_T}{a_L}\right)\;\sin\left[\frac{q\,d_H}{a_L}+\Delta\left(\frac{q\,d_T}{a_L}\right)\right] \tag{4.8}$$

where $a_L = a(t_L) = 1/(1+z_L)$, $z_L = 1090$, $d_T = 0.1331$ Mpc, $d_H = 0.1351$ Mpc, $d_D = 0.008130$ Mpc, $d_A = 12.99$ Mpc, and $R_L \equiv 3\Omega_B(t_L)/4\Omega_\gamma(t_L) = 0.6234$. It is noteworthy at this stage that all three transfer functions are completely determined again by (well measured) cosmological parameters. So the only remaining ingredient to fully determine the C_l coefficient is an initial spectrum $\mathcal{R}_q^0$, which is usually parameterized by an amplitude N and spectral index n_s,

$$\mathcal{R}_q^0 = N\,q^{-3/2}\left(\frac{q}{q_{\mathcal{R}}}\right)^{(n_s-1)/2}\quad. \tag{4.9}$$

Here the reference "pivot scale" is usually taken to be $q_{\mathcal{R}} = 0.05\,\mathrm{Mpc}^{-1}$ by convention. As a consequence, once the primary function $\mathcal{R}_q^0$ is somehow determined, classical cosmology then fully determines the form of the C_l spectral coefficients. It is therefore possible to write the C_l's fully, and explicitly, in terms of the primary function $\mathcal{R}_q^0$. After expanding the original plane wave factor in a complete set of spherical Harmonics and spherical Bessel functions, one obtains

$$C_l = 16\pi^2\,T_0^2\int_0^\infty q^2\,dq\;\left(\mathcal{R}_k^0\right)^2\left[\,j_l(qr_L)\widetilde{F_1}(q) + j_l'(qr_L)\widetilde{F_2}(q)\,\right]^2\quad. \tag{4.10}$$

Here $r_L = r\,(t_L)$, and we have factored out the function $\mathcal{R}_q^0$ explicitly $F_1(q) = (\mathcal{R}_q^0)\,\widetilde{F_1}(q)$

and $F_2(q) = (\mathcal{R}_q^0)\,\widetilde{F_2}(q)$. Recall that, since the matter power spectrum is given by

$$P\,(k) = C_0\,\left(\mathcal{R}_k^0\right)^2\;k^4\,[\mathcal{T}(\kappa)]^2\;\;, \tag{4.11}$$

we can use $\mathcal{R}_q^0$ to obtain a direct relation between the C_l's and $P(k)$,

$$C_l = 16\pi^2\,T_0^2\int_0^\infty q^2 dq\,P(q)\;\left[\,C_0\,k^4\,\mathcal{T}(\kappa)^2\,\right]^{-1}\left[\,j_l(qr_L)\widetilde{F_1}(q) + j_l'(qr_L)\widetilde{F_2}(q)\,\right]^2\;\;, \tag{4.12}$$

where q and k are related by $q = a_0 k$, and the scale factor "today" a_0 can be taken to be 1.

4.3 Quantum Gravity Results

The Quantum theory of Gravity, as outlined in the earlier sections, predicts the form of the full matter power spectrum function $P(k)$. Using Eq. (4.12), one can therefore translate the quantum gravity prediction on $P(k)$ to the angular coefficients C_l's. Figure 4.1 shows a plot of the ensuing result, represented by the top blue curve, for $l = 2$ to $l = 50$. One can see that the theoretical prediction (obtained here by numerical integration) is in generally rather good agreement with most of the observational data. Again, it should be emphasized here that reproducing the full expression for the C_l's does not require the inclusion of a scalar field anywhere. Instead, the spectrum for gravitational fluctuations is used to set the scaling in a particular regime, which is chosen to be the galaxy regime for its most direct connection, and the rest is then fully governed by classical general relativity and standard kinetic theory. Another way of expressing this result is that the entire expression for the C_l's, or for $P(k)$, except for the spectral index n_s and the amplitude N, is fully governed by classical general relativity and kinetic theory (and by finely measured cosmological parameters such as Ω_M, Ω_Λ, H_0, etc. ...). That is, n_s and N are the only two remaining theoretically undetermined quantities in this framework. Whereas inflation provides one perspective on how these two

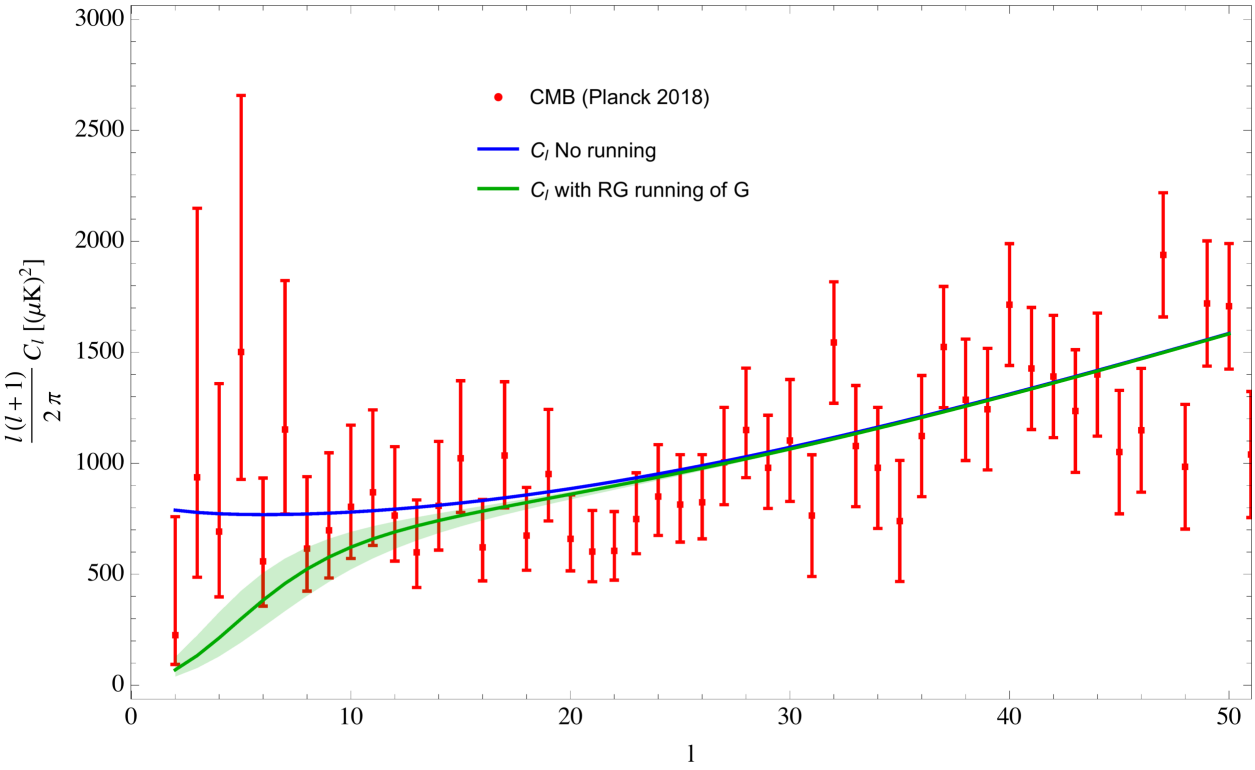

Figure 4.1: Plot of the angular power spectrum coefficients $l(l+1)C_l/2\pi$. The upper (blue) curve shows the quantum gravity prediction of the angular CMB power spectrum C_l's as obtained from the matter power spectrum $P(k)$ (and thus with scaling exponent ν=1/3), without any IR regulation effect from ξ, and without the RG running of Newton's constant G. The bottom (green) curve shows the combined quantum gravity effect now with IR regulation and the lattice RG running of Newton's constant G, with the original lattice quantum amplitude $2\,c_0 = 16.04$. The upper and lower bands on the bottom curve represent a factor of 2 variance on the quantum amplitude c_0, i.e., $2\,c_0 = (8.02, 32.08)$.

parameters can be derived, quantum gravity provides in our view an equally well-motivated alternative.

However, as before, additional quantum gravity effects are expected to manifest themselves at very large distances comparable to ξ. In angular space, this corresponds to the widest angles, or very low-l regime. In this context one can then investigate how the IR regularization and the RG running of Newton's constant G affects the standard prediction, thus providing potentially testable predictions and alternatives, to distinguish between this quantum gravity fluctuation picture and the inflation one. In the case of the matter power spectrum $P(k)$, the RG running of Newton's constant G was implemented by modifying

$$P(k) \;\rightarrow\; \left[\frac{G_0}{G(k)}\right]^2 P(k) \tag{4.13}$$

where G_0 is the Newton's gravitational constant measured in the laboratory or on solar system scales. In the angular spectrum coefficients C_l, this will introduce an extra factor of $[G_0/G(q)]^2$ in the integrand. The resulting modification is shown by the lower green curve in Figure 4.1. As for the case of $P(k)$, the RG running of Newton's constant G causes a significant drop in the magnitude of the C_l's at large distance scales (low l). The green bands around the curve with the RG running of Newton's constant G shows the effects of varying by factor of 2 the quantum running amplitude c_0.

Note that in particular the last point at $l = 2$, which corresponds to measuring the CMB on the largest scales on the sky, is significantly below the classical prediction, and has represented a well-known anomaly for quite some time. Although that last point is plagued with large uncertainties due to cosmic variance - the lack of independent samples on this scale from our sky - many do agree that the error bars as shown already account for our best assessments of the associated variances. If these judgements are believable, then the classical prediction seems just marginally consistent with the allowed uncertainties. If the

matter power spectrum indeed originates from inflation, then there are currently no widely agreed solutions that can reasonably explain the sudden drop in power at the extreme low l's. This is a general consequence of inflation, providing a scale-invariant normalization at very large scales.

Quantum gravity, however, tells us that the effects from a running Newton's constant G must be included, whether by an expression calculated from the lattice approach as represented by the green curve above, or by one calculated via the Hartree-Fock approximation. Figure 4.2 shows a comparison between them.

So it seems that for distance scales roughly $r < \xi$, both quantum gravity and inflation produce a spectrum that agrees rather well with observations. Although one can argue the gravity induced perspective is more natural to the principle of Ockham's Razor, being able to explain the same physical phenomena without the need of a new field, the question of which picture is more desirable remains largely a philosophical one. However, for distance scales roughly $r > \xi$ (i.e., small k or small l), both the observed matter power spectrum $P(k)$ and the corresponding observed angular power spectrum C_l seem to hint towards the quantum gravity picture. Of course, ultimately, much more precise data will be needed to conclude this decisively. Nevertheless, the current context presents an intriguing possibility for a new explanation for the nature of correlations and for the origin of cosmic fluctuations, and also beyond that an interesting testing ground for quantum gravity.

It is of some interest here to compare the running of Newton's constant G obtained from the lattice to the analytical result of the Hartree-Fock approximation. Using the Hartree-Fock expression Eq. (3.32), the corresponding result is displayed by the orange curve in Figure 4.2. One notes that, similarly to $P(k)$, the Hartree-Fock expression analogously (i) predicts a smaller power in the low-l's ($l < 50$), (ii) has a less dramatic dip compared to the lattice running at the very large scales ($l < 10$), and finally (iii) predicts a somewhat unwieldly upward turn at the extreme large scales ($l < 3$). As is the case of the matter power

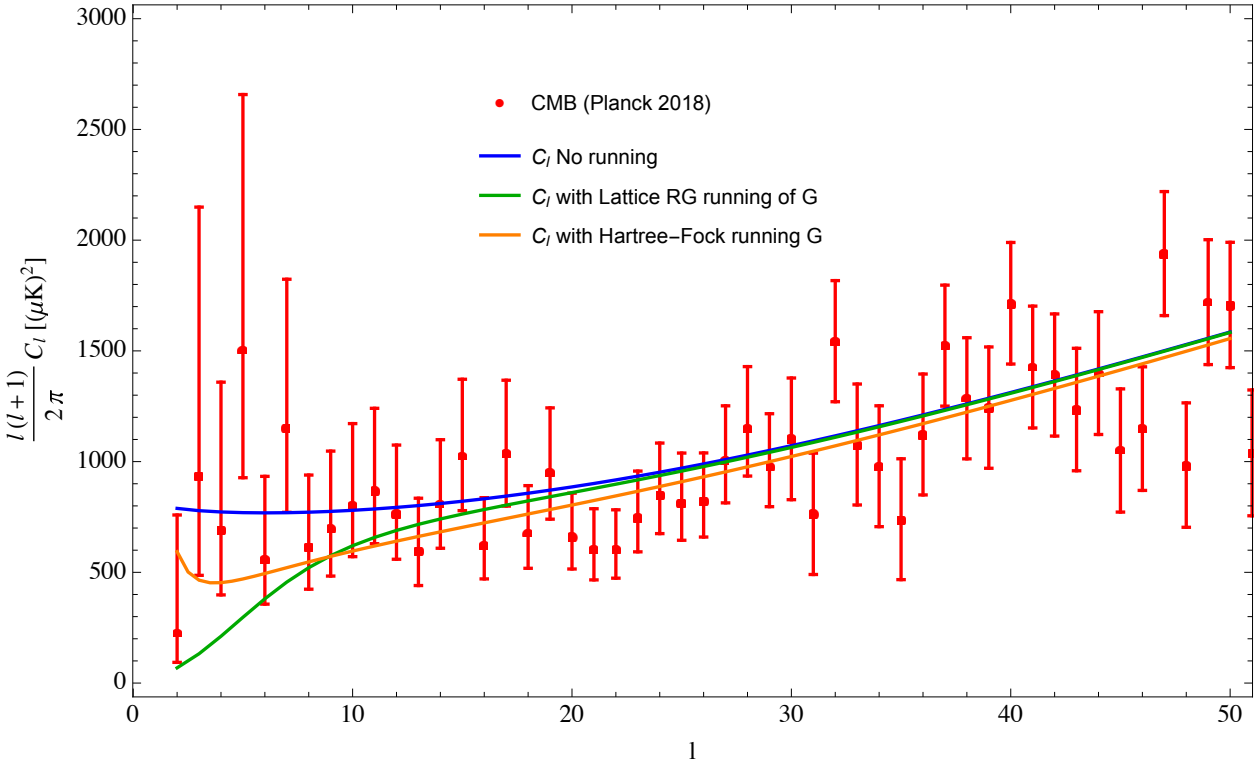

Figure 4.2: A comparison of the lattice versus Hartree-Fock RG running of Newton's constant G on the angular spectrum coefficients C_l. The middle (orange) curve shows C_l implemented with a Hartree-Fock running of Newton's constant G factor, in comparison with the original lattice RG running of Newton's constant G (with the original lattice coefficient $2\,c_0 = 16.04$), represented by the lower (green) curve. The original angular spectrum with no running of G is shown by the upper (blue) curve for reference.

spectrum $P(k)$, some of these features, especially the unwieldy upturn at extremely large scales, may be an artifact from the fact that Hartree-Fock is essentially a mean-field type approximation. Nevertheless, while the lattice prediction may be more trust-worthy due to it being an exact, numerical evaluation of the path integral, the Hartree-Fock expression provides a good independent consistency check for this picture.

Finally, it is possible to investigate the effect of varying the lattice quantum amplitude c_0 appearing in the running of G, as in Eqs. (2.12) and (2.17). From the investigation of $P(k)$, the value of c_0 that best fits the large scale data at small k is $2\,c_0 = 16.04/7 \approx 2.29$. Figure 4.3 plots the effect of this modification. As before, this choice seems to fit rather well with most of the data in the low-l regime. Nevertheless it should be noted that this modification can also be mimicked by modifying the correlation length $\xi \approx 5300$ Mpc to $\xi \approx 13000$ Mpc, or by any combined adjustments of the two parameters ξ and c_0. Although at first sight it may seem impossible to eventually distinguish the difference between the classical and quantum picture by the still highly uncertain data, it may not be so with better telescopes in the near future. Table 4.1 shows the percentage difference between the classical prediction, and one with the RG running of Newton's constant G included, in accordance with Eq. (2.17), with the choice $2\,c_0 = 16.04/7 \approx 2.29$. From Table 4.1, one can see a 58% difference in the C_l for $l = 2$, which future experiments may be able to distinguish. However, too much emphasis should not be put in the extreme low-l points due to statistical limitations arising from cosmic variance, which under reasonable assumptions (mainly Gaussianity) is expected to grow rapidly as l decreases, by $\Delta C_l \sim 2/\sqrt{2l+1}$ [18]. Nevertheless, focusing on the $l = 6$ to $l = 10$ points, the narrowing of errors needed to distinguish between the classical and the quantum predictions may very much be achievable. Thus, for example, for $l = 6$, the percentage difference between the predictions is 13%. In comparison, the current errors on the Planck data for the $l = 6$ value is $^{+67\%}_{-36\%}$. For $l = 10$, the current uncertainties in the Planck data is $^{+46\%}_{-29\%}$, whereas the difference between the classical and quantum prediction is only 3.53%, which may be more difficult to resolve with future satellite

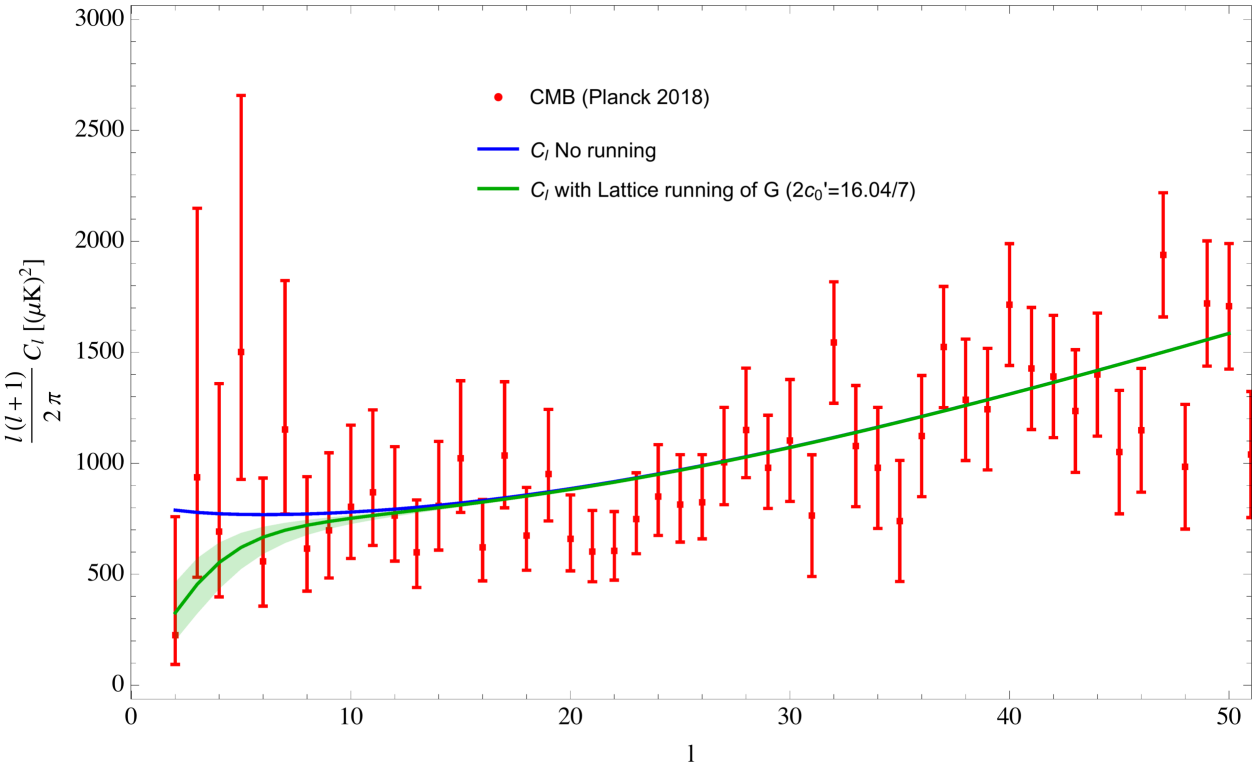

Figure 4.3: Angular power spectrum shown, with a comparison between various choices for the lattice RG running of G parameters of Eq. (2.17). For reference, the top blue curve represents the original spectrum with no RG running of Newton's constant. The bottom green curve shows the effect of the lattice RG running of Newton's constant G with a modified value for the lattice amplitude $2\,c_0 = 16.04/7 \approx 2.29$. This new curve, represented by the modified amplitude $2\,c_0$, appears to fit best through the last few ($l < 10$) data points. Here the green bands represent a factor of two in variance around this modified c_0. The last curve reveals that although the original value of $2\,c_0$, as obtained from numerical lattice simulations, is around the correct order of magnitude, nevertheless when looked at more carefully, a slightly smaller value seems to be favored by the very low l cosmological data. It seems therefore that future data from the CMB could be useful in further constraining the precise value for the quantum amplitude. Note that a coefficient of $2\,c_0 \approx 16.04/3.13$ will allow the green curve to precisely go through the last point at $l = 2$. However cosmic variance suggests $\Delta C_l \sim 2/\sqrt{2l+1}$, which disfavors giving too much weighting to the final point.

l	$l(l+1)C_l/2\pi$ Classical	$l(l+1)C_l/2\pi$ Quantum	Difference	%-Difference
2	788.78	328.47	460.31	58.36 %
3	778.43	457.41	321.02	41.24 %
4	772.58	555.42	217.16	28.11 %
5	769.52	623.18	146.34	19.02 %
6	768.55	668.59	99.96	13.01 %
7	769.30	699.51	69.80	9.07 %
8	771.56	721.59	49.97	6.48 %
9	775.17	738.51	36.67	4.73 %
10	780.04	752.51	27.53	3.53 %

Table 4.1: Values of, and percentage differences between, the classical predictions for the angular spectrum coefficients C_l's, and the prediction with a quantum RG running for Newton's constant G included. The quantum gravity values for the C_l's were computed here with a lattice RG running quantum amplitude of $2\,c_0 = 16.04/7 = 2.29$.

experiments. Nonetheless, while the magnitude of the errors in the CMB observational data may initially seem unpromising to make any claims, this table shows there may still be hope in distinguishing the various theoretical predictions. Within the $l = 6$ to $l = 10$ points range, the improvements in technology needed to improve the measurements and support the validity of the gravitational fluctuation picture may actually be within reach in the next decades, which provides an exciting prospect for the future.

In conclusion, in this section we showed how the quantum gravitation prediction for $P(k)$ unambiguously translates to a prediction for the C_l's - which is essentially related to the former via a spherical Bessel transform, weighted by some suitable combination of transfer functions. The transfer functions in turn are ultimately just solutions to the classical Friedmann equations and associated Boltzmann transport equations which, apart from the measured values of standard cosmological parameters such as H_0, Ω_m, etc., require no further theoretical input. As a result, we were able to show how the quantum gravity prediction for the matter power spectrum $P(k)$ directly and unambiguously translates to the angular coefficients C_l. It can be seen that the prediction is rather consistent with current cosmological data.

We also discussed several theoretical parameters, which in this picture potentially have some variance and related uncertainties. The first two key parameters in the quantum gravity motivated picture are the universal scaling exponent ν, and the fundamental vacuum condensate correlation length ξ. A third additional parameter here is the quantum amplitude c_0, which governs the amplitude of quantum correction in the RG running of Newton's constant G as given in Eqs. (2.12) and (2.17). Of the three parameters, as shown above in Section 3.5, ν is pretty much highly constrained (both theoretically and observationally) around $\nu^{-1} \simeq 3$. The value of this last parameter should also be the most trustworthy of the three since, as a universal scaling exponent, it is expected to be entirely independent of schemes and regularization. On the other hand, the values of ξ and c_0 are somewhat less definite. Here the nonperturbative length scale ξ is quite analogous (via the observed scaled cosmological constant $\lambda = 3/\xi^2$) to the vacuum condensate scale in QCD $\langle F_{\mu\nu}^2 \rangle \sim 1/\xi^4$, or to the scaling violation parameter $\Lambda_{\bar{MS}} \propto \xi^{-1}$. This implies that its absolute value in physical units is not determined theoretically, and can ultimately only be fixed by experiment. Current cosmological data seem to suggest the best – and most consistent – estimate for ξ is roughly $\xi \simeq 2.5 \times 5300$ Mpc, whereas for the quantum amplitude $2\,c_0 \simeq 16.04/7$, or some degenerate combination between the two (as discussed in the beginning of this chapter). Finally, we explicitly listed the percentage differences between the classical prediction and the quantum one implemented with an RG running of Newton's G, which should provide a useful guide as to how improved observational data must trend in order to support the picture advocated here. Although such precision has not been achieved yet, it should hopefully be attainable in the near future, and thus provide an additional significant test for the quantum gravity picture.

Nevertheless, with these flexibilities in mind, the quantum gravity picture outlined here provides a radically different perspective to the origin of matter and radiation fluctuations, as compared to the other common perspectives, for example, from inflation. In addition, the inflation picture normalizes the spectrum at large scales (i.e., small-k), so that for the C_l's

it predicts a flat scale-invariant plateau for small-l's. If the last point of $l = 2$ is to be taken seriously, despite the flexibility inherent in various inflation models, it would be difficult to account naturally for the reduction in power on the very largest scales. In contrast, the demand of a renormalization group running Newton's constant in the quantum gravity picture appears to explain the dip quite naturally. Of course, due to the large uncertainties in the data at small l's, significant improvements on the errors needs to be made before definite conclusions can be drawn.

4.4 Conclusion

In this chapter, we have revisited some key procedures in how the angular CMB temperature spectrum is related to the matter power spectrum and showed, mostly analytically, how the gravitationally motivated fluctuations can give rise to the angular temperature spectrum. We also showed how the additional quantum effects are predicted to affect the spectrum in the low-l regime.

To reiterate, the primary benefit of the quantum gravity explanation over inflation is the non-necessity of additional and untested physics ingredients, other than standard Einstein's gravity and accepted modern quantum field theory methods. The basis of the methods begins with the path integral formulation of gravity [27, 28] which, unlike inflation, provides a very constrained theoretical framework. Also, given the well-known fact that the theory is not perturbatively renormalizable, standard nonperturbative methods and approaches must be used. While a lot of the results used here are derived from the lattice numerical treatment, additional confirmations via analytical methods are also briefly discussed, including the $2+\epsilon$ and the Hartree-Fock approximation. The general consistencies of these numerical and analytical methods gives confidence to the results. The lattice treatment in particular has

a long history of high precision success in other fields from QCD to condensed matter and statistical systems, and thus provides us with particularly trustworthy results.

On the other hand, for inflation, a new (minimum of one) inflaton field, usually scalar in nature, must be invoked. The details of the particular theory are also highly flexible, leading to a myriad of models, see for example [88] and references therein. In addition, recent studies have shown that a majority of single-field inflation models have either been ruled out or highly constrained. The amount of flexibility for inflation has thus led many to question the predictability and ultimate naturalness of such scalar-field based solutions [10–12, 85, 86]. Although the original model of inflation was invented to explain the flatness and horizon problem, it has been convincingly argued that it is not a necessary ingredient to do so [92–102]. We have argued therefore that the gravitational picture provides a more concrete and natural explanation to the origin and distribution of cosmological matter fluctuations.

Finally, we have pointed out that the gravitational fluctuation picture also provides a clear set of predictions that diverge from scalar field induced predictions on very large scales. As advanced satellite experiments are continuously being conducted, and increasingly accurate measurements are becoming available, the predictions originating in quantum gravity outlined in Section 4.3 could be verified or disproved in the near future.

We should add that it is certainly possible for our picture of gravitational fluctuations to even coexists with inflation, with both effects providing significant contributions to the power spectra. Nevertheless, we do not explore this idea in depth here, as the primary aim of this thesis is to show that the same power spectra can be reproduced purely from macroscopic quantum fluctuations of gravity, independent of any inflation mechanism, making use of well-accepted and tested methods for dealing with perturbatively nonrenormalizable theories. Still, this could be a potential avenue for future explorations.

In addition to the results presented here, there are also a number of exciting future directions

which seem meaningful to explore. For example, the quantum gravity-based explanation is most certainly not Gaussian, due to the presence of non-trivial anomalous scaling dimensions [13] which affect all gravitational n-point functions, although they may seem to be Gaussian in certain regimes. While the corresponding predictions for the two-point functions, or power spectra, are similar to those motivated by inflation, a divergence will definitely be expected on higher order n-point functions, commonly known as bispectra and trispectra in the cosmology context. For example, the two-point function scalar curvature result of Eq. (3.6), derived from quantum gravity, will also determine the form of the connected reduced three-point function, or bispectrum, for large scale scalar curvature correlations [13]

$$\langle\, R(x_1)\, R(x_2)\, R(x_3)\,\rangle_{c,R} \quad \underset{d_{ij} \ll \xi}{\sim} \quad \frac{C_{123}}{d_{12}\, d_{23}\, d_{31}} \quad , \tag{4.14}$$

with constant amplitude C_{123}, and relative geodesic distances $d_{ij} = |x_i - x_j|$ in coordinate space. It is easy to see that this last correlation leads to a Fourier transform in momentum- or wavenumber-space of the form

$$B_R(\mathbf{k}_1, \mathbf{k}_2, \mathbf{k}_3) \;\equiv\; \langle\, R(\mathbf{k}_1)\, R(\mathbf{k}_2)\, R(\mathbf{k}_3)\,\rangle_{c,R} \quad \underset{k_i \gg m}{\sim} \quad \frac{\log\left(k_1 + k_2 + k_3\right) + \gamma_E}{k_1\, k_2\, k_3}\; \delta^{(3)}\left(\mathbf{k}_1 + \mathbf{k}_2 + \mathbf{k}_3\right) \quad , \tag{4.15}$$

where $\mathbf{k}_1, \mathbf{k}_2, \mathbf{k}_3$ are the three momenta conjugate to d_{12}, d_{23}, d_{31}, the scale $m = 1/\xi$, and γ_E is Euler's constant. One can then follow the same line of argument given in Section 1.2 to relate this to measured quantities from the CMB. Here we outline the main points of the argument. Firstly, the Einstein's field equations of Eq. (3.3) allow this bispectrum for curvature to directly translate to the bispectrum for matter $\langle\, \delta\rho\, \delta\rho\, \delta\rho\,\rangle$. Secondly, the transfer function, responsible for turning the two-point spectrum from $\sim 1/k$ to $\sim k$ when connecting the late-time galaxy regime to the early-time CMB regime, essentially supplies

an extra factor of k for each fluctuating field. This then leads to the result

$$B_{\delta\rho}^{(\mathrm{CMB})}(\mathbf{k}_1,\mathbf{k}_2,\mathbf{k}_3) \;\equiv\; \langle\, \delta\rho(\mathbf{k}_1)\, \delta\rho(\mathbf{k}_2)\, \delta\rho(\mathbf{k}_3)\,\rangle \underset{k_i \gg m}{\sim} \left[\, \log\left(k_1+k_2+k_3\right) + \gamma_E \,\right]\, \delta^{(3)}\left(\mathbf{k}_1+\mathbf{k}_2+\mathbf{k}_3\right) \quad . \tag{4.16}$$

Nevertheless, most CMB bispectrum measurements are presented nowadays in terms of the Bardeen field Φ, which roughly relates (as it describes a specific metric component) to the curvature by $R \simeq \Box\,\Phi$ in the weak field limit. This supplies an additional factor of $-k^2$ for each field, giving the following explicit prediction for the bispectrum of the Φ field

$$B_{\Phi}^{(\mathrm{CMB})}(\mathbf{k}_1,\mathbf{k}_2,\mathbf{k}_3) \;\equiv\; \langle\, \Phi(\mathbf{k}_1)\, \Phi(\mathbf{k}_2)\, \Phi(\mathbf{k}_3)\,\rangle \underset{k_i \gg m}{\sim} f_{\mathrm{NL}} \cdot \frac{\log\left(k_1+k_2+k_3\right)+\gamma_E}{k_1^2\, k_2^2\, k_3^2}\, \delta^{(3)}\left(\mathbf{k}_1+\mathbf{k}_2+\mathbf{k}_3\right) \quad . \tag{4.17}$$

Here the quantity f_{NL} here represents the overall amplitude for the expected non-Gaussian effects. However, these non-Gaussian amplitudes are expected to be rather small, with very significant suppressions by extra factors of $1/\xi$ [13]. This follows simply from the fact that in real space one has for the two-point function $\langle\, R\, R\,\rangle \sim 1/\xi^2 r^2$, whereas for the scalar curvature three-point function $\langle\, R\, R\, R\,\rangle \sim 1/\xi^3 r^3$, and also $\langle\, R\, R\, R\, R\,\rangle \sim 1/\xi^4 r^4$ etc., where r represents the relevant and appropriate combination of relative distances for each reduced curvature n-point function. More detailed analyses on this issue, and on the magnitude of these bispectra, shall be left for further work. Nevertheless, it should be clear at this point that analogous results, as hinted above, can also be derived for various four-point functions. We note here that the relevance and measurements of such nontrivial (non-Gaussian) three- and four-point matter density correlation functions in observational cosmology were already discussed in great detail some time ago by Peebles in [2]. The results presented here imply that further observational constraints on these higher order n-point functions could potentially provide additional tests on the vacuum condensate picture

for quantum gravity, and more specifically the implications of a non-trivial gravitational scaling dimensions scenario as described previously.

In addition, it is clear that the gravitational fluctuation-based explanation presented here should also give rise to nontrivial tensor perturbations, and with their magnitudes comparable to the scalar one. This could lead to new insights on the corresponding tensor-to-scalar ratio parameter r [87], and to a number of potentially interesting and testable consequences to be explored. Here we note that tensor perturbations first require the knowledge of the semi-classical Ricci tensor (as opposed to scalar curvature) correlation functions,

$$\langle\, R_{\mu\nu}(x_1)\, R_{\rho\sigma}(x_2)\,\rangle \underset{d_{12}\ll\xi}{\sim} \frac{P_{\mu\nu,\rho\sigma}}{(d_{12})^{\Delta}} \ , \tag{4.18}$$

with polarization tensor P and relative geodesic distance $d_{12} = |x_1 - x_2|$ in coordinate space. These correlations have not been measured yet on the lattice, but should be calculable in the near future. Nevertheless, based on the known scaling dimension for the scalar curvature, one would expect here the same result for the operator $R_{\mu\nu}(x)$, namely $\Delta = 2$, as in Eqs. (2.11) and (4.14) for the scalar curvature R case. In turn, these curvature correlation functions can then be related to suitable matter and radiation sources, via the quantum equations of motion

$$R_{\mu\nu}(x) \ = \ 8\pi G\, \left[T_{\mu\nu}(x) - \tfrac{1}{2}\, g_{\mu\nu}(x)\, T^{\lambda}_{\ \lambda}(x)\right] \tag{4.19}$$

with the (trace reversed) $T_{\mu\nu}$ here representing either matter or radiation contributions, and thus in complete analogy to what was used earlier in Eq. (3.3), and following, for the scalar (trace) case. Since the scalar curvature correlation function of Eq. (2.11) involves traces of the Ricci tensor (using the weak field limit here)

$$\langle\, (\, R_{00}(x_1)+R_{11}(x_1)+R_{22}(x_1)+R_{33}(x_1)\,) \cdot (\, R_{00}(x_2)+R_{11}(x_2)+R_{22}(x_2)+R_{33}(x_2)\,)\,\rangle$$

versus say the intrinsically tensor correlation $\langle\, R_{12}(x_1)\, R_{12}(x_2)\,\rangle$, one would expect for the ratio of tensor over scalar correlation amplitudes, based just on Lorentz symmetry, to be $1/4^2 = 1/16$. The translation of these simple results into measurable cosmological predictions is of course a lot more complicated.

In conclusion, the ability to reproduce the cosmological matter power spectrum has long been considered one of the "major successes" for inflation-inspired models. Although within our preliminary study, further limited by the accuracy of present observational data, it is not yet possible to clearly prove or disprove either idea, the possibility of an alternative explanation without invoking the machinery of inflation suggests that the power spectrum may not be a direct consequence nor a solid confirmation of inflation, as some literature may suggest. By exploring in more detail the relationship between gravity and cosmological matter and radiation, together with the influx of new and increasingly accurate observational data, one can hope that this hypothesis can be subjected to further stringent physical tests in the near future.

Chapter 5

Numerical Results

Power spectra play an important role in the theory of inflation, and their ability to reproduce current observational data to high accuracy is often considered a triumph of inflation, largely because of a lack of credible alternatives.

In previous chapters we introduced the alternative picture for the cosmological power spectra – based on the nonperturbative features of the quantum version of Einstein's gravity, instead of currently popular inflation models based on scalar fields.

The key ingredients in the gravitational picture are the appearance of a nontrivial gravitational vacuum condensate (directly related to the observed cosmological constant), and a calculable renormalization group running of Newton's G on cosmological scales. More importantly, one notes the absence of any fundamental scalar fields in this approach.

Results obtained previously were largely based on a semi-analytical treatment, and thus, while generally transparent in their implementation, often suffered from the limitations of various approximations and simplifying assumptions.

In this chapter, we extend and refine our previous calculations by laying out an updated and

extended analysis that utilizes a set of suitably modified state-of-the-art numerical programs (ISiTGR, MGCAMB and MGCLASS) developed for observational cosmology. As a result, we are able to remove some of the approximations employed in our previous studies, leading to a number of novel and detailed physical predictions. These should help in potentially distinguishing the vacuum condensate picture of quantum gravity from that of other models such as scalar field inflation. Besides the matter power spectrum $P_m(k)$, here we work out, in detail, predictions for what are referred to as the TT, TE, EE, BB angular spectra, as well as their closely related lensing spectra. However, the current limited precision of observational data today (especially on large angular scales) does not allow us yet to clearly prove or disprove either set of ideas. Nevertheless, by exploring in more details the relationship between gravity and cosmological matter and radiation both analytically and numerically, together with an expected future influx of increasingly accurate observational data, one can hope that the new quantum gravitational picture can be subjected to further stringent tests in the near future. The chapter is organized as follows. In Section 5.1, we introduce the various numerical programs we used in the study, and in Section 5.2 we present the numerical results and analysis. Finally, key points and future work will be summarized in the overall conclusion next chapter.

5.1 Numerical Programs

There are a variety of publicly available Einstein–Boltzmann (EB) solvers that have been in use for the past two decades starting with CMBFAST [103]. The main independent programs are CAMB [104] and CLASS [105] which solve the coupled Einstein–Boltzmann equations in a background FRW metric. These codes are computed for ΛCDM cosmology with a limited set of choices for a parameterization of equation of state for the Dark Energy (w). In all our programs we use $w = -1$, which considers dark energy as a vacuum energy.

For modifications of gravity with a scale dependent gravitational constant, there are three EB solvers. We used Integrated Software in Testing General Relativity (ISiTGR) [106] as the primary code to generate power spectra. Then we compare with two other programs Modified Growth with CAMB (MGCAMB) [107] and MGCLASS (CLASS version for phenomenological modified gravity) [108]. ISiTGR and MGCAMB are patches for CAMB and COSMOMC [109] which are written in the FORTRAN language, while MGCLASS is a patch for CLASS written in C. All three programs have implemented the parameterization effective gravitational coupling (μ)—gravitation slip parameter (η) which sometimes is denoted as γ. Those two parameters are defined as $\mu(a,k) \equiv G(a,k)/G_0$ and $\eta(a,k) \equiv \Phi/\Psi$ where G_0 is the laboratory value of Newton's gravitational constant and Φ, Ψ are scalar potentials in the conformal Newtonian gauge. The comparison of the three programs for no RG running of G as in standard ΛCDM cosmology is shown in Figures 5.1 and 5.2.

One can see that while all three program's ΛCDM predictions are generally consistent, only ISiTGR's modified Newton's constant patch with $\mu(a,k) \equiv G_{\rm mod}/G_{Newt} = 1$ (or equivalently $c_0 = 0$ in Eq. (2.17)) is consistent with its original default-ΛCDM prediction. Matter power spectrum from MGCLASS has a noticeable upper trend for small k from the ΛCDM curve, as shown in the left plot in Figure 5.1. Figure 5.2 shows a significant deviation of MGCAMB's $C_l^{T\phi}$ from the ΛCDM curve. Primarily due to this reason we chose ISiTGR over these two other programs.

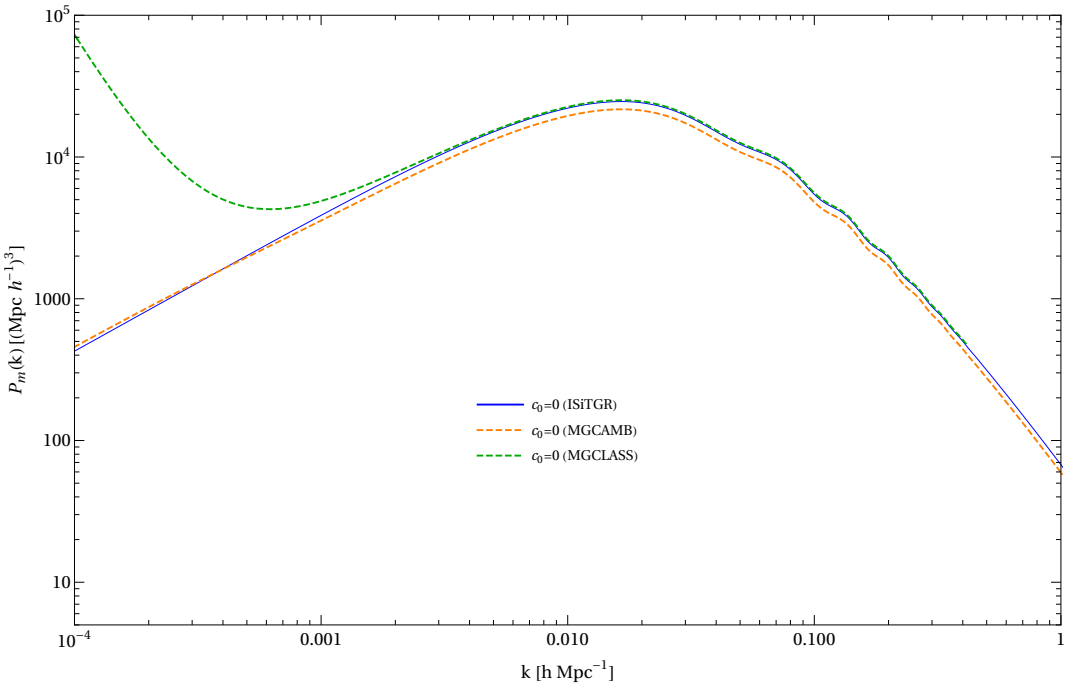

Figure 5.1: As an example we illustrate the $P_m(k)$ predictions between the three programs—Integrated Software in Testing General Relativity (ISiTGR) (blue), Modified Growth with CAMB (MGCAMB) (orange) and Modified Growth with CLASS (MGCLASS) (green)—with their corresponding patches for a modified Newton's constant. This serves as a consistency check between the programs and a validity check for their patches. The solid curves are generated from the respective original ΛCDM programs, while the dashed curves are generated by each program's modified Newton's constant patch setting $\mu(a,k) \equiv G_{\rm mod}/G_{Newt} = 1$. It can be seen that ISiTGR is the most consistent, and hence reliable program of the three, to investigate the effects of a modified Newton's constant.

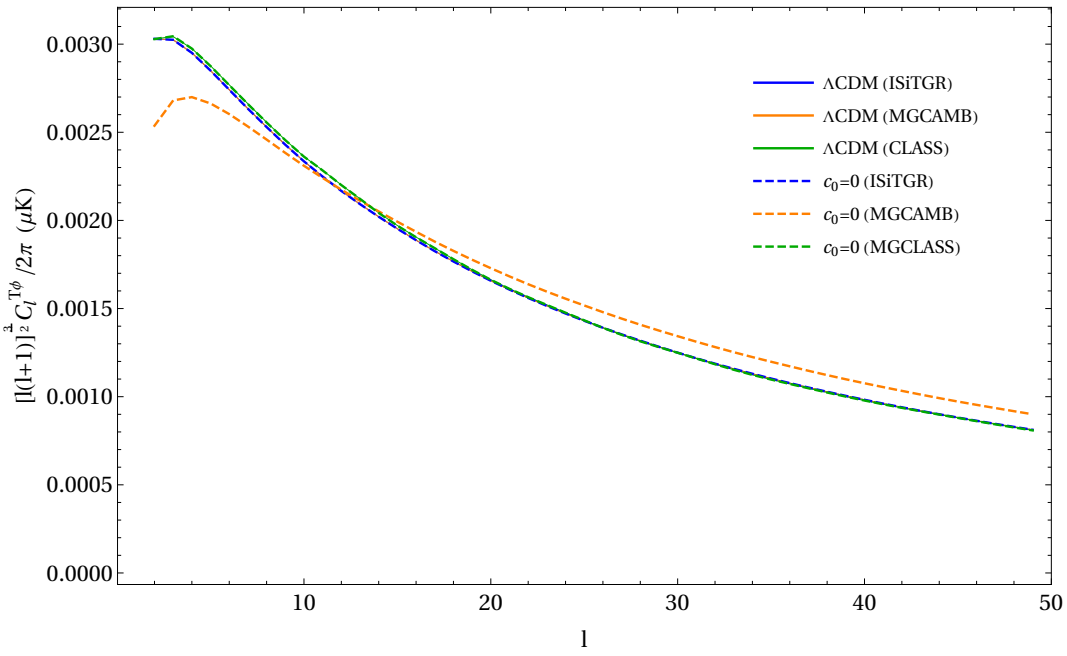

Figure 5.2: Comparison of the $C_l^{T\phi}$ predictions between the three programs—ISiTGR (blue), MGCAMB (orange) and MGCLASS (green)—with their corresponding patches for a modified Newton's constant. This serves as a consistency check between the programs and a validity check for their patches. The solid curves are generated from the respective original ΛCDM programs, while the dashed curves are generated by each program's modified Newton's constant patch setting $\mu(a,k) \equiv G_{\rm mod}/G_{Newt} = 1$. It can be seen that ISiTGR is the most consistent, and hence reliable program of the three, to investigate the effects of a modified Newton's constant.

In the ISiTGR program all times are in conformal time, as is the case for CAMB. The growth equations are written based on a perturbed FLRW metric in the Newtonian gauge,

$$ds^2 = a(\tau)^2 \left[-(1+2\Psi)d\tau^2 + (1-2\Phi)\gamma_{ij}dx^i dx^j\right], \tag{5.1}$$

where Φ and Ψ are scalar gravitational potentials, x_i represents comoving coordinates and $a(\tau)$ is scale factor at conformal time τ. For a flat universe the three dimensional spatial metric γ_{ij} in cartesian coordinates is given by

$$\gamma_{ij} = \delta_{ij}, \tag{5.2}$$

From now on we only discuss cosmology for a spatially flat universe.

There are four built-in functional forms for selected modified cosmologies [110] and we used (μ)- gravitation slip parameter (η) form. The modified growth equations are

$$k^2\Psi = -4\pi\, G a^2 \mu(a,k) \sum_i \left[\rho_i \Delta_i + 3\rho_i \left(1+w_i\right)\sigma_i\right], \tag{5.3}$$

and

$$k^2\left[\Phi - \eta(a,k)\Psi\right] = 12\pi\, G a^2 \mu(a,k) \sum_i 3\rho_i \left(1+w_i\right)\sigma_i \tag{5.4}$$

where w_i and ρ_i are respectively the equation of state and density of ith particle species. Generally there are three species which are radiation, non-relativistic matter and dark energy. Δ_i is the gauge-invariant, rest-frame overdensity defined by,

$$\Delta_i = \delta_i + 3H\frac{q_i}{k} \quad , \tag{5.5}$$

where $H = \dot{a}/a$ is the Hubble's constant in conformal time, fractional overdensity $\delta_i = \delta\rho/\bar{\rho}$ and q_i is the heat flux, related with the peculiar velocity (θ_i)

$$q_i = \theta_i \frac{1+w_i}{k} \quad . \tag{5.6}$$

From the conservation of energy-momentum tensor of the perturbed matter fluids and for uncoupled fluid species Δ_i evolution is given by

$$\Delta_i = 3(1+w_i)\left(\dot{\Phi} + H\Psi\right) + 3Hw_i\Delta_i - \left[k^2 + 3(H^2 - \dot{H})\right]\frac{q_i}{k} - 3H(1+w_i)\sigma_i \quad . \tag{5.7}$$

Secondary effects considered by ISiTGR are reionization, weak gravitational lensing and the integrated Sachs–Wolfe (ISW) effect. For reionization it uses the same approach as in

CAMB [111], namely a simple tanh model for reionization fraction (x_e), given by

$$x_e(y) = \frac{f}{2}\left[1 + \tanh\frac{y(z_{re}) - y}{\Delta_y}\right] \quad , \tag{5.8}$$

where $y(z) = (1+z)^{3/2}$, z_{re} is the red shift value where the $x_e = f/2$, and Δ_y is the fractional change in y. The latter agrees with a Thomson scattering optical depth for an instantaneous reionzation which occurred at z_{re}. The treatment of weak lensing is discussed here later in Section 5.2.

Since the required formulation for $\mu(a, k)$, as appropriate for the quantum RG running of Newton's G as described earlier, does not appear as a built-in function, we added a part with newly defined functions $\mu(a, k)$, $\dot{\mu}(a, k)$ for our need in the above equations. In accordance with Eq. (2.17) we have

$$\mu(a, k) = 1 + 2c_0\left(\frac{m^2}{k^2 + m^2}\right)^{\frac{1}{2\nu}} \quad , \tag{5.9}$$

and $\dot{\mu}(a, k) = 0$.

As secondary effects, ISiTGR considers reionization, weak gravitational lensing and the ISW effect. $\eta(a, k) = 1$ is assumed since there are no different modifications to the potentials. ISiTGR has two binning methods but here we only used the traditional binning method. For all the power spectra computations we set the tensor part to zero. The program computes 2-point self- and cross-correlation functions for the temperature, E-mode and B-mode polarization and weak lensing potential. Each generated power spectrum appears in two separate files, one with lensing and the other without. In the following we use power spectra with gravitational lensing included. The values of the cosmological parameters we used here as initial conditions are shown in Table 5.1.

In our published work [15, 16] we used semi-analytic methods to solve for the matter power

spectra using semi-numerical approximations for the relevant transfer functions. In the current approach the numerical programs solve the full set of Boltzmann equations, and uses integration techniques such as adaptive Runge–Kutta method to integrate all the tightly coupled equations. Secondary effects accounted for like reionization and integrated Sachs–Wolfe (ISW) effect are treated as a more general case compared to our published work.

Table 5.1: Values used here for cosmological parameters in the ΛCDM model. We have used the Planck-18 68% interval from CMB power spectra, in combination with CMB lensing reconstruction and Baryonic Acoustic Oscillations (BAO).

Parameter	**Symbol**	**Value**
barryon density	$\Omega_b h^2$	2.242×10^{-2}
cold dark matter density	$\Omega_c h^2$	1.1933×10^{-1}
acoustic scale angle	$100\ \theta_*$	1.04
scalar amplitude	A_s	2.105×10^{-9}
reionization optical depth	τ	5.61×10^{-2}
scalar tilt	n_s	0.9665
Hubble constant	H_0	67.66 km $s^{-1}$$Mpc^{-1}$
curvature density	Ω_k	0
effective extra relativistic degrees of freedom	N_{eff}	3.046
CMB temperature	*temp_cmb*	2.7255 K
equation of state of dark energy	w	-1

5.2 Numerical Results

In this section we present numerical results for the quantum gravitational corrections to the various cosmological spectra ($P_m(k)$, C_l^{TT}, C_l^{TE}, C_l^{EE}, ...). This includes both the effects of

an RG running of Newton's constant and the IR regulation, collectively achieved by replacing

$$G \;\to\; G(k) = G_0 \left[1 + 2\, c_0 \left(\frac{m^2}{k^2 + m^2} \right)^{3/2} + \mathcal{O}\left(\left(\frac{m^2}{k^2 + m^2} \right)^3 \right) \right] \quad . \tag{5.10}$$

For simplicity, of the three numerical programs used for our analysis (ISiTGR, MGCAMB, MGCLASS), only the results from the ISiTGR numerical program shall be plotted. The reason for this choice is that we expect this program to provide better consistency and reliability in the particular region considered (small k, small l), as explained in Section 5.1. Furthermore, all numerical results presented here are generated using the latest values of the cosmological parameters as given by Planck (2018) [17].

In the above, c_0 is the coefficient that governs the amplitude of quantum corrections. For all the following spectra, three different values of $c_0 = 0$, 1.146 and 8.02 will be plotted. Lattice calculations give $c_0 \approx 8$. However, being a non-universal parameter, it can depend on specific choices arising from the way an ultraviolet cutoff is imposed. Therefore, not too much weight should not be placed on this specific value, beyond perhaps the order of magnitude. In practice, this value could be further constrained by experiments, which is precisely what these observations of cosmological spectra can achieve. From our work published in [16], using the approximate semi-analytical methods, we see that a value of $8.02/7 \simeq 1.146$ is generally favored.

5.2.1 Matter Power Spectrum $P_m(k)$

We start with the matter power spectrum $P_m(k)$. Recall the definitions

$$G_\rho(r; t, t') \equiv \langle\, \delta_\rho(\mathbf{x}, t)\; \delta_\rho(\mathbf{y}, t') \,\rangle \quad , \quad P_m(k) \sim \langle\, \delta_\rho(\mathbf{k})\; \delta_\rho(-\mathbf{k}) \,\rangle \quad , \tag{5.11}$$

where the variable $\delta_\rho \equiv (\rho - \bar{\rho})/\bar{\rho}$ is the fractional density fluctuations above the average, referred to in cosmology as the mass-density contrast. The numerical results for $P_m(k)$ obtained from the numerical program (ISiTGR) for both the classical ΛCDM (i.e., $c_0 = 0$) and quantum ($c_0 > 0$) results, as well as the respective analytical results (as derived in [15, 16]), are shown and compared in Figure 5.3.

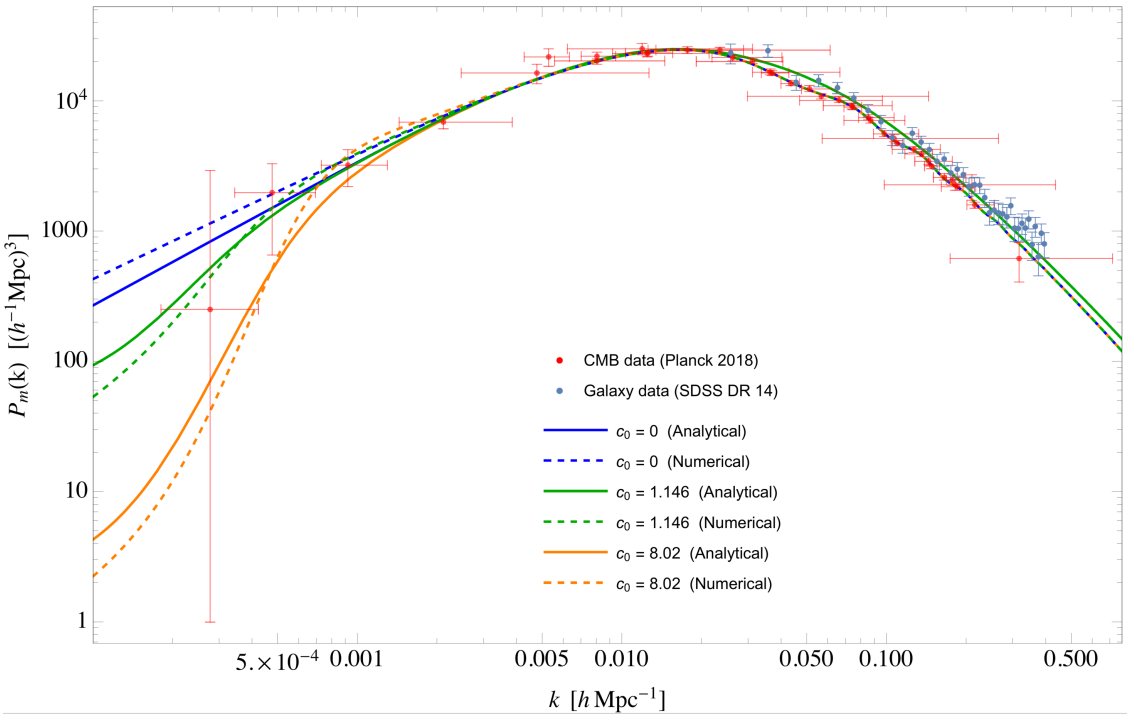

Figure 5.3: Comparison between analytical vs. numerical predictions of the RG running of Newton's constant's effect on the matter power spectrum $P_m(k)$. The solid curves represent the analytical predictions, with the top (blue), middle (green) and bottom (orange) representing the quantum amplitude quantum amplitudes (see Eq. (2.17)) $c_0 = 0, 1.146, 8.02$, respectively (see Eq. (2.17)). The corresponding dashed curves represent the corresponding numerical predictions generated by ISiTGR, showing very good general consistency with the trend derived from analytical methods. The observational CMB and galaxy data points taken from the Planck (2018) collaboration and Sloan Digital Sky Survey (SDSS)'s 14th Data Release (DR14) are also shown.

From Figure 5.3, we see that all the numerical results are generally consistent with the corresponding analytical results from the work obtained by following the semi-analytical interpolating formulas from [18], and the implementation of the RG running following dimensional arguments. The small deviations may be attributed to the slightly older values of cosmo-

logical parameters [112] and some analytic approximations used by Weinberg and Dicus' interpolating formula for the transfer function in [18], whereas the numerical results presented here use the latest cosmological parameter values from the Planck collaboration [17]. Despite the small discrepancies, we see that the overall trends, and the extra downwards bend due to the inclusion of the (IR regulated) RG running of Newton's constant as predicted analytically using the semi-analytical formulas, are in very good agreement with the numerical predictions using the latest-fitted cosmological parameters. This overall general agreement between the analytical and numerical result provides a good verification and confidence that the procedure of including a running Newton's constant as presented above is reliable.

The same numerical analysis has now been repeated with the other two numerical programs MGCAMB and MGCLASS, besides ISiTGR. The result of MGCAMB is in extremely good agreement with ISiTGR, with its predictions for all three values of c_0 almost completely overlapping with ISiTGR's result, giving additional confidence to the latter. However, while MGCLASS is relatively consistent with ISiTGR for most of the angular spectrum results (as we will discuss later), its prediction for $P_m(k)$ shows a rather radical upturn below $k = 10^{-3}$, which is at odds with both ISiTGR and MGCAMB, as well as the analytical predictions (also shown and discussed earlier in Figure 5.1 and then in Section 5.1), even for the $c_0 = 0$ ΛCDM case. The pathological upturn at small-k and resultant disagreement of MGCLASS (even with CLASS, the original ΛCDM program that MGCLASS is based on, when setting $c_0 = 0$) suggests some potentially unresolved issues in MGCLASS's prediction for $P_m(k)$, while the consistent results between ISiTGR, MGCAMB and the analytical predictions should be treated in our opinion with a higher reliability.

Given the more reliable (and in principle more accurate) predictions from the numerical programs as shown in Figure 5.3, it can be seen that the value of $c_0 \simeq 1.146$ is a better overall fit to the observational data from Planck, which is a consistent conclusion from our

work that was based exclusively on the early analytical results [16]. Armed with the new tools of numerical programs, we now move on to present the numerical results for the other various correlation functions, which will hopefully shed new insights to the validity of the quantum gravity effects in cosmology.

It should be noted that there is a slight degeneracy between c_0 and ξ in the original expression for the RG running of Newton's G, as in Eq. (2.17). Support of a smaller c_0 from the observational data can equivalently be mimicked by an increase in the vacuum condensate scale ξ. In fact, the apparently better fit value of $c_0 \simeq 1.146$, seven times smaller than the lattice predicted value of $\approx 8.0 \pm 3.1$, can be mimicked by simply a factor of ~ 1.9 times larger in ξ. Technically, including IR regulation will change the shape of the curve and break the degeneracy, which in principle could be fitted in a more sophisticated way, say, with a Monte Carlo simulation. However, not only is such an exercise beyond the current scope of this dissertation, the scarcity and imprecision of data points in the small-k regime do not render this exercise fruitful as well at this stage either.

On the other hand, it may be instructive, amongst other physical motivations, to look at the quantum effects on a variety of other spectra of cosmological significance with these numerical programs. With independent quantities and measurements, the new plots may not only provide additional constraints to these quantum gravitational parameters, but also potential insights to the physics.

5.2.2 Angular Temperature Power Spectrum C_l^{TT}

The TT power spectrum is one of the most important cosmological spectra since it has been measured to a high degree of accuracy, thus potentially allowing for great insights in constraining various cosmological models. Figure 5.4 shows the numerical predictions for the temperature-temperature (TT) angular power spectrum C_l^{TT} with and without the quantum

effects. We will first briefly recall the definitions for C_l^{TT} and how theoretical predictions for it can be obtained, and then compare them against observational data. Following notations in Weinberg [18], the temperature fluctuations ΔT can first be resolved into spherical harmonics $Y_l^m(\hat{n})$'s,

$$\Delta T(\hat{n}) \equiv T(\hat{n}) - T_0 = \sum_{lm} a_{lm}^T Y_l^m(\hat{n}) \ , \tag{5.12}$$

where $T(\hat{n})$ is the temperature in the direction $\hat{n}$, $T_0 \equiv (1/4\pi)\int d^2\hat{n}\ T(\hat{n})$ is the average temperature over the sky and the coefficients a_{lm}^T quantifies the fluctuation for each harmonic. Since ΔT's are real, and the products of ΔTs are rotationally invariant, one has

$$\left\langle \Delta T(\hat{n})\, \Delta T(\hat{n'}) \right\rangle = \sum_{lm} C_l^{TT}\, Y_l^m(\hat{n}) Y_l^{-m}(\hat{n'}) = \sum_l C_l^{TT} \left(\frac{2l+1}{4\pi}\right) L_l(\hat{n}\cdot\hat{n'}) \ . \tag{5.13}$$

Here the L_l's are the Legendre polynomials, and C_l^{TT} is defined as

$$\left\langle a_{lm}^T\, a_{l'm'}^T \right\rangle \equiv \delta_{ll'}\delta_{m-m'}\, C_l^{TT} \ , \tag{5.14}$$

the 2-point correlation functions of a_{lm}^T, the temperature fluctuation in "l"-space. Or equivalently,

$$C_l^{TT} = \frac{1}{4\pi}\int d^2\hat{n}\, d^2\hat{n'}\ \left\langle \Delta T(\hat{n})\, \Delta T(\hat{n'}) \right\rangle L_l(\hat{n}\cdot\hat{n'}) \ , \tag{5.15}$$

by inverting the transformation. As a result, the correlations for temperature-temperature fluctuations are fully quantified with the C_l^{TT}s. (Note that here we use L_l instead of the usual notation P_l for the Legendre polynomials in order to avoid confusion with the matter power spectra.)

Theoretically, since CMB photon temperatures and matter density are coupled, the C_l^{TT}s are therefore related to the matter power spectrum $P_m(k)$ via integral transforms that involve

spherical Bessel functions and appropriate form factors and transfer functions. However, from transforming the predictions from one set of observable to another, new insights (and potential constraints) to the theory can be derived.

To do so, one can first use the Friedmann and continuity equations to relate temperature fluctuations to metric perturbations via suitable form factors $F_{1,2}(q)$, through

$$\left(\frac{\Delta T(\hat{n})}{T_0}\right) = \int d^3q \; e^{i\mathbf{q}\cdot\hat{n}\, r(t_L)} \left[\, F_1(q) + i\hat{q}\cdot\hat{n}\; F_2(q)\,\right] \quad , \tag{5.16}$$

where the latter are defined as

$$F_1(q) = -\frac{1}{2}\, a^2(t_L)\ddot{B}_q(t_L) - \frac{1}{2} a(t_L)\, \dot{a}(t_L)\dot{B}_q(t_L) + \frac{1}{2}E_q(t_L) + \frac{\delta T_q(t_L)}{\bar{T}(t_L)} \quad , \tag{5.17}$$

and

$$F_2(q) = -q\left(\frac{1}{2}\, a(t_L)\dot{B}_q(t_L) + \frac{\delta u_{\gamma q}(t_L)}{a(t_L)}\right) \quad . \tag{5.18}$$

Here the B and E functions are suitable decompositions of the metric perturbations, and δu_γ is the velocity potential for the CMB photons. It is known that these form factors become simplified in certain gauge choices. In the synchronous gauge, one has $E = 0$, whereas in the Newtonian gauge $B = 0$ and $E = 2\Phi$, which then gives

$$F_1(q) = \Phi_q(t_L) + \frac{\delta T_q(t_L)}{\bar{T}(t_L)} \quad , \tag{5.19}$$

and

$$F_2(q) = -\frac{\delta u_{\gamma q}(t_L)}{a(t_L)} \quad . \tag{5.20}$$

(Note that $F_1(q)$ and $F_2(q)$ are referred to as "$F(q)$" and "$G(q)$", respectively, in [18]. Here

we use the former in order to avoid confusion with the expression for the running of Newton's constant $G(k)$, as it will be implemented below. The above equations also assume a sudden transition to opacity on the CMB at a time t_L, which does not change the form of the basic equations and only some of the details, and are later taken into account fully with the numerical programs, as discussed below.)

Hence, given appropriate initial conditions, the functions Φ and δu_γ, as well as the scale factor $a(t)$ and the function $T(t)$, can all be obtained as solutions of the classical Friedmann equations. These are then combined with the Boltzmann transport equations, as is done in standard cosmology, which eventually leads to unambiguous predictions for the C_l's. The solutions for $F_{1,2}(q)$ can be parameterized in terms of transfer functions $\mathcal{T}(\kappa)$, $\mathcal{S}(\kappa)$ and $\Delta(\kappa)$, leading to the following expressions for $F_1(q)$ and $F_2(q)$

$$F_1(q) = \frac{\mathcal{R}_q^o}{5}\left[3\,\mathcal{T}\left(\frac{q\,d_T}{a_L}\right)R_L\,-\,(1+R_L)^{-\frac{1}{4}}\,e^{-\left(\frac{q\,d_D}{a_L}\right)^2}\mathcal{S}\left(\frac{q\,d_T}{a_L}\right)\,\cos\left[\frac{q\,d_H}{a_L}+\Delta\left(\frac{q\,d_T}{a_L}\right)\right]\right]\,, \tag{5.21}$$

and

$$F_2(q) = \sqrt{2}\,\frac{\mathcal{R}_q^o}{5}\,(1+R_L)^{-\frac{3}{4}}\,e^{-\left(\frac{q\,d_D}{a_L}\right)^2}\mathcal{S}\left(\frac{q\,d_T}{a_L}\right)\,\sin\left[\frac{q\,d_H}{a_L}+\Delta\left(\frac{q\,d_T}{a_L}\right)\right] \tag{5.22}$$

where $a_L = a(t_L) = 1/(1+z_L)$, $z_L = 1090$, $d_T = 0.1331$ Mpc, $d_H = 0.1351$ Mpc, $d_D = 0.008130$ Mpc, $d_A = 12.99$ Mpc and $R_L \equiv 3\Omega_B(t_L)/4\,\Omega_\gamma(t_L) = 0.6234$ (the latest set of suitable parameters are taken from Planck 2018 [17]). It is noteworthy at this stage to point out again that all three transfer functions are completely determined by standard measured cosmological parameters, so that the only remaining ingredient to fully determine the C_l^{TT} coefficients is the initial (or primordial) spectrum $\mathcal{R}_q^o$, where q is the wavenumber, and "o" refers to outside the horizon. Conventionally, $\mathcal{R}_q^o$ is parameterized by an amplitude N and

spectral index n_s,

$$\mathcal{R}^o_q = N\, q^{-3/2} \left(\frac{q}{q_{\mathcal{R}}}\right)^{(n_s-1)/2} \quad . \tag{5.23}$$

Here the reference "pivot scale" is usually taken to be $q_{\mathcal{R}} = 0.05\,\mathrm{Mpc}^{-1}$ by convention. As a consequence, once the primary function $\mathcal{R}^o_q$ is somehow determined, classical cosmology is then expected to fully determine the form of the C_l^{TT} spectral coefficients. It is therefore possible to write the C_l^{TT}'s fully and explicitly in terms of the primary function $\mathcal{R}^o_q$. After expanding the plane waves factor in a complete set of spherical harmonics and spherical Bessel functions, C_l^{TT} from Eq. (5.15) becomes

$$C_l^{TT} = 16\pi^2\, T_0^2 \int_0^\infty q^2\, dq\ \left(\mathcal{R}^0_k\right)^2 \Big[\, j_l(qr_L)\widetilde{F_1}(q) + j_l'(qr_L)\widetilde{F_2}(q)\,\Big]^2 \quad , \tag{5.24}$$

where $r_L = r\,(t_L)$, and we have factored out the function $\mathcal{R}^o_q$ explicitly by defining $F_1(q) = (\mathcal{R}^o_q)\,\widetilde{F_1}(q)$ and $F_2(q) = (\mathcal{R}^o_q)\,\widetilde{F_2}(q)$.

Now, recall that the matter power spectrum $P_m(k)$ is given by

$$P_m\,(k) = C_0\left(\mathcal{R}^0_k\right)^2\ k^4\,[\mathcal{T}(\kappa)]^2 \ , \tag{5.25}$$

which tells us that we can obtain a direct relation between the matter power spectrum $P_m(k)$ and the angular temperature coefficients C_l^{TT},

$$C_l^{TT} = 16\pi^2\ T_0^2 \int_0^\infty q^2 dq\ P_m(q)\,\big[\, C_0\, k^4\, \mathcal{T}(\kappa)^2\,\big]^{-1}\,\Big[\, j_l(qr_L)\widetilde{F_1}(q) + j_l'(qr_L)\widetilde{F_2}(q)\,\Big]^2 \ , \tag{5.26}$$

where q and k are related by $q = a_0 k$, and the scale factor "today" a_0 can be taken to be 1. As a result, the predictions on $P_m(k)$ can be directly transformed into a prediction for C_l^{TT}. Utilizing the same parameters in numerical programs, the effects of with and without the RG running of Newton's constant (with IR regulation) on C_l^{TT} can then be generated.

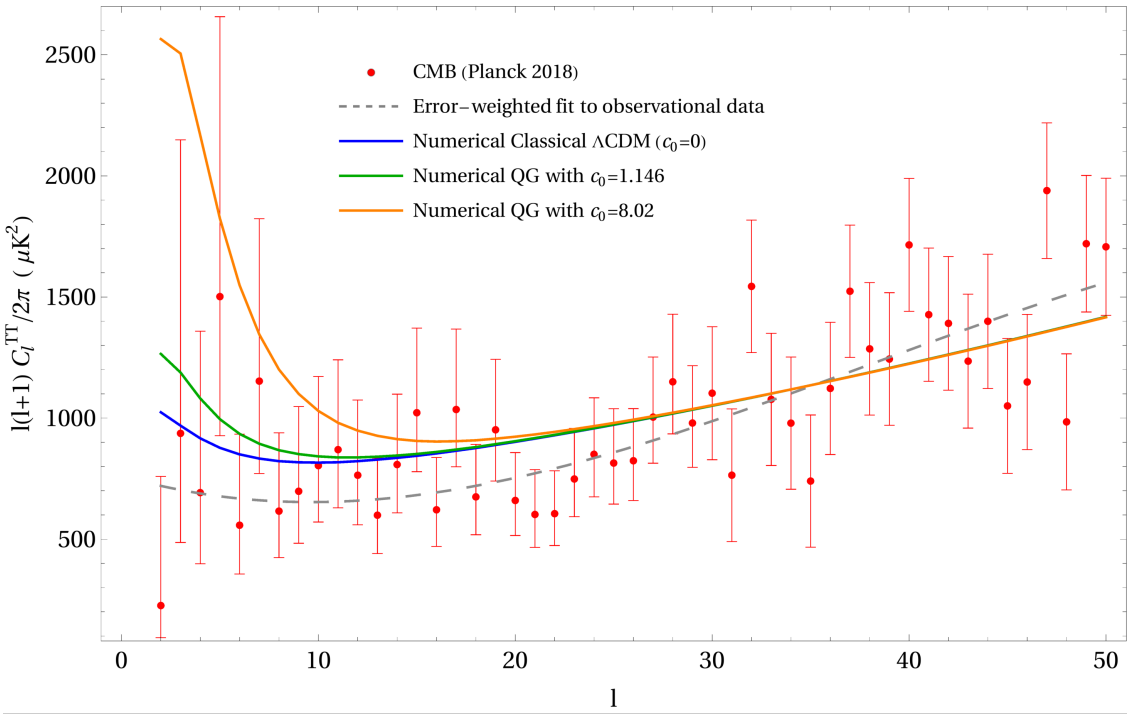

Figure 5.4: Comparison of the numerical prediction of the classical ΛCDM program vs. the numerical predictions of the renormalization group (RG) running of Newton's constant's effect on the temperature (TT) power spectrum C_l^{TT}. The solid curves represent the numerical predictions generated by the ISiTGR program, with the bottom (blue), middle (green) and top (orange) representing quantum amplitudes (see Eq. (2.17)) $c_0 = 0, 1.146, 8.02$, respectively (see Eq. (2.17)), showing a higher trend at large angular scales ($l < 20$) as compared to the classical ΛCDM (no running) numerical curve. The dashed curve represents an error-weighted cubic fit to the observational CMB data, from the Planck (2018) collaboration .

Figure 5.4 shows the numerical result of $c_0 = 0$ (no running), 1.146, and 8.02 with the blue, green and orange curves, respectively, generated by ISitGR. The observational CMB data from Planck (2018), as well as an error-weighted cubic fit for reference, are also shown. Noticing that the point $l = 2$ is anomalously low, with large uncertainty due to cosmic variance, the error-weighted fit shown in this plot has not included the $l = 2$ point.

From Figure 5.4, we see that the effects of a RG running of Newton's constant generally cause an upturn to the spectrum at low-ls, starting at roughly $l = 20$. It can also be seen that the orange curve with a quantum amplitude (see Eq. (2.17)) $c_0 = 8.02$ (or $\xi = 5300$ Mpc) creates

a much more dramatic deviation, reaching a maximum of 140% larger in value compared to the blue, classical ($c_0 = 0$) ΛCDM curve, while the green curve with $c_0 = 1.146$ (or roughly $\xi \simeq 2.65 \times 5300 = 14{,}000$ Mpc) has a milder deviation of ≈24% from the classical result. Again, neglecting the anomalous $l = 2$ point, the green curve with $c_0 = 1.146$ is generally consistent with all observational data, arguably also with the desirable feature of marginally going through the error bars of $l = 5$ and $l = 6$. On the other hand, the orange $c_0 = 8.02$ curve, while still lying within a few points' error margins, is less favorably supported by the data in this plot. It is also seen that its deviation starts earlier at a higher value around $l \sim 22$, which causes it to miss a few more error bars in the low l points. As a result, the numerical results of this TT plot shows that the green $c_0 = 1.146$ (or $\xi \approx 14{,}000$ Mpc) curve is currently a more favorable parameter than the orange one. Note that this is also consistent with the discussion and conclusion from the matter power spectrum $P_m(k)$ plot in Figure 5.3.

We also investigated the results with all 3 programs. However unlike $P_m(k)$, the three programs do not agree, despite being supplied with the same RG modified expression for Newton's constant. Figure 5.4 displays the result from ISiTGR, which seems to be the most consistent among all plots. MGCAMB produces a much more dramatic upturn effect from the RG running at small ls, roughly having its $c_0 = 1.146$ curve coinciding with ISiTGR's $c_0 = 8.02$ curve, and the MGCAMB $c_0 = 8.02$ curve even higher. On the other hand, MGCLASS predicts a much milder upturn, with its $c_0 = 8.02$ curve almost coinciding with ISiTGR's $c_0 = 1.146$ curve. In other words, MGCAMB seem to predict an upturn around 7 times larger than ISiTGR, while MGCLASS seem to predict an upturn that is 7 times smaller than ISiTGR. Given the blackbox nature of such programs, the cause of this difference is unclear given that all programs were supplied with the same modification in Newton's G. These programs, designed for modified gravity models, are known to be less well-tested compared to their base program (CAMB, CLASS), and it may not be surprising that two (or all) of them may be incorrect. One consistency is that all three programs predicts an

upturn at low l's, just to a different degree, roughly ± 1 order of magnitude. Hence, the best we can conclude from these available programs is that the RG running of Newton's G causes an upturn to roughly the order of magnitude presented in Figure 5.4.

Perhaps even more intriguing is the disagreement with a naive analytical analysis. From Eq. (5.26), the first order estimate is that since C_l^{TT} is the (weighted) integral of $P_m(k)$ over all k, a smaller $P_m(k)$ caused by an RG running (c.f. Figure 5.3) should cause a smaller value of C_l^{TT}. In fact, if one assumes the transfer functions are not affected by the quantum corrections, the integral Eq. (5.26) can be performed numerically (as done in [16]), since the classical interpolating formulas for the transfer functions are known, which does show a downturn, as naively expected, instead of an upturn. This work utilizes programs that in principle modifies the initial Friedmann and Boltzmann equations from the beginning, and includes any effects of the RG modified Newton's G into the solutions, and thus in principle more trustworthy. Given the opaque nature of such programs, it would require further investigations through a more detailed study of the entangled initial set of coupled differential equations to fully understand the disagreements between the programs and the first-order analytical result, as well as the disagreement (and hence the reliability) within the numerical programs.

Nevertheless, given that these programs represent the most sophisticated state-of-the-art tools to date, it is still constructive to look at their predictions of the quantum effects on other modes and variables of the CMB. For example, the theoretical predictions for the percentage deviations for $c_0 = 1.146$ curve with the classical curve is $\sim$37% on $P_m(k)$ at its further available data point, while it is only $\sim$24% on C_l^{TT}. This reveals the fact that the quantum effects maybe more significant in different physical variables. So by studying the predictions for different auto- and cross-correlations of different variables, and comparing them to potentially independent data (e.g., ground-based measurements of E- and B-mode polarizations as opposed to space-based measurements of CMB temperature), new

constraints and insight may be deduced. We will present the analysis and results of the other spectra of interest to cosmology in the remaining of this section.

5.2.3 Temperature-E-Mode Power Spectrum C_l^{TE}

The next few most popularly studied correlations on the CMB are the so-called E- and B-type polarization modes. Here we will give a brief recap of the physics, and present the numerical results of the quantum corrections from a RG running Newton's constant, later compared with the observational data.

Recall that observations of the CMB photons not only reveal their intensity (i.e., temperature) from various directions, but also the photons' polarizations, which can result from scattering on free electrons either at the time of recombination, or during the later period of reionization. Measurements on polarizations then reveal extra information in constraining the parameters arising from a running of Newton's constant.

Following notations in [18], CMB photon distributions are fully described through a number density matrices $n^{ij}(\mathbf{x}, \mathbf{p}, t)$, or, more usefully, the dimensionless version of its perturbation $J_{ij}(\mathbf{x}, \hat{p}, t)$ (referred to as the dimensionless photon intensity perturbation matrix), related to n^{ij} via

$$J_{ij}(\mathbf{x}, \hat{p}, t) \equiv \frac{1}{a^2(t)} \frac{1}{\bar{\rho_\gamma}(t)} \int_0^\infty 4\pi\, p^3 dp\; \delta n^{ij}(\mathbf{x}, p\hat{p}, t)\ . \tag{5.27}$$

In a line-of-sight direction $\hat{n}$, J_{ij} can be parameterized via

$$J_{ij}(\mathbf{x}, -\hat{n}, t) = \frac{2}{T_0} \begin{pmatrix} \Delta T(\hat{n}) + Q(\hat{n}) & U(\hat{n}) - iV(\hat{n}) & 0 \\ U(\hat{n}) + iV(\hat{n}) & \Delta T(\hat{n}) - Q(\hat{n}) & 0 \\ 0 & 0 & 0 \end{pmatrix}\ , \tag{5.28}$$

where Q, U and V are three real functions of direction (with units of temperature), known as the Stokes parameters, describing the photon's polarizations. Notice that the photon temperature perturbations are given by the trace

$$\frac{\Delta T(\hat{n})}{T_0} = \tfrac{1}{4}\, J_{ii}(0, -\hat{n}, t_0) \ . \tag{5.29}$$

It is these Stokes parameters that are measured in current observations of the CMB. Since the scattering of light by non-relativistic electrons does not produce circular polarization, one expects that all CMB photons will be linearly polarized, so that J_{ij} is real, and therefore $V = 0$. For further convenience in comparing with observations of 2-point functions, which respect spherical symmetry, it is useful to expand the Stokes parameters $Q(\hat{n})$ and $U(\hat{n})$ seen in a direction $\hat{n}$ in a series of functions $\mathcal{Y}_l^m(\hat{n})$

$$Q(\hat{n}) + iU(\hat{n}) = \sum_{l=2}^{\infty} \sum_{m=-l}^{l} a_{P,lm}\, \mathcal{Y}_l^m(\hat{n}) \ , \tag{5.30}$$

$$\mathcal{Y}_l^m(\hat{n}) \equiv 2 \sqrt{\frac{(l-2)!}{(l+2)!}}\, e_{+i}(\hat{n})\, e_{+j}(\hat{n})\, \tilde{\nabla}_i \tilde{\nabla}_j\, Y_l^m(\hat{n}) \ , \tag{5.31}$$

where the subscript "P" in the coefficient $a_{P,lm}$ stands for "polarization", $\tilde{\nabla}$ is the angular part of the gradient operator and $\mathbf{e}_{\pm}(\hat{n}) = (1, \pm i, 0)/\sqrt{2}$ are the polarization vectors in the direction $\hat{n}$. To further satisfy the reality condition, one defines the amplitudes

$$a_{E,lm} \equiv -\left(a_{P,lm} + a_{P,lm}^*\right)/2 \ \ , \quad a_{B,lm} \equiv i\left(a_{P,lm} - a_{P,lm}^*\right)/2 \ , \tag{5.32}$$

so that their correlation functions

$$\left\langle a_{T,lm}^*\, a_{T,l'm'} \right\rangle = C_l^{TT}\, \delta_{ll'}\, \delta_{mm'} \ , \tag{5.33}$$

$$\left\langle a^*_{T,lm}\, a_{E,l'm'} \right\rangle = C_l^{TE}\, \delta_{ll'}\delta_{mm'} \ , \tag{5.34}$$

$$\left\langle a^*_{E,lm}\, a_{E,l'm'} \right\rangle = C_l^{EE}\, \delta_{ll'}\delta_{mm'} \ , \tag{5.35}$$

$$\left\langle a^*_{B,lm}\, a_{B,l'm'} \right\rangle = C_l^{BB}\, \delta_{ll'}\delta_{mm'} \ , \tag{5.36}$$

are real and rotationally invariant. The above relations define the various angular power spectrum functions C_l^{XX}, where $X = T, E, B$. The superscripts E and B are referred to as E- and B-type polarization, respectively, since under spatial-parity inversion, $a_{E,lm} \mapsto (-1)^l\, a^*_{E,lm}$, and similarly for $a_{T,lm}$, whereas $a_{B,lm} \mapsto -(-1)^l\, a^*_{B,lm}$. As a result of parity, there are no bilinear correlations between B and either E or T. (i.e., $C_l^{TB} = C_l^{EB} = 0$.)

With this background, we shall present the numerical predictions for the corresponding spectra with and without an RG running of Newton's G, compared against the latest observational data. We start with the TE spectrum. Figure 5.5 shows the numerical results with the observational data for C_l^{TE}. The lowest solid (blue) curve represents the classical ($c_0 = 0$) spectrum, while the solid middle (green) and top (orange) curve represents the effect of a RG running Newton's constant with $c_0 = 1.146$ and 8.02, respectively.

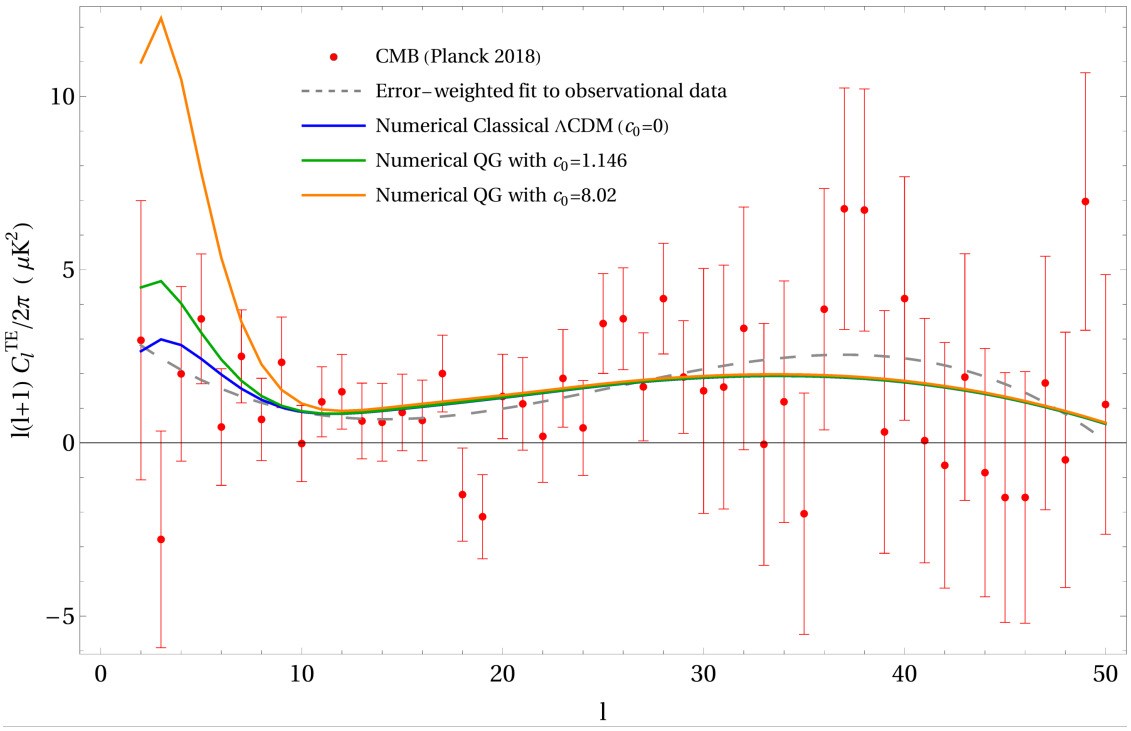

Figure 5.5: Comparison of the numerical prediction of the classical ΛCDM program vs. the numerical predictions of the RG running of Newton's constant's effect on the cross-temperature-E-mode-polarization (TE) power spectrum C_l^{TE}. The solid curves represent the numerical predictions generated by the ISiTGR program, with the bottom (blue), middle (green) and top (orange) representing quantum amplitudes (see Eq. (2.17)) $c_0 = 0, 1.146, 8.02$, respectively. Here again one finds higher trends at large angular scales ($l < 10$) as compared to the classical (no running) numerical ΛCDM curve. The dashed curve represents an error-weighted cubic fit to the observational CMB data from Planck (2018) .

It turns out new constraints for the RG running parameter c_0 can be deduced with this new plot. With the inclusion of the E-type polarization data, we see that this has further constraints on some of the error bars in the low-l data points. This is due to the smaller error bars from the observational data in the E-type polarization correlations in the low-l regime (see Figure 5.6). As a result, one sees that the top $c_0 = 8.02$ curve (orange) is strongly disfavored by this plot. Another observation is that the difference between the $c_0 = 1.146$ and the classical ΛCDM ($c_0 = 0$) curve is about 60% in this TE plot, which is a larger percentage deviation compared to ≈24% for the TT plot.

We also compared the results from the other two programs (MGCLASS and MGCAMB,

not shown on Figure 5.5). All the resultant curves of MGCLASS agree with ISiTGR for $l > 30$. But for $l < 30$, the $c_0 = 8.02$ curve of MGCLASS is about 36% lower than the corresponding ISiTGR curve. All two curves with RG running from MGCLASS are within the error bars but due to the mismatch as shown in the Figure 5.1, MGCLASS results should be investigated further. For MGCAMB, the curves with RG running are significantly higher than ISiTGR, making them disfavored. In addition, there is a slight horizontal shift for MGCAMB in l-space compared to the other two program, which should be investigated further.

5.2.4 EE- Power Spectrum C_l^{EE}

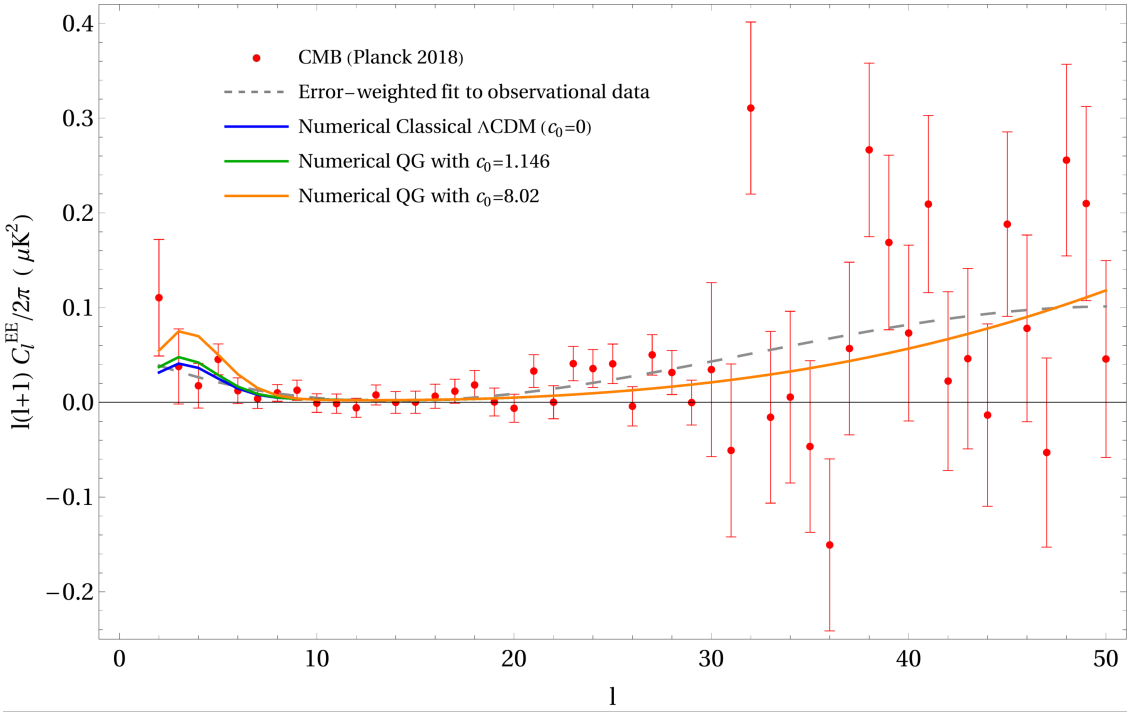

Figure 5.6: Comparison of the numerical prediction of the classical ΛCDM program vs. the numerical predictions of the RG running of Newton's constant's effect on the E-mode (EE) power spectrum C_l^{EE}. The solid curves represent the numerical predictions generated by ISiTGR, with the bottom (blue), middle (green) and top (orange) representing quantum amplitudes (see Eq. (2.17)) $c_0 = 0, 1.146, 8.02$, respectively, showing slightly higher trends for large angular scales ($l < 10$) as compared to the classical (no running) numerical ΛCDM curve. The dashed curve represents error-weighted cubic fit for observational CMB data from the Planck (2018) collaboration.

We move on to the EE spectrum. Figure 5.6 shows the numerical results with the observational data for C_l^{EE}. We also plotted an error-weighted cubic fit (dashed line) for the classical ($c_0 = 0$) spectrum (solid blue), as well as the quantum RG running of G for the above values for c_0 (green and orange). It can be seen that there is no significant deviation from standard ΛCDM prediction like in temperature power spectra and all the curves are well within the data point error bars. We can see that in the large scales ($l < 20$) the errors are significantly small which makes T-E spectrum having smaller error bars in the scale of interest in this paper.

When the other two programs are compared, there is no significant deviation to rule out any any curve. There is no noticeable deviation for MGCAMB curves from ISiTGR for $l < 20$ but there is a slight upward deviation for $l > 20$. With MGCLASS, the curves with RG running of G are lower than those of ISiTGR, making smaller deviation from ΛCDM curve.

5.2.5 BB- Power Spectrum C_l^{BB}

Next we discuss B-mode polarization power spectrum shown in Figure 5.7. We have plotted an error-weighted quadratic fit (dashed line) for the classical ($c_0 = 0$) spectrum (solid blue), as well as the RG varying of Newton's G for $c_0 = 1.146$ (green). It can be seen that there is no noticeable deviation from standard ΛCDM prediction like in the temperature power spectra, and all the curves are well within the data point error bars. As a result of the unnoticeable deviation, we did not include the $c_0 = 8.02$ curve. In standard cosmology, due to weak lensing, there is a partial conversion of the E-mode to the B-mode polarization that is predicted to be considerable around the $l \sim 1000$ scale, which leaves the actual values of C_l^{BB} close to zero on the large angular scales ($l < 30$). Also, due to limitations in dust modeling and telescope technology, there are only data up to $l = 29$, as shown in Figure 5.7.

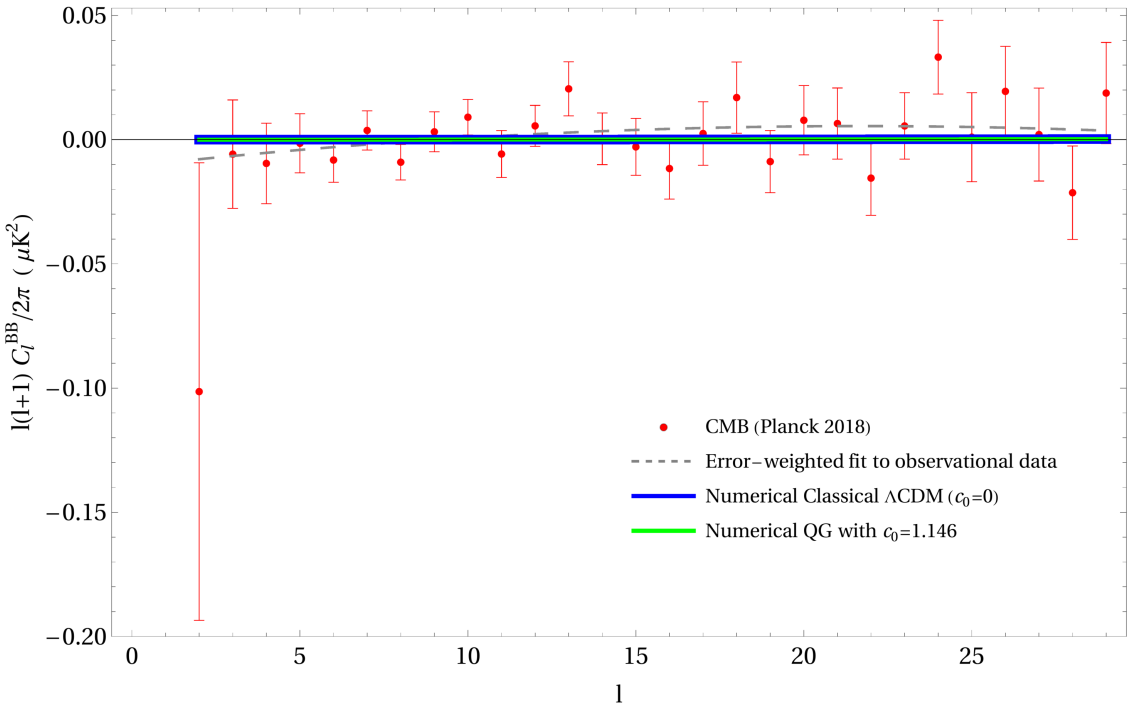

Figure 5.7: Comparison of the numerical prediction of the classical ΛCDM program vs. the numerical prediction of the RG running of Newton's constant's effect on the B-mode (BB) power spectrum C_l^{BB}. The solid curves represent the numerical predictions generated by ISiTGR, with the top (blue) and bottom (green, not quite visible due to substantial overlap with the blue one) representing $c_0 = 0, 1.146$ respectively, showing no significant deviation with the classical no running numerical ΛCDM curve. The dashed curve represents error-weighted quadratic fit for observational CMB data from the Planck (2018) collaboration. The other $c_0 = 8.02$ curve, like the $c_0 = 1.146$ (green) curve, is consistent with zero (to around 1 part in 10,000). So any deviations from the classical and $c_0 = 1.146$ curve are too insignificant to be seen, and negligible relative to the size of the error bars from the current latest data. Hence the $c_0 = 8.02$ curve is not included in this plot for clarity.

5.2.6 Lensing Power Spectrum $C_l^{\phi\phi}$

The theory of CMB lensing is a vast topic on its own. Here, we just attempt to present the key defining equations of the lensing spectrum, and then look at the numerical results of quantum gravitational effects on the lensing potential spectra. A more complete account for the physics and observations can be found in [18, 113, 114].

Consider a small deflection angle θ from the undeflected direction $\hat{n}$ of a CMB photon, with

θ describing perpendicular direction to $\hat{n}$, and $|\theta| \ll 1$. Define the shear matrix M_{ab} as

$$\Delta\theta_a = \sum_b M_{ab}(r_S, \hat{n})\, \theta_b \ , \tag{5.37}$$

where a, b run over the directions orthogonal to $\hat{n}$, r_S is the radial distance of the source from earth in a Robertson–Walker coordinate system and $\delta\theta_a$ is the amount of deflection of θ. From standard general relativistic calculations, the shear matrix can be related to the Newtonian potential of the lens source (ϕ), via

$$M_{ab}(r_S, \hat{n}) = 2 \int_0^{r_S} dr\, \frac{r(r_S, \hat{n})\, r}{r_S} \left[\frac{\partial^2}{\partial y_a \partial y_b}\, \delta\phi(r\hat{n} + \mathbf{y}, t) \right]_{\mathbf{y}=0, t=t_r} \ , \tag{5.38}$$

where $\mathbf{y}$ is a small perpendicular deflection vector to $\hat{n}$, and t_r is the time for a photon that just reached us from radial coordinate r. Hence, the measurements of the shear matrix can yield information about perturbations to the gravitational potential ($\delta\phi$) by masses spread along the line of sight. Define the so-called lensing convergence field κ as

$$\kappa \equiv \frac{1}{2}\, \mathrm{Tr} M \ = \int_0^{r_S} dr\, \frac{r(r_S, \hat{n})\, r}{r_S} \left[\left(\nabla^2 - \frac{\partial^2}{\partial r^2} \right) \delta\phi(r\hat{n} + \mathbf{y}, t) \right]_{\mathbf{y}=0, t=t_r} \ . \tag{5.39}$$

κ is particularly useful because, if the lensing is due to a collection of bodies all at about the same radial coordinate r_L, it can be directly related to the matter perturbations $\delta\rho_m$. More explicitly, $\delta\phi$ falls off rapidly for large distances, so that the factor $r(r, r_S)r$ can be replaced in a first approximation with $r(r_L, r_S)r_L$ and similarly the second term with $\partial^2/\partial r^2$ can be dropped. Then Poisson's equation $a^{-2}\nabla^2\delta\phi = 4\pi G\, \delta\rho_m$ gives

$$\kappa = \frac{4\pi\, G\, a^2(t_{r_L})\, d_A(LS)\, d_A(EL)}{d_A(ES)} \int_0^{r_S} dr\ \delta\rho_m(r\hat{n}, t_L)\, a(t_L) \ \ , \tag{5.40}$$

resulting in an expression directly linking κ to matter density fluctuations $\delta\rho_m$. Hence, a measurement of the value of κ for sources seen in one direction can reveal the total mass

density of a cluster of lensing masses that lies along that line of sight at distance r_L (projected onto a plane perpendicular to the line of sight). Since, as we have shown, gravity constraints the scaling of correlations of matter, it should also do so for κ.

So, to project the convergence field κ onto the sky, we decompose it in a way that is analogous to the other angular spectra,

$$\kappa(\hat{n}) = \sum_{lm} a_{\kappa,lm}\, Y_l^m(\hat{n}) \;, \tag{5.41}$$

with

$$a_{\kappa,lm} = -2\pi\, i^l \int d^3\mathbf{q}\, q^2\; \alpha(\mathbf{q})\, Y_l^{m*}(\hat{q}) \int_0^\infty dr\, g(r)\, \delta\phi_q(t_r)\, [j_l(qr) + j_l''(qr)] \;, \tag{5.42}$$

with quantum noise fluctuation correlation

$$\langle \alpha(\mathbf{q})\, \alpha^*(\mathbf{q}') \rangle = \delta^3(\mathbf{q} - \mathbf{q}') \;, \tag{5.43}$$

which defines $C_l^{\kappa\kappa}$

$$\left\langle a_{\kappa,lm}\, a^*_{\kappa,l'm'} \right\rangle = \delta_{ll'}\, \delta_{mm'}\, C_l^{\kappa\kappa} \;\; . \tag{5.44}$$

Or more explicitly, by inverting the expression in Eq. (5.44), we have

$$C_l^{\kappa\kappa} \;=\; 4\pi^2 \int_0^\infty q^6\, dq \;\left| \int_0^\infty dr\, g(r)\, \delta\phi_q(t_r)\, [j_l(qr) + j_l''(qr)] \right|^2 \;. \tag{5.45}$$

In the literature [113, 114], often the correlation for the lensing potential $C_l^{\phi\phi}$ is plotted, instead of that of the lensing convergence field $C_l^{\kappa\kappa}$, which are related by

$$\kappa\,(\hat{\mathbf{n}}) \;=\; \tfrac{1}{2}\, \nabla^2 \phi(\hat{\mathbf{n}}) \;\; . \tag{5.46}$$

Finally, the cross-correlations $C_l^{T\phi}$ and $C_l^{E\phi}$ can be similarly defined in analogous to Eq. (5.44) with their respective expansion coefficients $a_{T,lm}$ and $a_{E,lm}$, similar to those from Eqs. (5.33)–(5.36). With this background, we hereby present the numerical results of including a quantum RG running of Newton's constant for these spectra.

In Figure 5.8, for $C_l^{\phi\phi}$ we have plotted the classical ($c_0 = 0$) spectrum (solid blue), as well as the ones for an RG running of G with the previously used values for c_0 (green and orange). One can see significant deviation which is up to 80% for $c_0 = 8.02$, but only 10% for $c_0 = 1.146$, compared to the standard ΛCDM prediction. Due to current observational limitations, only three data points lie inside our region of interest ($l < 50$). Apart from Planck collaboration (2018) data, other projects such as the South Pole Telescope (SPT) [115] and the Atacama Cosmology Telescope (ACT) [116] have few observational data points and they mostly lie in the region $l > 100$.

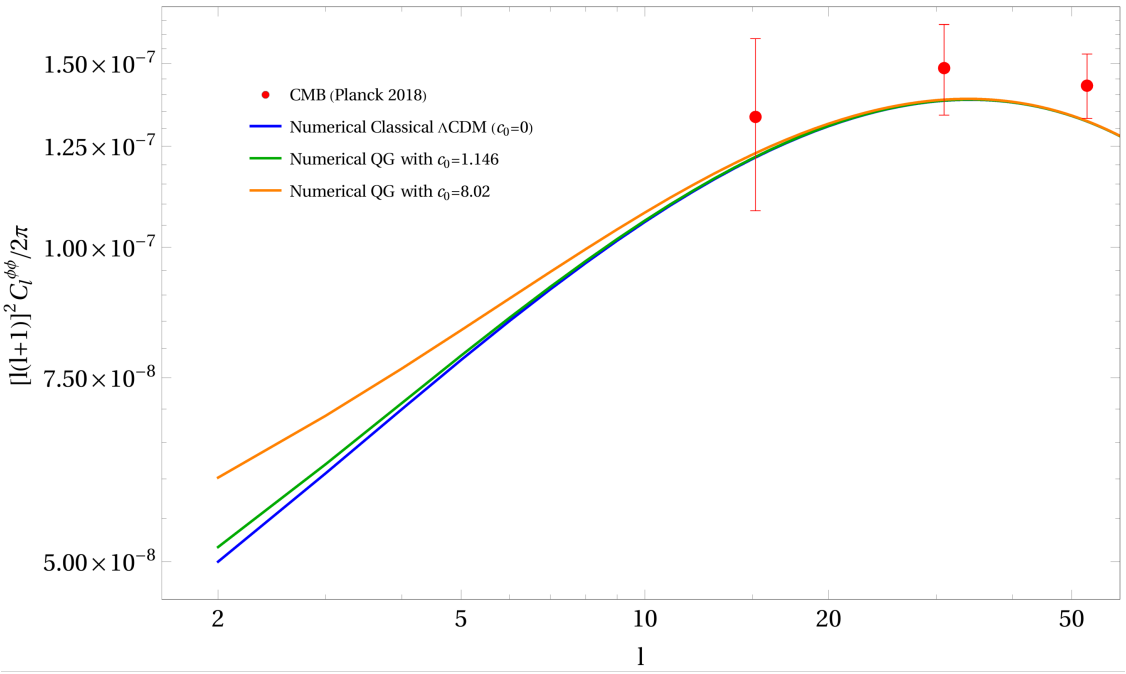

Figure 5.8: Comparison of the numerical prediction of the classical ΛCDM program vs. the numerical predictions of the RG running of Newton's constant's effect on the deflection lensing ($\phi\phi$) power spectrum $C_l^{\phi\phi}$. The solid curves represent the numerical predictions generated by ISiTGR, with the bottom (blue), middle (green) and top (orange) representing the quantum amplitudes (see Eq. (2.17)) $c_0 = 0, 1.146, 8.02$, respectively, showing just slightly higher trends at the very large angular scales ($l < 5$) as compared to the classical (no quantum running) numerical ΛCDM curve. Only limited observational data are available currently, especially at large angular scales (below $l < 15$).

5.2.7 Temperature-Lensing Power Spectrum $C_l^{T\phi}$

For the $C_l^{T\phi}$ and $C_l^{E\phi}$ power spectra, there are no observational data points so far. Since there are only limited data points for $C_l^{\phi\phi}$, especially in the large scale regions of $l < 50$, so it is not surprising there are no significantly useful data for the cross-correlations of $C_l^{T\phi}$ and $C_l^{E\phi}$. Nevertheless, we present the numerical program's predictions here. In Figure 5.9, we have plotted the classical ($c_0 = 0$) spectrum solid blue and the ones with RG running of G (with $c_0 = 1.146, 8.02$) in green and orange, respectively, for $C_l^{T\phi}$. We do see more significant deviations, with the $c_0 = 8.02$ (orange) curve running down to negative values in the vertical axis. For example, at scales of around $l \approx 5$, we see the $c_0 = 1.146$ (green) curve

gives around a 16% deviation from the classical one, and the $c_0 = 8.02$ (orange) curve gives an almost 83% difference from the classical one. Should there be any data points for this spectrum in the future in these ranges, this spectrum can potentially be a good candidate to test for the RG running of G effects.

5.2.8 Lensing-E-mode Power Spectrum $C_l^{E\phi}$

In Figure 5.10, we show the results for $C_l^{E\phi}$, and we have plotted the classical ΛCDM ($c_0 = 0$) spectrum (solid blue) compared with the RG running of Newton's G spectrum using the values 1.146 and 8.02 for c_0 (green and orange, respectively). In this spectrum, the deviation begins similarly around the scale of $l < 30$. But the deviations with classical are small, especially with the $c_0 = 1.146$ curve, going up to $\sim 30\%$ only at $l \approx 3$. On the other hand, the $c_0 = 8.02$ curve does show larger deviations, and also starting at a larger value of l. Since for now there are limited observational data points for this, nothing can be done about ruling out any specific c_0 value from this. In the near future with CMB-S4 (the next generation "Stage-4" ground-based CMB experiment) [117], perhaps more data on $C_l^{\phi\phi}$, and hence $C_l^{T\phi}$ and $C_l^{E\phi}$, might provide a good test for these parameters – especially with the potential to rule out the $c_0 = 8.02$ value.

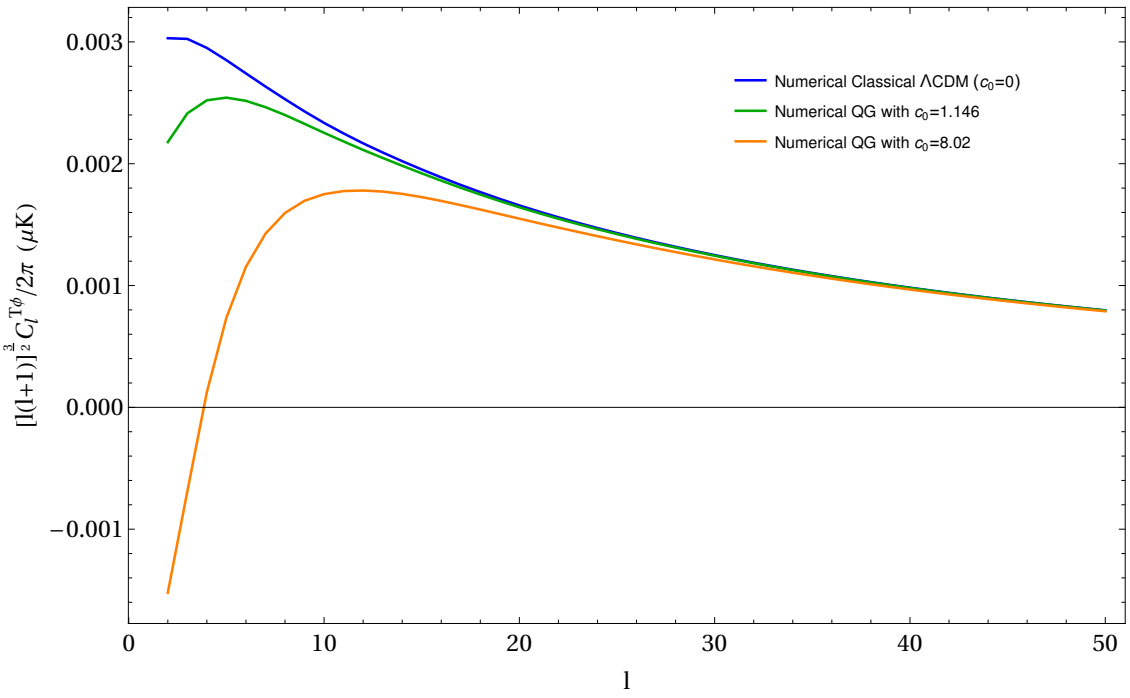

Figure 5.9: Comparison of the numerical prediction of the classical ΛCDM program vs. numerical predictions of the RG running of Newton's constant's effect on the cross-temperature-lensing (Tϕ) power spectrum $C_l^{T\phi}$. The solid curves represent the numerical predictions generated by ISiTGR, with the top (blue), middle (green) and bottom (orange) representing quantum amplitudes (see Eq. (2.17)) $c_0 = 0, 1.146, 8.02$, respectively, showing again just slightly higher trends at the large angular scales ($l < 20$) as compared to the classical no running numerical ΛCDM curve. No data with reasonable errors are found so far for $C_l^{T\phi}$.

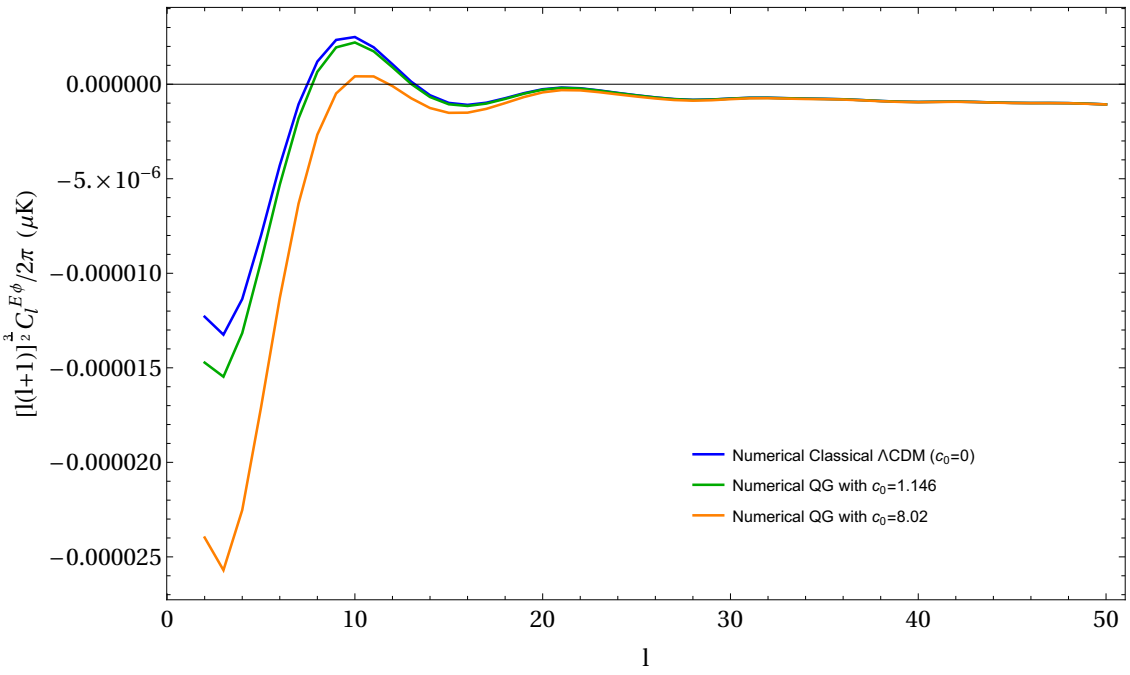

Figure 5.10: Comparison of the numerical prediction of the classical ΛCDM program vs. numerical predictions of the RG running of Newton's constant's effect on the cross-E-mode-lensing (Eϕ) power spectrum $C_l^{E\phi}$. The solid curves represent the numerical predictions generated by ISiTGR, with the top (blue), middle (green) and bottom (orange) representing quantum amplitudes (see Eq. (2.17)) $c_0 = 0, 1.146, 8.02$, respectively, showing this time smaller trends at the large angular scales ($l < 20$) as compared to the classical no running numerical ΛCDM curve. No data with reasonable errors are found so far for $C_l^{E\phi}$.

Chapter 6

Conclusion

6.1 Summary

In this thesis, we have revisited the derivation of the matter and temperature power spectra from the quantum theory of gravity without invoking any additional scalar fields from inflation. To our knowledge, our treatement is the first of its kind. We reviewed that while the short-distance quantum theory of gravity remains speculative, the long-distance behaviors are well known and primarily governed by the renormalization group (RG) behaviors near its critical point. In particular, we reviewed how the critical scaling dimension "s" of the correlation function of the scalar curvature fluctuations at large distances directly governs the scalar spectral index "n_s" of the cosmological spectra, as well as the additional quantum gravitational effects, such as the (IR-regulated) renormalization group running of the coupling constant (Newton's constant) G, that will affect these spectra subtly at large distances. We then presented the various numerical programs that we used in this work, as well as their main results in Chapter 5, to complement the primarily analytical analysis from Chapter 3 and 4. We further utilized these programs to study other cosmological spectra of

different modes. We compared these spectra using the latest available observational data, and provided new constraints and insights to the parameters (c_0, ξ) of the quantum theory. We also discussed the possibility of verifying, or falsifying, some of these hypotheses with increasingly powerful observational cosmology experiments in the future.

Using the numerical results, we find that especially the plots of the matter power spectrum $P_m(k)$, the angular temperature spectrum C_l^{TT}, and the angular temperature-E-mode spectrum C_l^{TE}- all play an important role in revealing new insight to constraining the quantum amplitude c_0, a parameter that governs the size of quantum corrections due to the RG running of Newton's constant. We find that all three plots consistently favor a value of c_0 closer to around 1.15, rather than the naive estimate of $\sim$8.0. This is particularly obvious in the new C_l^{TE} plot from this work, with the $c_0 = 1.146$ curve showing a $\sim$60% deviation from the classical ΛCDM (no quantum running) curve. On the other hand, the angular E-mode spectrum C_l^{EE} and angular B-mode spectrum C_l^{BB} plots are the least useful in distinguishing the running effect, with the EE plot showing only a mild deviation of about 15% from the classical prediction for the $c_0 = 1.146$ curve, and the deviations on the BB plot are essentially consistent with zero. The three angular lensing spectra, namely, $C_l^{\phi\phi}, C_l^{T\phi}$ and $C_l^{E\phi}$, are potentially feasible candidates in providing further insights and constraints. Of particular note is that the $T\phi$ plot, shows around 20% and almost 150% deviation, respectively, for the $c_0 = 1.146$ and $c_0 = 8.02$ curves from the classical curve, on the largest angular scales. However, all these latter ($C_l^{\phi\phi}, C_l^{T\phi}$, $C_l^{E\phi}$) spectra suffer from the scarcity or lack of observational data in the low-l regime, making it impossible to draw any conclusion about the favorability of the parameter or the RG running in general at this stage.

However, although the percentage differences between the spectra with and without quantum corrections are decently significant for scales below $l < 10$—ranging from $\sim$15–60% even with the milder value of 1.146 for c_0, the uncertainties from current observational data in those ranges are unfortunately even larger. As a result, it is not yet possible to conclude at this

stage the visibility of these effects. At best, one can claim the slight hints of RG running from the smallest data point in $P_m(k)$, as well as the last few points ($3 < l < 7$, ignoring the anomalous $l = 2$ point) of C_l^{TT}. Nevertheless, with technology and precision of cosmological experiments improving at a rapid pace, better observational data in this regime perhaps form one of the most promising area where quantum effects of gravity can be revealed and tested for the first time. This is a consequence of the concrete predictions of the long-distance quantum effects, based on well-established renormalization group analysis, as opposed to the still rather speculative short-distance theories of gravity.

From a theoretical perspective, the numerical results from this work also serve an important purpose in ruling out the less favorable value of $c_0 = 8.0$ for the quantum amplitude, but instead suggesting a value around seven times smaller, closer to $c_0 = 1.15$. We also noted that the uncertainties in the observational data at low-ls cannot yet fully constrain the precise shape of the RG running, allowing for the possibility that these various deviations can all be mimicked instead by a modified value of $\xi \approx 14{,}000$ Mpc, or around 2.5 times larger than the naive estimate $\xi \simeq \sqrt{3/\lambda} = 5300$ Mpc. As we discussed in the theory section (Section 3.4), unlike the universal critical scaling index ν (shown from various methods to have a value very close to $\nu = 1/3$), the parameters c_0 and ξ do not necessarily follow from universality, but are instead reliable only up to order of magnitudes. While the observational data at this stage cannot yet exhibit the effects of RG running, they do provide a useful constraint to the possible values of these theoretical parameters. In particular, as discussed in detail in our work [16], even with the current observational data's (im-)precision, our work shows an extremely stringent constraint on the allowed values of ν, down to at most a 1–2% deviation from 1/3. This result not only provides a great verification of the values obtained from various theoretical methods such as the Regge lattice calculations of the path integral, but perhaps the first phenomenological test of the quantum theory of gravity in cosmology. It is thus hopeful that as observational technology continues to improve, more insights can be gained regarding the values for c_0 and ξ. With more data and smaller error bars, one can further

narrow down a best-fit value for the quantum amplitude c_0 or vacuum condensate scale ξ by Markov Chain Monte Carlo (MCMC) sampling in the ISiTGR program. In addition, ISiTGR is also capable of calculating tensor perturbations, which can be used to test this quantum gravitational picture as soon as more observational data on that becomes available. As a fundamentally tensor theory, this gravitational fluctuation picture is expected to produce nontrivial predictions to those of scalar field based inflation models.

It should also be noted that the numerical programs show very encouraging agreement with the analytical results on the matter power spectrum $P_m(k)$, as shown here in Figure 5.3. This agreement provides great confidence in the analytical methodology used in [15], or as summarized in Section 3.4. The concordance between numerical and analytical results provides extra support on how the quantum fluctuations of the gravitational field are linked to the fluctuations of the matter density field. However, the numerical results for the effects of a RG running of G, suggesting an upturn at low ls, seem to challenge the analytical intuition that a lower $P_m(k)$ should give a lower C_l^{TT}, as suggested in Equation (4.12). Since the derivation of Equation (4.12) is purely classical and does not involve any quantum gravitation input, this suggests a lack of analytical understanding of the effects of a having a modified RG running Newton's constant on the Boltzmann equations, and hence also their solutions of the form factors F_1 and F_2 (Equations (4.7) and (4.8)). It is unclear analytically from the coupled differential equations how the running of Newton's G from Equation (5.10) affects their solutions, making it difficult to translate the predictions on $P_m(k)$, which agrees with the numerical results, to C_l^{TT}. This is an area under active further theoretical investigations, and has to be addressed in future work. Nevertheless, armed with the supposedly more comprehensive and reliable numerical programs, new insights should be gained regarding the various quantum effects of gravity on the different cosmological spectra.

At first, the results presented in this dissertation might appear puzzling, since one usually associates quantum fluctuations with microscopic, very short distance phenomena. This is in

fact generally incorrect, with well-known examples of condensation and macroscopic quantum cooperative behavior in areas such as superconductors, superfluids, phase transitions and white dwarf stars. The point here is: experience shows that the magnitude and scale for quantum fluctuations in quantum field theory is instead generally related to an intrinsic dynamical length scale, here the gravitational correlation length ξ, or equivalently the vacuum condensate $\langle R \rangle \sim 1/\xi^2$ connected to it. In this QCD-like picture, supported by extensive nonperturbative calculations on the lattice and in the continuum, quantum fluctuations exist on all length scales and propagate from the microscopic to the macroscopic regime, all the way up to the cosmological domain (since in the quantum theory the only relevant scale is the vacuum condensate $\langle R \rangle$, which we know from observation is exceedingly small). This is not unexpected, as the graviton is massless and macroscopic effects thus arise because of strong infrared divergences (again in a way that is similar to what happens in QCD) where perturbation also fails completely in the infrared regime. Consequently, quantum fluctuations of the gravitational field are not just primordial ($t \to 0$) or microscopic ($r \to 0$) in nature. Instead, they occur on all length scales (including infrared scales) at all times, with specific features (such as a weak running of G) predicted by the existence of those scale invariant quantum fluctuations, and with the parameter ξ setting the scale for those very subtle quantum effects, again in close analogy to QCD. Of course, such effects are entirely missed in ordinary perturbation theory, which is badly divergent due to a (largely invisible) nontrivial vacuum condensation.

In conclusion, we have presented in this dissertation a compelling alternative picture for the various observed cosmological spectra that is motivated by gravitational fluctuations. In this work, we have provided updated- and extended-analyses utilizing numerical programs in cosmology, as well as new physical predictions that can potentially distinguish this perspective from that of standard scalar field inflation. To this day, inflation still forms one of the more popular approaches, but its full acceptance has remained controversial [10, 12]. While there exist a number of alternatives to the standard horizon and flatness problems [85, 98], the

ability to explain the various cosmological power spectra has long been one of the unique predictions from inflation-motivated models, and thus often considered as one of the "major successes" for inflation. It is thus significant that this work provides an entirely new alternative, which is in principle arguably more elegant as it only uses Einstein gravity and standard (and well established) nonperturbative quantum field theory methods, without the usual burden of flexibilities associated with inflation. Nevertheless, because of the limited precision of current observational data, it is not yet possible to clearly prove or disprove either idea. In addition, a complete account of various other cosmological problems such as the horizon and flatness problem, the issue of cosmological initial conditions, quantum coherence of the initial state, etc., are certainly interesting and important though quite beyond the scope of this work. Future work is pending to see how these issues can be integrated into the picture. Still, the possibility of an alternative explanation without invoking the artificial machinery of scalar fields is significant, as it suggests that the observed power spectra may not be a direct consequence nor a solid confirmation of inflation, as some literature may suggest. By exploring in more details the relationship between gravity and cosmological matter and radiation both analytically and numerically, together with the influx of new and increasingly accurate observational data, one can hope that this hypothesis can be subjected to further stringent tests in the future.

6.2 Related Issues and Future Work

Given the vastness of the subject, we have to reiterate that it is impossible to address all the cosmological problems related to inflation in a single work, nor is this the intent of this dissertation work here. Hence, the work primarily focuses on the central problem of explaining the matter power spectrum. As a result, our scope here is restricted to two-fold: (i) to describe this perspective and present detailed calculations of the power spectrum as

reproduced from macroscopic gravitational fluctuations, and (ii) to describe predictions of deviations from the classical picture, which serves as a test for this gravitational picture as experimental accuracies in the large-scale regions improve in the near future. Nevertheless, the other cosmological problems addressed by inflation, including an explanation of why the universe is flat, isotropic and homogeneous, remain of great interest. These, amongst other inflation related problems such as B-mode polarizations and quantitative tests against higher order correlation functions, are intended to be pursued in future work.

According to current established physical laws, two main aspects determine the cosmological evolution. The first aspect involves the use of the correct field equations for a coupled matter gravity system, and these in turn follow from Einstein's classical field equations, coupled with an exhaustive specification of all the various matter and radiation components and their mutual interactions. The second main ingredient is a set of suitable initial conditions for all the fields in question, which should then lead to a hopefully unambiguous determination of the complete subsequent time evolution.

While there is currently very little controversy on the nature of the correct cosmological evolution equations themselves (which largely follow from the choice of a suitable metric based on physical symmetry arguments and on a complete list of matter and radiation constituents based on our current understanding of fundamental particle physics), the same cannot be said for the choice of initial conditions. The latter are largely unknown, and generally involve a number of explicitly stated, and sometimes implicitly assumed, assumptions of what the universe might have looked like close to the initial singularity. Furthermore, it is generally expected that quantum effects do play a major role at such early stages, be it for the matter fields and their interactions, or for the gravitational field itself for which a classical description is clearly inadequate in this regime. Indeed, over the years, attempts have been made to partially include some quantum effects, for instance, by assuming non-trivial Gaussian (free field) correlations for some matter and gravity two-point functions.

Recent attempts at overcoming our admitted ignorance regarding the initial conditions for the evolution equations have explored a number of different avenues. In one popular scenario [92–95], it is argued that the universe might have evolved initially from a state that could not even remotely be described in terms of a simple and symmetric physical characterization. If, as suggested by particle physics and string theory, a modified quantum dynamics becomes operative at short distance, then one would expect a complete removal of the initial spacetime singularity, replaced herewith instead by some sort of bounce. One key, but nevertheless natural, consequence of this perspective is that the universe must have evolved into and out of the initial singularity in a highly coherent quantum state, with non-trivial quantum correlations arising between all fields, and with the latter presumably operating on all distance scales. These highly coherent and complex initial conditions would then represent the surviving physical imprint of a previous, presumably very long, cycle of cosmological evolution, thus generating a set of suitable initial conditions for the cosmology of our current universe.

Another possibility regarding the initial conditions is inspired by the semi-classical approach to quantum gravity [96, 97], and entail a more geometric point of view regarding the nature of gravity. In this approach, the universe naturally evolves instead from an initial simple, symmetric and elegant geometric construct, as described in practice for example by the so-called no-boundary proposal for homogeneous isotropic closed universes, endowed with a cosmological constant and a variety of other fields. Another popular attempt to explain features of the early universe, and more specifically properties of the matter power spectrum, is through inflation models [5–7]. These models propose that structures visible in the Universe today get formed from quantum fluctuations in a hypothetical primordial scalar inflaton field. Although the precise behavior and dynamics of the inflaton field are to this day still largely controversial [9–12, 85, 86], one nevertheless finds some general features that are common among these models, and which allow one to derive predictions about the nature of the power spectrum.

In broad terms, the approach adopted in this dissertation can be viewed as more in line with the first scenario, where as little as possible is assumed about the nature of the initial quantum state of the universe given that, as mentioned previously, the latter might be quite far from a simple and symmetric physical characterization. Instead, in this work, we make extensive use of prior knowledge from nonperturbative studies of quantum gravity regarding the large distance behavior of gravitational and matter two-point functions. An important ingredient in the results presented here will therefore be the nontrivial scaling dimensions obtained from these studies, and how these relate to current observational data. We note here that the quantum-field theoretic treatment of perturbatively nonrenormalizable theories – in particular the determination of their generally nontrivial scaling dimensions – has a rather distinguished history: originally developed in the context of scalar field theories by Wilson and Parisi [33–35,38], and recently reviewed in great detail in [30], as well as in many other excellent monographs [31,118–120]. Attempts at quantizing gravity within established rules of quantum field theory also have a long and distinguished history, dating back to Feynman's original investigations, and the subsequent formulation of a consistent covariant path integral framework [27,28]. Quantum gravity, and by now the rather compelling theoretical evidence of a nontrivial ultraviolet (UV) renormalization group fixed point in four spacetime dimensions, in principle leads to a number of unambiguous predictions, recently reviewed and summarized in [13,14]. Perhaps the most salient observational effects of such an approach include a running of Newton's constant G with scale on very large cosmological distances [40], the modification of classical results for the growth of relativistic matter density perturbations and their associated growth exponents, and a non-vanishing slip function in the conformal Newtonian gauge [41,42]. Moreover, the existence of a nontrivial UV fixed point, arising from the highly nonlinear nature of the Einstein-Hilbert action, leads in a natural way to a nontrivial quantum condensate in the curvature. Such a condensate effectively produces long-distance correlations between local curvature fluctuations, and these curvature fluctuations couple locally to matter density fluctuations unambiguously through

the field equations. The fluctuations in matter density, which are in principle unambiguously calculable in this perspective, should lead to gravitational clumping of matter in the over-dense areas, which eventually brings about the formation of galaxies. In other words, the correlations of galaxy distributions should in principle become predictable from correlations of curvature fluctuations derived from quantum gravity. The calculated results can then be compared with observations, and thus viewed as a potential test for the proposed vacuum condensate picture of quantum gravity.

Bibliography

[1] P. J. E. Peebles. "Principles of Physical Cosmology". *Princeton series in Physics* (Princeton University Press), (1993).

[2] P. J. E. Peebles. "Issues for the Next Generation of Galaxy Surveys". *Phil. Trans. Roy. Soc. Lond.* **A357**, 21-34, (1999).

[3] C. Baugh. "Correlation Function and Power Spectra in Cosmology". *Encyclopedia of Astronomy and Astrophysics* (IOP, London), ISBN 0333750888, (2006).

[4] M. Tegmark and M. Zaldarriaga. "Separating the Early Universe from the Late Universe: Cosmological parameter estimation beyond the black box". *Phys. Rev.* **D66**, 103508, (2002).

[5] A. H. Guth. "Inflationary universe: A possible solution to the horizon and flatness problems". *Phys. Rev.* **D23**, 347-356, (1981).

[6] A. D. Linde. "A new inflationary universe scenario: A possible solution of the horizon, flatness, homogeneity, isotropy, and primordial monopole problems". *Phys. Lett.* **108B** 389, (1982).

[7] A. Albrecht and P. J. Steinhardt. "Cosmology for grand unified theories with radiation induced symmetry breaking". *Phys. Rev. Lett.* **48**, 1220, (1982).

[8] A. R. Liddle and D. H. Lyth. *Cosmological Inflation and Large-Scale Structure*. Cambridge University Press, (2000).

[9] P. J. Steinhardt. "The inflation debate: Is the theory at the heart of modern cosmology deeply flawed?". *Scientific American* 304N4:18-25, (2011).

[10] M. Tegmark. "What does inflation really predict?". *JCAP*, 4:001, April 2005, (2005).

[11] A. Ijjas, P. J. Steinhardt, and A. Loeb. "Inflationary paradigm in trouble after Planck 2013". *Phys. Lett.* **B** 723, 261-266, (2013).

[12] A. Ijjas, P. J. Steinhardt, and A. Loeb. "Inflationary Schism". *Phys. Lett.* **B736**, 142-146, September 2014, (2014).

[13] H. W. Hamber. "Vacuum Condensate Picture of Quantum Gravity". arXiv 1707.08188 [hep-th], and references therein, (2017).

[14] H. W. Hamber. "*Quantum Gravitation*". *Springer Tracts in Modern Physics* (Springer Publishing, Berlin and New York), (2009).

[15] H. W. Hamber and L. H. S. Yu. "Gravitational Fluctuations as an Alternative to Inflation". *Universe* **2019**, 5(1), 31; arXiv:1807.10704v3 [gr-qc], (2018).

[16] H. W. Hamber and L. H. S. Yu. "Gravitational Fluctuations as an Alternative to Inflation II. CMB Angular Power Spectrum". *Universe* **2019**, 5(11), 216, (2019).

[17] Y. Akrami et al. "Planck 2018 results. I. Overview and the cosmological legacy of Planck". *Planck Collaboration,* arXiv:1807.06205v1 [astro-ph.CO], (2018).

[18] S. Weinberg. *Cosmology*. Oxford University Press , (2008).

[19] N. A. Bahcall et al. "The Richness-dependent Cluster Correlation Function: Early Sloan Digital Sky Survey Data". *Astrophys. J.* **599**, 814, (2003).

[20] M. Longair. *Galaxy Formation*. Springer Publishing New York, 2nd ed., (2007).

[21] M. Tegmark et al. "The 3D Power Spectrum of Galaxies from the SDSS". *Astrophys. J.* **606**, 702-740, `astro-ph/0310725`, (2004).

[22] A. Durkalec et al. "The evolution of clustering length, large-scale bias and host halo mass at $2 < z < 5$ in the VIMOS Ultra Deep Survey (VUDS)". *astro-ph.CO* arXiv:1411.5688, (2014).

[23] Y. Wang et al. "The SDSS Galaxy Angular Two-Point Correlation Function". *Mon. Not. Astron. Soc.* 432, 1961, arXiv:1303.2432 [astro-ph.CO], (2013).

[24] A. L. Coil, T.D. Oswalt, and W.C. Keel. *Large Scale Structure in the Universe in Planets, Stars, and Stellar Systems*. Springer, New York , Vol. 8; arXiv:1202.6633 [astro-ph.CO], (2012).

[25] H. Gil-MarÌn et al. "The clustering of the SDSS-IV extended Baryon Oscillation Spectroscopic Survey DR14 quasar sample: structure growth rate measurement from the anisotropic quasar power spectrum in the redshift range $0.8 < z < 2.2$". *SDSS collaboration*, (2018).

[26] T. Damour. "Experimental Tests of Gravitational Theory". *Review of Particle Physics, J. Phys.* **G** 33, 1. `http://pdg.lbl.gov/2009/reviews/rpp2009-rev-gravity-tests.pdf`, (2006).

[27] R. P. Feynman. "*Quantum Theory of Gravitation*". *Acta Phys. Polon.* **24**, 697-722, (1963).

[28] R. P. Feynman, F. B. Morinigo, W. Wagner, and B. Hatfield. "Lectures on Gravitation, Caltech lecture notes, 1962-1963". *Advanced book program* (Addison-Wesley), (1995).

[29] B. S. DeWitt. "Quantization of Fields with Infinite-Dimensional Invariance Groups. III. Generalized Schwinger-Feynman Theory". *Journal of Mathematical Physics* **3**, 1073, (1962).

[30] J. Zinn-Justin. *Quantum Field Theory and Critical Phenomena*, 4th ed. Oxford University Press, Oxford, UK, (2002).

[31] E. Brezin. *Introduction to Statistical Field Theory*. Cambridge University Press Cambridge, UK, (2010).

[32] H. W. Hamber. "*Simplicial Quantum Gravity*". Critical Phenomena, Random Systems and Gauge Theories 1984 Les Houches Summer School, Session XLIII, edited by K. Osterwalder and R. Stora (North-Holland, Amsterdam), (1986).

[33] K. G. Wilson. "Feynman-graph expansion for critical exponent". *Phys. Rev. Lett.* **28**, 548, (1972).

[34] K. G. Wilson. "Quantum field-theory models in less than 4 dimensions". *Phys. Rev.* **D7**, 2911, (1973).

[35] G. Parisi. "On the Renormalizability of not Renormalizable Theories". *Lett. Nuovo Cimento* **6S2**, 450, (1973).

[36] G. Parisi. "Theory of Non-Renormalizable Interactions - The large N expansion". *Nucl. Phys.* **B100**, 368, (1975).

[37] G. Parisi. "Symanzik's Improvement Program". *Nucl. Phys.* **B254**, 58, (1985).

[38] G. Parisi. "On Non-Renormalizable Interactions". *Proceedings of the 1976 Cargese NATO Advances Study Institute, on New Developments in Quantum Field Theory and Statistical Mechanics*, edited by M. Levy and P. Mitter (Plenum Press, New York, 1977), (1977).

[39] H. W. Hamber. "Invariant Correlations in Simplicial Gravity". *Phys. Rev.* **D50**, 3932, (1994).

[40] H. W. Hamber and R. M. Williams. "Nonlocal effective gravitational field equations and the running of Newton's G". *Phys. Rev.* **D72**, 044026, (2005).

[41] H. W. Hamber and R. Toriumi. "Cosmological Density Perturbations with a Scale-Dependent Newton's G". *Phys. Rev.* **D82**, 043518, (2010).

[42] H. W. Hamber and R. Toriumi. "Cosmological Density Perturbations with a Scale-Dependent Newton's G". *Phys. Rev.* **D84**, 103507, (2011).

[43] H. W. Hamber and R. Toriumi. "Inconsistencies from a Running Cosmological Constant". *Int. J. Mod. Phys.* **D22**, 36, (2013).

[44] H. W. Hamber and R. Toriumi. "Group Invariant Scale Corresponding to a Gravitational Condensate". *Frontiers of Fundamental Physics* **PoS**, FFP14:178, (2016).

[45] H. W. Hamber. "Scaling Exponents for Lattice Quantum Gravity in Four Dimensions". *Phys. Rev.* **D92**, 064017, (2015).

[46] H. W. Hamber. "Scalar fields coupled to four-dimensional lattice gravity". *Nucl. Phys.* **B400**, 347, (1993).

[47] H. W. Hamber. "Gravitational scaling dimensions". *Phys. Rev.* **D61**, 124008, (2000).

[48] H. W. Hamber and R. M. Williams. "Gravitational Wilson Loop and Large Scale Curvature". *Phys. Rev.* **D76** 084008, (2007).

[49] H. W. Hamber and R. M. Williams. "Gravitational Wilson Loop in Discrete Gravity". *Phys. Rev.* **D81** 084048, (2010).

[50] S. Weinberg. "Ultraviolet Divergences in Quantum Gravity" in *General Relativity - An Einstein Centenary Survey*, edited by S. W. Hawking and W. Israel. Cambridge University Press, Cambridge, UK, (1979).

[51] R. Gastmans, R. Kallosh, and C. Truffin. "Quantum Gravity Near Two-Dimensions". *Nucl. Phys.* **B133** 417, (1978).

[52] S. M. Christensen and M. J. Duff. "Quantum Gravity in $2 + \epsilon$ Dimensions". *Phys. Lett.* **B79** 213, (1978).

[53] H. Kawai and M. Ninomiya. "Renormalization Group and Quantum Gravity". *Nucl. Phys.* **B336**, 115, (1990).

[54] H. Kawai, Y. Kitazawa, and M. Ninomiya. "Scaling Exponents in Quantum Gravity near Two Dimensions". *Nucl. Phys.* **B393**, 280, (1993).

[55] H. Kawai and M. Ninomiya. "Ultraviolet stable fixed point and scaling relations in (2 + ϵ)-dimensional quantum gravity". *Nucl. Phys.* **B404**, 684, (1993).

[56] Y. Kitazawa and M. Ninomiya. "Scaling behavior of Ricci curvature at short distance near two dimensions". *Phys. Rev.* **D55**, 2076, (1997).

[57] T. Aida and Y. Kitazawa. "Two-loop Prediction for Scaling Exponents in (2 + ϵ)-dimensional Quantum Gravity". *Nucl. Phys.* **B491**, 427, (1997).

[58] H. W. Hamber and R. M. Williams. "Nonperturbative gravity and the spin of the lattice graviton". *Phys. Rev.* **D70**, 124007, (2004).

[59] H. W. Hamber and R. M. Williams. "Quantum gravity in large dimensions". *Phys. Rev.* **D73**, 044031, (2006).

[60] H. W. Hamber, R. Toriumi, and R. M. Williams. "Wheeler-DeWitt Equation in 2+1 Dimensions". *Phys. Rev.* **D86**, 084010, (2012).

[61] H. W. Hamber, R. Toriumi, and R. M. Williams. "Wheeler-DeWitt Equation in 3+1 Dimensions". *Phys. Rev.* **D88**, 084012, (2013).

[62] M. Reuter. "Nonperturbative Evolution Equation for Quantum Gravity". *Phys. Rev.* **D57**, 971, (1998).

[63] M. Reuter and H. Weyer. "Quantum Gravity: Challenges and Perspectives, Bad Honneff (Hermann Nicolai ed.)". *General Relativ. Gravit.* **41**, 983, (2009).

[64] D. F. Litim. "Fixed Points of Quantum Gravity". *Phys. Rev. Lett.* **92** 201301, (2004).

[65] P. Fischer and D. F. Litim. "Fixed points of quantum gravity in extra dimensions". *Phys. Lett.* **B638**, 497, (2006).

[66] D. Becker and M. Reuter. "En route to background independence: Broken split-symmetry, and how to restore it with bi-metric average actions". *Annals Phys.* **350**, 225, (2014).

[67] K. Falls. "Critical scaling in quantum gravity from the renormalisation group". arXiv:1503.06233 [hep-th], (2015).

[68] K. Nikolakopoulo K. Falls, D. F. Litim and C. Rahmede. "Further Evidence for Asymptotic Safety of Quantum Gravity". arXiv:1501.05331 [hep-th], (2015).

[69] N. Ohta, R. Percacci, and A. D. Pereira. "Gauges and functional measures in quantum gravity I: Einstein theory". *JHEP* **1606**, 115, (2016).

[70] H. Gies, B. Knorr, and S. Lippoldt. "Generalized Parametrization Dependence in Quantum Gravity". *Phys. Rev.* **D92**, no. 8, 084020, (2015).

[71] N. Ohta, R. Percacci, and G. P. Vacca. "Renormalization Group Equation and scaling solutions for f(R) gravity in exponential parametrization". *Eur. Phys. J.* C76 no. 2, 46, (2016).

[72] M. Demmel, F. Saueressig, and O. Zanusso. "RG flows of Quantum Einstein Gravity in the linear-geometric approximation". *Annals Phys.* **359**, 141, (2015).

[73] E. Manrique, M. Reuter, and F. Saueressig. "Bimetric Renormalization Group Flows in Quantum Einstein Gravity". *Annals Phys.* **326**, 463, (2011).

[74] A. Codello, G. D'Odorico, and C. Pagani. "Consistent closure of renormalization group flow equations in quantum gravity". *Phys. Rev.* **D89** no. 8, 081701, (2014).

[75] K. Falls. "Asymptotic safety and the cosmological constant". arXiv:1408.0276 [hep-th], (2014).

[76] K. Nikolakopoulo K. Falls, D. F. Litim and C. Rahmede. "On the Renormalization of Newton's constant". arXiv:1501.05331 [hep-th], (2015).

[77] S. Dodelson. *Modern Cosmology*. Academic Press, Amsterdam, The Netherlands, (2003).

[78] P. J. Steinhardt. "Cosmological Perturbations". *Mod. Phys. Lett. A* **19**, 967-982, (2004).

[79] W. Hu and D. J. Eisenstein. "Baryonic Features in the Matter Transfer Function". *arXiv* astro-ph/9709112, (1997).

[80] E. R. Harrison. "Fluctuations at the Threshold of Classical Cosmology". *Phys. Rev.* **D1**, 2726, (1970).

[81] Y. B. Zeldovich. "A hypothesis, unifying the structure and the entropy of the Universe". *Mon. Not. Roy. Astron. Soc.* **160**, (1972).

[82] P. J. E. Peebles and J. T. Yu. "Primeval Adiabatic Perturbation in an Expanding Universe". *Astrophys. J.* **162**, 815, (1970).

[83] P. A. R. Ade et al. "Planck 2015 Results. XIII. Cosmological Parameters". *Astron. Astrophys.* 594:A13, (2016).

[84] N. MacCrann et al. "Cosmic Discordance: Are Planck CMB and CFHTLenS weak lensing measurements out of tune?". arXiv:1408.4742v2 [astro-ph.CO], (2015).

[85] P. J. Steinhardt. *The Cyclic Theory of the Universe*. Princeton University Press , (2012).

[86] P. J. Steinhardt, A. Ijjas, and A. Loeb. "Pop Goes the Universe". *Scientific American*; `https://www.cfa.harvard.edu/~loeb/sciam3.pdf`, (2017).

[87] L. A. Boyle, P. J. Steinhardt, and N. Turok. "Inflationary Predictions for Scalar and Tensor Fluctuations Reconsidered". *Phys. Rev. Lett.* **96** (11):111301, (2006).

[88] A. H. Guth, D. I. Kaiser, and Y. Nomura. "Inflationary paradigm after Planck 2013". *Phys. Lett.* **B**, 733:112-119, (2014).

[89] R. Dashen and D. J. Gross. "Relationship between lattice and continuum definitions of the gauge-theory coupling". *Phys. Rev.* **D23**, 2340, (1981).

[90] M. Beneke. "Renormalons". *CERN-TH/98-233, Physics Reports* **317**, 1, and references therein, (1999).

[91] H. W. Hamber and L. H. S. Yu. "Dyson's Equations for Quantum Gravity in the Hartree-Fock Approximation". arXiv:2010.10500 [hep-th], (2020).

[92] G. Veneziano. "String Cosmology: The Pre-Big Bang Scenario". *CERN-Th*/2000-42, hep-th/0002094., (2000).

[93] G. Veneziano. "The Myth of the Beginning of Time". *Scientific American*, May, pp. 54-65., (2004).

[94] M. Gasperini and G. Veneziano. "Pre-Big Bang in String Cosmology". *Astropart. Phys.* 1, 317, (1993).

[95] A. Buonanno, T. Damour, and G. Veneziano. "Pre-Big Bang Bubbles from the Gravitational Instability of Generic String Vacua". *Nucl. Phys.* **B543** 275-320, (1999).

[96] J. B. Hartle and S. W. Hawking. "Wave function of the Universe". *Phys. Rev.* **D28** 2960, (1983).

[97] J. B. Hartle, S. W. Hawking, and T. Hertog. "No-Boundary Measure of the Universe". *Phys. Rev. Lett.* **100**, 201301, (2008).

[98] S. Hollands and R. M. Wald. "An Alternative to Inflation". arXiv: gr-qc/0205058, (2002).

[99] S. V. Mukhanov and G. V. Chibisov. "Quantum fluctuations and a nonsingular universe". *Sov. Phys. JETP Lett.* **33**, 532, (1981).

[100] S. Hawking. "The development of irregularities in a single bubble inflationary universe". *Phys. Lett.* **115B**, 295, (1982).

[101] A. A. Starobinsky. "Dynamics of phase transition in the new inflationary universe scenario and generation of perturbations". *Phys. Lett.* **117B**, 175, (1982).

[102] A. Guth and S Y. Pi. "Fluctuations in the New Inflationary Universe". *Phys. Rev. Lett.* **49**, 1110, (1982).

[103] E. Bellini, A. Barreira, N. Frusciante, B. Hu, S. Peirone, M. Raveri, et al. "Comparison of Einstein-Boltzmann solvers for testing general relativity". *Phys. Rev.* **D97**, 023520, (2018).

[104] A. Lewis, A. Challinor, and A. Lasenby. "Efficient Computation of CMB anisotropies in closed FRW models". arXiv:astro-ph/9911177, (1999).

[105] J. Lesgourgues. "The Cosmic Linear Anisotropy Solving System (CLASS) I: Overview". arXiv:astro-ph.IM [astro-ph.IM], (2011).

[106] C. Garcia-Quintero and M Ishak. "ISiTGR Version 3.1 released in February 2020 (with python wrapper)". GitHub repository, `https://github.com/mishakb/ISiTGR`, (2020).

[107] S. Alessandra Z. Alex, P. Levon and Z. Gong-Bo. "MGCAMB with massive neutrinos and dynamical dark energy". arXiv:1901.05956 [astro-ph.CO], (2019).

[108] B. Tessa and B. Philip. "Observational signatures of modified gravity on ultra-large scales". arXiv:1506.00641 [astro-ph.CO], (2015).

[109] L. Antony and B. Sarah. "Cosmological parameters from CMB and other data: A Monte-Carlo approach". arXiv:astro-ph/0205436, (2002).

[110] C. Garcia-Quintero, L. Fox M. Ishak, and J. Dossett. "ISiTGR: Testing deviations from GR at cosmological scales including dynamical dark energy, massive neutrinos, functional or binned parametrizations, and spatial curvature". arXiv:1908.00290 [astro-ph.CO], (2019).

[111] Antony Lewis. "CAMB Notes". *DAMTP/CITA/IoA/Sussex* `https://cosmologist.info/notes/CAMB.pdf`, (2014).

[112] D. N. Spergel et al. "First Year Wilkinson Microwave Anisotropy Probe (WMAP) Observations: Determination of Cosmological Parameters". *WMAP Collaboration* arXiv:astro-ph/0302209v3 [astro-ph], (2003).

[113] A. van Engelen, S. Bhattacharya, N. Sehgal1, G. P. Holder, O. Zahn, and D. Nagai. "CMB Lensing Power Spectrum Biases from Galaxies and Clusters using High-angular Resolution Temperature Maps". *Astrophys. J.* **786**, 13, (2014).

[114] N. Aghanim et al. "Planck 2018 results. VIII. Gravitational lensing". *Planck Collaboration* arXiv:1807.06210v2 [astro-ph.CO], (2018).

[115] G. Simard, Y. Omori, K. Aylor, E. J. Baxter, B. A. Benson, L. E. Bleem, Carlstrom J. E, C. L. Chang, H-M. Cho, R. Chown, et al. "Constraints on Cosmological Parameters from the Angular Power Spectrum of a Combined 2500 deg2 SPT-SZ and Planck Gravitational Lensing Map". *The Astrophysical Journal* **860**, 2, (2018).

[116] S. Das, T. Louis, M. R. Nolta, G. E. Addison, E. S. Battistelli, J. R. Bond, E. Calabrese, D. Crichton, M. J. Devlin, S. Dicker, et al. "The Atacama Cosmology Telescope: Temperature and gravitational lensing power spectrum measurements from three seasons of data". *The Astrophysical Journal* **04**, 014–014, (2014).

[117] K. N. Abazajian et al. *CMB-S4 Science Book*, First Edition. arXiv:1610.02743 [astro-ph.CO], (2016).

[118] G. Parisi. *Statistical Field Theory*. Benjamin Cummings, San Francisco, CA, (1981).

[119] C. Itzykson and J. M. Drouffe. *Statistical Field Theory*. Cambridge University Press, Cambridge, UK, (1991).

[120] J. L. Cardy. "Scaling and Renormalization in Statistical Physics". Cambridge Lecture Notes in Physics, Cambridge University Press, Cambridge, UK, (1996).

Appendix A

Quantum Gravity on Solar-System Scales

A.1 Magnitude of Quantum Gravity Effects on Solar-System Scales

It is of some interest to investigate the magnitude of quantum gravitational effects on Solar System scales, and see if they could become potentially significant. This paper utilizes three particular results from a quantum treatment of gravity - the two-point correlation functions, the infrared (IR) regulator, and the renormalization group (RG) running of Newton's constant G. First, it is easiest to see the IR regulator and RG running of Newton's constant G play completely negligible roles in the Solar System. Using

$\xi \sim \sqrt{3/\lambda} \simeq 5300\,\mathrm{Mpc} = 1.093 \times 10^{15}$ AU, the respective modifications

$$\frac{1}{k^2} \to \frac{1}{k^2 + m^2} \ , \tag{A.1}$$

and

$$G \to G + \delta G(k) + \mathcal{O}\left(\delta G^2\right) \quad , \text{ where } \frac{\delta G}{G} \equiv 2\, c_0 \left(\frac{m^2}{k^2 + m^2}\right)^{3/2} \tag{A.2}$$

are only significant when k falls below $\sim m \equiv 1/\xi$, or equivalently r above $\simeq \xi$. Taking the Solar System size as $r_{\mathrm{sol}} \approx 100$ AU, such quantum effects in the Solar System are suppressed by large factors of $r_{\mathrm{sol}}/\xi \simeq 10^{-13}$. For example, for the running of Newton's constant G, one can estimate

$$\frac{\delta G}{G} \sim \left(\frac{r_{\mathrm{sol}}}{\xi}\right)^3 \sim 10^{-39} \ . \tag{A.3}$$

Next, for the scaling of correlation functions, the fluctuations are governed by the Einstein field equations

$$\langle\, \delta R\, \delta R \,\rangle \ = \ (8\pi G)^2\, \bar{\rho}^2 \left\langle \frac{\delta\rho}{\bar{\rho}}\, \frac{\delta\rho}{\bar{\rho}} \right\rangle \simeq \ G^2\, \bar{\rho}^2 \left(\frac{r_0}{r}\right)^2 \ , \tag{A.4}$$

where $r_0 \simeq 10\,\mathrm{Mpc} \sim 10^{-2}\,\xi$, and $\bar{\rho}$ is the average matter density of the Universe, which is roughly given by

$$\bar{\rho} \simeq \frac{M}{\xi^3} \ , \tag{A.5}$$

where M is of the order of the mass of the currently observable Universe, roughly $M \simeq 10^{80}$ protons, and ξ is roughly the size of the currently observable Universe. In the following, again, we are just interested in rough order of magnitude estimates. The value of Newton's

constant G, as argued for example in [28], is roughly

$$G \simeq \frac{\xi}{2\,M} \ . \tag{A.6}$$

So, putting together the numbers, one has

$$\langle \delta R\, \delta R \rangle \simeq \left(\frac{\xi}{M}\right)^2 \left(\frac{M}{\xi^3}\right)^2 \left(\frac{10^{-2}\,\xi}{r}\right)^2 \ = \ \frac{1}{\xi^2\, r^2} \cdot 10^{-4} \tag{A.7}$$

In a semi-classical approach, one can relate fluctuations in the curvature to metric fluctuations via the weak field relationship

$$\delta R \ \simeq \Box\, h \ , \tag{A.8}$$

and inserting the value for ξ then gives

$$\langle\ \delta R\, \delta R\ \rangle \simeq \ \langle\ \Box h\, \Box h\ \rangle \ \simeq \ \frac{10^{-4}}{\xi^2\, r^2} \ \sim \ \frac{10^{-34}}{(1\,\mathrm{AU})^2} \cdot \frac{1}{r^2} \ \ . \tag{A.9}$$

Therefore, if we use Poisson's equation $\Box h \simeq \Delta\Phi \simeq \delta\rho$ to relate the metric to matter density in the Solar System, it should still obey a $1/r^2$ scaling law, but with an amplitude suppressed by a very large factor 10^{-34}. In conclusion, within Solar System scales, any other Newtonian dynamics will completely dominate over the (very tiny) correlations due to quantum fluctuations of the gravitational field.